COPYRIGHT NOTICE

SPACE-TIME MULTIUSER DETECTION OF MULTI-CARRIER DS-CDMA SYSTEMS

James Bruce Whitehead
University of Natal
2001

Submitted in fulfilment of the academic requirements for the degree of MScEng in the School of Electrical and Electronic Engineering, University of Natal, South Africa, Dec. 2001.

Abstract

Personal wireless communications networks have flourished over the last decade as advances in digital cellular technology have made them more accessible to the general public. Third Generation Cellular Communication systems based on code division multiple access (CDMA) as the multiple access technique, show great scope for improvement in terms of capacity, through the use of advanced signal processing techniques. Two of the leading areas that encompass these techniques are space-time processing (smart antennas) and multiuser detection (MUD). Space-time-MUD (ST-MUD) is a relatively new field that hopes to bring together these two techniques. The focus of this thesis is ST-MUD in the context of a multi-carrier direct sequence CDMA (MC-DS-CDMA) communications system, which is one of the adopted multiple access techniques for the upcoming third generation cellular communications systems.

The concepts of MUD and smart antennas are discussed, and their performance enhancing capabilities are demonstrated. The use of vector channel models and their role in modelling the propagation phenomena of the communications channel in terms of the space, time and frequency domains is also illustrated. A ST-MUD receiver architecture is presented, and the performance of the architecture with a minimum mean square error (MMSE) decision criterion is analysed in a frequency selective Rayleigh fading channel. The analysis results are verified via simulation. Three subspace MUD techniques are adapted for ST-MUD, and the joint space-frequency-multipath MMSE solution on these subspaces is given. Simulation results are used to quantify their relative performance. The relevance and applications of the subspace techniques are elaborated.

Preface

The research work presented in this dissertation was performed by Mr. James Whitehead, under the supervision of Prof. F. Takawira, at the University of Natal's School of Electrical and Electronic Engineering Centre for Radio Access Technologies, which is sponsored by Telkom SA Ltd and Alcatel Altech Telecomms.

Parts of this dissertation have been presented by the student at the COMSIG'2000 conference in Somerset West, South Africa, and at the SATNAC'2001 conference at the Wild Coast, South Africa.

This dissertation is completely the student's own work, unless otherwise stated in the text. It has not been submitted in part, or in its entirety, to any other University.

Acknowledgements

I wish to thank my supervisor, Prof. Takawira, for his valuable help and advice provided during the last two years. It is much appreciated.

Thanks is also owed to Telkom and Alcatel Altech Telecomms for providing financial support and equipment for the completion of this masters degree.

Finally, thanks go to my Dad, and Shelley, for their support and time spent proof reading parts of this document.

Table of Contents

List of Figures

List of Tables

List of Acronyms

AAA	Adaptive Antenna Array
AMPS	Advanced Mobile Phone System
AOA	Angle Of Arrival
AWGN	Additive White Gaussian Noise
BER	Bit Error Rate
CDMA	Code Division Multiple Access
COST	European Cooperation in the field of Science and Technology
CMA	Constant Modulus Algorithm
DECT	Digital Enhanced Cordless Telecommunications
DOA	Direction Of Arrival
DS-CDMA	Direct Sequence CDMA
EDGE	Enhanced Data rates for Global Evolution
ETSI	European Telecommunications Standards Institute
FDMA	Frequency Division Multiple Access
FIR	Finite Impulse Response (filter)
FEC	Forward Error Correction
FH-CDMA	Frequency Hopping CDMA
FM	Frequency Modulation
GPRS	General Packet Radio Service
GSM	Global System for Mobile communication
ICI	Inter-carrier Interference
IF	Intermediate Frequency
IMT-2000	International Mobile Telecommunications 2000
ISI	Inter-symbol Interference

ITU	International Telecommunications Union
MC-CDMA	Multicarrier CDMA
MAI	Multiaccess Interference
MIP	Multipath Intensity Profile
MMSE	Minimum Mean Square Error
MSE	Mean Square Error
MT-CDMA	Multitone CDMA
MUD	Multiuser Detection
PCN	Personal Communications Network
PSK	Phase Shift Keying
PN-Sequence	Pseudo-random Noise Sequence
RF	Radio Frequency
SINR	Signal to Interference plus Noise Ratio
SNR	Signal to Noise Ration
STAP	Space-time Adaptive Processing
TACS	Total Access Communications Systems
TDD-CDMA	Time Division Duplexing CDMA
TDMA	Time Division Multiple Access
TH-CDMA	Time hopping CDMA
TOA	Time Of Arrival
UCA	Uniform Circular Array
ULA	Uniform Linear Array
UMTS	Universal Mobile Telecommunications System
UTRAN	UMTS Terrestrial Radio Access Network
MC-DS-CDMA	Multicarrier direct sequence CDMA
W-CDMA	Wideband CDMA

Notation and Common Parameters

Bold capital	Matrix
Bold lower case	Column vector
Lowercase	Scalar (complex or real valued)
Capital	Constant
$(.)^T$	Transpose
$(.)^H$	Hermitian transpose
$(.)^-$	Lower Bound, (limit taken from above)

P	Number of antenna elements
M	Number of subcarriers
L	Number of multipath receivers
N	Processing gain
L_{tot}	Total number of resolvable multipaths
K	Number of users

Chapter 1 Introduction

1.1 Mobile Wireless Communications

Personal wireless communications is a global phenomenon that seems to have captured the imagination of the every day person. Known as "cellphones", "mobiles", "handsets", or simply as a "phone" to the man in the street, they are expected to work every where (at home and away in different countries), hardly ever need charging, be simple to use, and are often required to connect seamlessly to portable devices for email retrieval and the like. These features must also be provided inexpensively. An example of the incredible public interest in cellular telephones can be found in the South African market. The first cellular service provider was only launched in South Africa in 1994. Their initial prediction was to have 250 000 subscribers within ten years; they now provide service to approximately 5.5 million South Africans (2001). Every month 1.3 billion calls are made on the network and almost five million SMS messages from cellphones were sent on New Year's Day (2001) alone.

With a growing demand in terms of the number of subscribers and potential high data rate applications, like video on demand, video conferencing, web browsing and email retrieval, current second generation (2G) technologies like GSM and cdmaOne™ (IS-95) are unable to provide the levels of service required by the customers. These 2G technologies cannot be efficiently scaled to provide the bandwidth required by customers. They also fall short in terms of spectral efficiency when compared to advanced spread spectrum solutions that are coupled with advanced signal processing capabilities.

1.1.1 3G Standards

There are two large standards bodies governing the evolutionary path to 3G technologies, namely, the ITU (International Telecommunications Union) and ETSI (European Telecommunications Standards Institute). The ITU is a United Nations department responsible for co-ordinating global telecommunications activities, especially in the area of standards. ETSI

is a non-profit European body comprised of representatives from administrations, network operators, manufacturers, service providers, research bodies and users.

The ITU's 3G network solution is called IMT-2000 (International Mobile Telecommunications 2000) [1]. There are five radio access technologies which fall under this banner, namely: UMTS (Universal Mobile Telecommunications System) using W-CDMA (Wideband CDMA) [2], CDMA2000 using MC-CDMA (Multicarrier CDMA) [3], TDD-CDMA (Time Division Duplexing CDMA), UWC-136/ EDGE (Enhanced Data rates for Global Evolution) using single carrier TDMA, and lastly DECT (Digital Enhanced Cordless Telecommunications) which is a combination of FDMA and TDMA. The CDMA [4] approaches have attracted the most amount of research. CDMA2000 provides a logical evolutionary path for IS-95 based networks.

The ETSI 3G network solution is called UTRA or UTRAN (UMTS Terrestrial Radio Access/ Network), which will be driven by UMTS, whose radio access technology will be W-CDMA based. UMTS is the logical upgrade path for GSM networks. A conceptual overview of W-CDMA is provided in [2].

A comparison between the ITU and ETSI standards can be found in [1]. More detail on UMTS and IMT2000 standards based on W-CDMA is contained in [5].

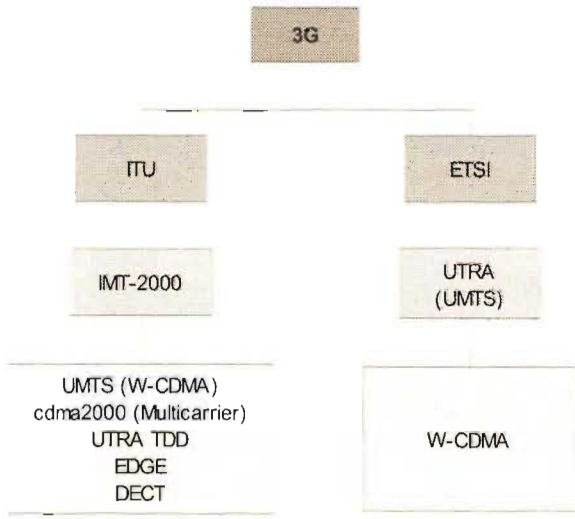

Figure 1-1 Organisation of standards bodies (ITU and ETSI) and their proposed 3G standards followed by their respective air interface schemes.

1.2 Problem formulation

Third generation air interface standards will be based on W-CDMA and some form of combination of MC-CDMA. 3G technologies far exceed the capabilities of 2G CDMA and

TDMA schemes because they will use a wider bandwidth/ higher chip rate, provide packet data services, use complex spreading, and make provision for optional multiuser detection and smart antennas (adaptive antenna arrays - AAA). The nominal bandwidth is 5MHz and data rates of 144 and 384 kb/s will be supported. These requirements, together with the need for high spectral efficiency, require advanced signal processing techniques to make 3G systems possible.

The 5MHz bandwidth is larger than 2G systems and thus it is capable of resolving more multipaths (section 2.2.4), which provide a valuable form of diversity; techniques should therefore be used to exploit the multipath diversity in 3G systems. Multiuser detection (MUD) is an option that has been considered [1] to improve the performance of 3G systems. It can reduce the amount of interference, thereby increasing capacity, and can also reduce the negative effects of loose power control, and the near-far problem. The use of smart antennas has been shown to offer many positive effects for CDMA networks [6], [7], [8]. The varying levels of sophistication in smart antennas provide varying levels of performance enhancement or capability. On a macro scale these devices can perform sector synthesis, which is the function whereby the AAA adjusts its radiation pattern to optimise hand-off boundaries, redistribute traffic loads, and control the levels of interference in neighbouring cells. Traffic load balancing is the shifting of traffic load from heavily loaded sectors to underused sectors, which reduces the call blocking probability. On a smaller scale, the most advanced AAA techniques would be able to track individual users and their multipaths in order to maximise the signal-to-interference-plus-noise-ratio (SINR) of those users.

ST-MUD for MC-DS-CDMA, encompasses all these signal processing related techniques to enable 3G communications systems. The performance of such a receiver with a realistic channel model needs to be understood. This dissertation provides a framework to analyse the effects of multipath diversity, antenna arrays, and MUD with different channel models. The system model is based on W-CDMA, and with the addition of subcarriers, can be made to model CDMA2000 like systems. An analytical technique is derived for analysing these CDMA schemes using a MMSE ST-MUD receiver. The MMSE criterion was chosen because it is a common criterion of many adaptive schemes that are likely to be used in 3G systems [9], [8]. It is a useful performance criterion that could either be used as a lower bound for many different adaptive receiver systems or as a bench mark for other advanced signal processing techniques used in ST-MUD.

When a MUD scheme is implemented using a transversal filter [10], the number of filter coefficients that need adapting can become large in asynchronous channels that have long delay spreads. The use of short spreading codes helps this problem somewhat [11], but the number of

coefficients to adapt is still prohibitively large and the tracking and convergence properties suffer a performance penalty. Subspace techniques have been investigated in an attempt to improve the tracking and convergence performance of adaptive algorithms when the number of filter coefficients to adapt is large. The performance of the ST-MUD architecture, when using subspace techniques, is therefore also important. This dissertation modifies three subspace techniques to work with the ST-MUD architecture. Their respective trade offs in performance, when compared to the MMSE solution, is investigated.

1.3 Outline of thesis

The first chapter attempts to summarise the background material to this dissertation, and motivates the use of ST-MUD as a unifying framework for the smart antenna and MUD techniques used in either W-CDMA or MC-DS-CDMA 3G cellular networks.

Chapters 2, 3 and 4 are intended to introduce the three fields with which this dissertation overlaps, to present the current research trends in the respective fields, as well as highlight concepts and models that directly apply to the ST-MUD concept. Chapter 2 covers the topic of vector channel models, propagation in wireless communications channels and the relationship between the fading in the space, time and frequency domains. In chapter 3, smart antenna techniques are reviewed and a geometrical model is used to formulate the optimal beamforming problem. Array performance criteria and combined space-time processing is also introduced. Chapter 4 reviews important MUD concepts and performance criteria that are relevant to DS-CDMA systems, with emphasis on optimal MUD and MMSE MUD.

In chapter 5, a new ST-MUD receiver architecture for the reception MC-DS-CDMA and multipaths is developed. The joint space-frequency-multipath MMSE solution is derived, and the performance of such is analysed in a frequency selective Rayleigh fading channel. A full derivation of a simplified term for the SINR at the output of the MMSE ST-MUD was performed to this end. The analysis is compared with simulation results, garnered from a custom simulation environment.

Chapter 6 describes the subspace projection of the received vector of samples and three subspace techniques for use in the ST-MUD of MC-DS-CDMA. The respective performance of the subspace techniques is compared using simulation results. For comparative purposes, a simulation of the matched filter receiver and the MMSE receiver is presented along with these results. The relevance and application of the subspace techniques is also explored.

A summary of the dissertation and concluding remarks are made in chapter 7, together with some ideas for future study. Appendix A contains the formulas for the received vector of samples used in chapter 5. In Appendix B, the elements of the multiaccess-interference-plus-noise covariance matrix of chapter 5 are derived. Appendix C summarises the details pertinent to the implementation and configuration of the custom simulation environment, and the results thereof.

1.4 Original Contribution

There have been several contributions in this dissertation to the body of research of communication systems engineering, namely:

- A joint space-frequency correlation function was developed in section (2.4.2), from existing separate frequency and space correlation models. This enabled the modelling of the fading correlation between the antenna elements and subcarriers of the MC-DS-CDMA transmission scheme.
- In section (5.4), a ST-MUD receiver structure was developed for MC-DS-CDMA with the capability to exploit time resolvable multipaths. The joint space-frequency-multipath MMSE MUD solution on this architecture was derived.
- Existing subspace based MUD techniques were modified for the ST-MUD architecture, in Chapter 6, for the reception of asynchronous MC-DS-CDMA. These were the: Principle Components, Cross-Spectral filtering, and Partial Despreading methods. In particular, a novel block matrix form of the projection matrix was developed for the partial despreading subspace in section (6.5).

Chapter 2 Vector Channel Models and Propagation

2.1 Introduction

The advent of smart antennas and spatial processing techniques has led to the need for more advanced propagation models which accurately predict or simulate the received signal across an antenna array. These are vector channel models. Vector channel models attempt to model the received signal in both the space and time domains. This enables: network planning with smart antenna technology, increased capacity and performance estimations, as well as the development and analysis of smart antenna algorithms. Vector channel models should include effects modelled by traditional single sensor antenna models such as fading, delay spread and power level prediction. Some of the challenges include modelling angle of arrival (AOA) information, spatial correlation, angle spread, and joint AOA and time of arrival (TOA) statistics.

Some recent work in this field includes [12] and an overview of vector channel models can be found in [13], [14].

This chapter reviews existing vector channel models, and provides a brief summary of the propagation phenomena relevant to the vector channel models under discussion. The vector channel models are grouped into either geometrical or statistically based models. The joint space-frequency vector model used in the analysis of the proposed ST-MUD system is derived, and this joint space-frequency function is computed to show the fading correlation surface.

2.2 Mobile Radio Propagation

The propagation of radio waves that are used in wireless communications systems is complex and has been analysed extensively [17]. Radio waves can propagate from transmitter to receiver

by the following mechanisms: transmission, diffraction, scattering, refraction and reflection. Radio waves are transmitted through the atmosphere and can pass through such obstacles as windows also via transmission. This enables radio coverage inside buildings. Reflection is important since it is the cause of multipath propagation which gives rise to fading. Propagation models generally try to predict path loss over distance, and use statistical models to predict the effects that scattering and reflection have on the received signal amplitude.

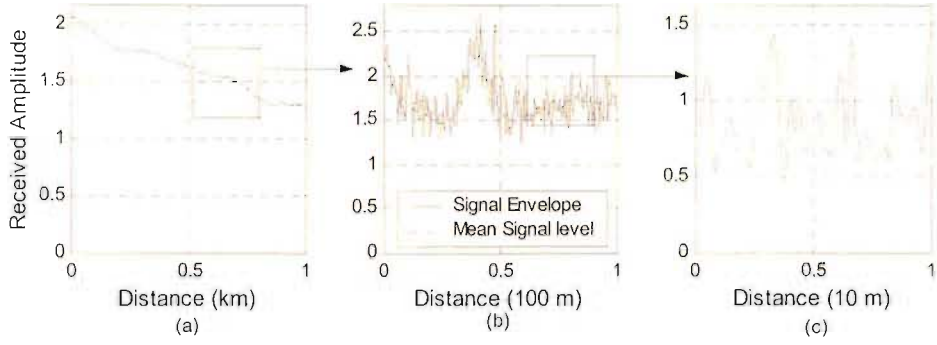

Figure 2-1 Different propagation phenomena can be characterised on different time (or distance) scales. Propagation loss (a) occurs on then largest scale. On a shorter time scale, log-normal fading of the mean signal level occurs (b). A closer look at the signal fluctuation in (c) illustrates the Rayleigh fading phenomenon, which occurs on the smallest scale.

2.2.1 Propagation Loss

Propagation loss models commonly try to model the received signal level as a function of the distance between the transmitter and receiver, whilst taking into account the type of terrain over which the radio waves propagate. The simplest path loss model calculates the path loss factor L, by raising the distance between transmitter and receiver R, relative to a reference distance r_0, to a power n.

$$L(R) = \left(\frac{R}{r_0}\right)^n \tag{2.1}$$

The factor n can be quite low (less than 2) when considering propagation along a street between tall buildings, but typically varies between 2.5 and 5, depending on the severity of the terrain. More sophisticated propagation loss models need to factor in such quantities as:

- Free space loss
- Height of the transmit and receive antennas
- Antenna gains
- Whether they be in urban, suburban or rural areas

They should also make use of site-specific factors, such as:

- Geometry of buildings
- Street width

Examples of outdoor propagation models include: Okumura, Sakagmi and Kuboi, Hata, Egli, Ibrahim and Parson, Lee, Walfish and Ikegami (COST 231), [17], [14], [18]. They are generally a combination of theoretical path loss models based on free space propagation, and some empirical data gathered from measurements of the typical environment under consideration. As an example, Lee's model is given as [18]

$$P_r = P_{r0} - \gamma \log_{10}(r/r_0) - n \log_{10}(f/f_0) + \alpha \tag{2.2}$$

where P_r is the received signal power relative to the power received at a 1 mile intercept point P_{r0}, γ is the path loss slope, n is the frequency dependence factor and α is correction factor to account for antenna gains, transmitter power and antenna heights. A sample of the empirical data used in the Lee model is found in Table 1.

Environment	1-Mile Intercept P_{r0}	Path Loss Slope γ
Free Space	-45.0 dBm	20.0 dB/dec
Open Area	-49.0 dBm	43.5 dB/dec
Suburban Area	-61.7 dBm	38.4 dB/dec
Urban (Philadelphia)	-70.0 dBm	36.8 dB/dec
Urban (Newark)	-64.0 dBm	43.1 dB/dec
Urban (Tokyo)	-84.0 dBm	30.5 dB/dec

Table 1 Lee Model empirical data [18].

2.2.2 Shadowing (Log-normal slow fading)

Measurements have shown that the mean value of the received signal level has a log-normally distributed value. This phenomenon is called shadowing and is caused by the movement of the mobile station and/or the movement of dominant reflectors in the propagation environment. The received signal is composed of multipaths originating from reflectors and scatterers. When the mobile moves around, new multipaths arrive at the receiver and old propagation paths vanish, inflicting a fluctuation in the mean signal level. In a similar fashion, scatterers and reflector could change position while the mobile remains stationary, and also generate a variation in the mean signal level. This fluctuation is characterised by a log-normally distributed random variable, and its probability distribution function is given by

$$f(r) = \frac{20\log_{10} e}{r\sigma_p\sqrt{2\pi}} \exp\left(-\frac{(20\log_{10} r)^2}{2\sigma_p^2}\right) \tag{2.3}$$

where $1.02686^{\sigma_p^2}$ is the second moment of the log-normally distributed random variable.

2.2.3 Fading

One of the most significant performance effecting aspects of the mobile radio communications channel is fading, and many diversity techniques have been designed specifically to combat it. When the received signal is made up of many randomly phased multipaths, the envelope of the received signal amplitude r follows a Rayleigh distribution,

$$f(r) = \frac{r}{\sigma^2} e^{\frac{-r^2}{2\sigma^2}} \tag{2.4}$$

and the received signal phase has a uniform distribution on $[0,\ 2\pi]$. The first and second moments of a Rayleigh distribution are given, respectively, by

$$E\{r\} = \sqrt{\frac{\pi}{2}}\sigma \tag{2.5}$$

$$E\{r^2\} = 2\sigma^2 \tag{2.6}$$

This same result is obtained if one models the in-phase and quadrature-phase amplitudes of the received signal envelope as independent, zero mean, Gaussian random variables, with variance σ^2. The Rice distribution better models the received amplitude level when there is a direct line of site between the transmitter and the receiver. If one then models the in-phase and quadrature-phase components of the received signal envelope as nonzero mean, independent, Gaussian random variables, the received signal envelope follows the Rice distribution,

$$f(r) = \frac{2r}{\sigma^2} \exp\left(-\frac{r^2+\mu^2}{\sigma^2}\right) I_0\left(\frac{2r\mu}{\sigma^2}\right) \tag{2.7}$$

where μ^2 is the average power of the direct line of site path, and $I_0(.)$ is the zero-order modified Bessel function[1]. The Nakagami distribution [19] has an extra degree of freedom over the Rayleigh and Rice probability distribution functions that enables it to more closely fit experimental data. Its probability distribution function is given by,

---

[1] $I_0(x) = \frac{1}{2\pi}\int_0^{2\pi} e^{x\cos(\alpha+\beta)} d\alpha$

$$f(r) = \frac{2m^m r^{2m-1}}{\Gamma(m)\sigma^2} \exp\left(-\frac{mr^2}{\sigma^2}\right) \tag{2.8}$$

where $\Gamma(.)$ is the gamma function. When $m = 1$, the Nakagami distribution is the same as the Rayleigh distribution, and as m increases, the Nakagami distribution more closely approximates the Rice distribution.

Another formulation of the fading problem would be from the frequency domain. When the mobile station is moving, with respect to the base station, there is a Doppler shift in the received signal. This Doppler shift has the effect of broadening the received signal's bandwidth. The maximum amount of Doppler shift is $f_m = v/\lambda$ where v is the velocity of the mobile and λ is the wavelength of the carrier frequency. The Doppler power spectrum $(R(\lambda))$ of the signal quantifies the time varying properties, like the fading rate, of the received signal. It is related to the time correlation function via the Fourier transform. The maximum Doppler shift is known as the Doppler spread, B_d, of the channel. The inverse of the Doppler spread is referred to as the coherence time of the channel (Δt_c), and gives an indication of how rapidly the channel fade level changes.

2.2.4 Frequency Selective Fading

Frequency selective fading occurs when the time delay between multipaths is greater than the symbol duration. These multipaths are said to be time resolvable, and are the cause of inter-symbol interference (ISI). For the benefit of this dissertation, a tapped delay line model will be used to model a frequency selective fading channel. The impulse response of the channel is one way to characterise the frequency selectivity, and for L resolvable multipaths it takes the form

$$h(t,\tau) = \sum_{i=1}^{L} \beta_i \delta(t-\tau) \tag{2.9}$$

where β_i is the complex amplitude of the ith multipath and $\delta(.)$ is the delta function. The difference in propagation time of the longest path to the shortest path is known as the delay spread, and the inverse of which is known as the coherence bandwidth of the channel. If the bandwidth of the transmitted signal exceeds the coherence bandwidth of the channel then there will be frequency selective fading.

The fading on these multipaths is considered to be independent, and as such can be a valuable source of diversity. The RAKE combiner [19] is a common method used to exploit multipath diversity, and it does so by using maximal ratio combining on the multipaths.

There are various techniques used to model the spread of energy between the time resolvable multipaths. An exponential multipath intensity profile (MIP) is considered here, which is similar to the typical urban profile used in the GSM COST 207 power delay profile [20]. If the time delay τ is given in microseconds (μs), then the fraction of the power contained in multipath l relative to multipath 1, where $\tau = 0$, is given by

$$P_l(\tau) = \begin{cases} \exp(-\tau), & \text{for } 0 < \tau < 7, \\ 0, & \text{elsewhere} \end{cases} \tag{2.10}$$

2.2.5 Frequency Diversity Model

In a MC-DS-CDMA transmission system, data is transmitted on different frequency bands called subcarriers, if these bands are not sufficiently far apart it is possible that the bands do not have completely independent fading. Using a more general form of equation (2.10), it is possible to compute the fading correlation coefficient as a function of frequency separation (Δf), and the standard deviation of the multipath delays (σ_d). The standard deviation of the multipath delays is defined as

$$\sigma_d = \sqrt{E\{\tau^2\} - E\{\tau\}^2} \tag{2.11}$$

Modifying (2.10) and adding the σ_d parameter, the MIP becomes

$$P(\tau) = \begin{cases} \frac{1}{\sigma_d}\exp\left(-\frac{\tau}{\sigma_d}\right) & for\ \tau \geq 0 \\ 0 & \tau < 0 \end{cases} \tag{2.12}$$

The correlation in frequency is defined from the Fourier transform of the MIP function,

$$\begin{aligned} R_f(\Delta f) &= E\{y^H(f_c, t)\, y(f_c - \Delta f, t)\} \\ &= \int_{-\infty}^{\infty} P(t)\exp(j2\pi\Delta f \Delta t)\, d(\Delta t) \end{aligned} \tag{2.13}$$

The normalised correlation coefficient [23] can then be written as

$$\rho(\Delta f) = \frac{1}{\sqrt{1 + (2\pi\Delta f \sigma_d)^2}} \tag{2.14}$$

When either the frequency separation or the standard deviation of the multipath delays increases, the fading correlation decreases.

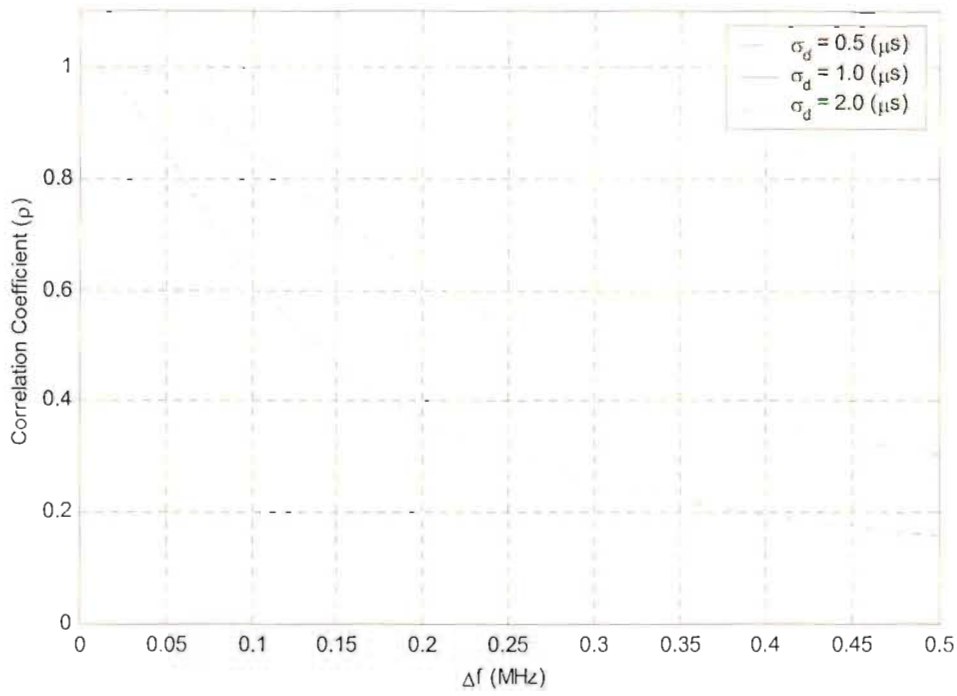

Figure 2-2 Fading correlation coefficient of two sinusoids as a function of their frequency separation using the exponential model in (2.14).

2.3 Vector/Spatial Channel models

The fading and propagation models covered thus far do not impart any information about the received signal in the space domain. The received signal characteristics, such as phase, amplitude or fade level, change as one moves across the antenna array in space. These characteristics are functions of phenomena that are not relevant for single sensor receivers and as such it has not been necessary to model them in the past. One of the outputs of the vector channel model is the array response vector (2.15). It gives the relative phase of the wave front at the N-sensors of the array, which is a function of the AOA and array geometry.

$$\mathbf{a}(t) = \begin{bmatrix} e^{j\psi_1(t)} \\ \vdots \\ e^{j\psi_N(t)} \end{bmatrix} \tag{2.15}$$

For a uniform linear array, $\psi(t)$ is given in (3.3). From the array response vector, it is possible to construct the vector channel impulse response (compare (2.9)) for a multipath fading channel,

$$\mathbf{h}(t,\tau) = \sum_{l=1}^{L} \mathbf{a}_l(t)\beta_l\,\delta(t-\tau_l) \tag{2.16}$$

Fading correlation information is contained in the array covariance matrix, and certain vector channel models are better than others at producing analytically tractable forms of such. The array covariance matrix is constructed from the vector of received signals at each antenna element, i.e. if the received signal at antenna element n is $r_n(t)$ then the received vector for an N-element antenna array is

$$\mathbf{r}(t) = \begin{bmatrix} r_1(t) \\ r_2(t) \\ \vdots \\ r_N(t) \end{bmatrix} \tag{2.17}$$

and the array covariance matrix is then

$$\mathbf{R} = E\left\{\mathbf{r}(t)\mathbf{r}^{H}(t)\right\} \tag{2.18}$$

where $(.)^{H}$ is the Hermitian transpose, which is the complex conjugate transpose.

2.3.1 Geometric Models

Geometrically based models define the location of scatterers, or scattering clusters, and the location of the mobile. These locations in turn determine properties of the received signal. The geometric single bounce models assume that the transmitted signal bounces off the scatterer and then goes directly to the receiver. The time of arrival (TOA), τ, and AOA, θ, can then be directly computed from the geometry illustrated in figure (2-3).

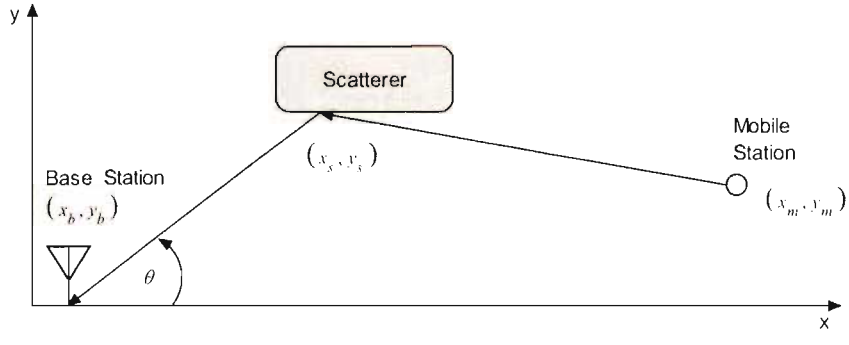

Figure 2-3 AOA and TOA calculations from discrete locations of scatterers.

$$\theta = \tan^{-1}\left(\frac{y_s - y_b}{x_s - x_b}\right) \tag{2.19}$$

$$\begin{aligned} \tau &= \frac{\text{distance traveled}}{\text{speed of light, c}} \\ &= \left[\sqrt{(y_m - y_s)^2 + (x_m - x_s)^2} + \sqrt{(y_s - y_b)^2 + (x_s - x_b)^2}\right] / c \end{aligned} \tag{2.20}$$

The scatterers' locations may be discrete or be distributed throughout a particular region.

2.3.1.1 Geometric Models Using Discrete Scatterers

Discrete models were developed to predict the signal correlation between two sensors as a function of their separation and AOA. Examples of discrete distribution models are Lee's (also known as "Effective Scatterer Model") [13], modified Lee's [24], the uniform distribution [25], and typical urban and bad urban [26].

Lee's model assumes that there is a ring of scatterers surrounding the mobile and the radius of the ring R, number of scatterers N, and distance from mobile to base station D, are parameters of the model. The discrete AOA's are given by

$$\theta_i = \frac{R}{D}\sin\left(i\frac{2\pi}{N}\right) \quad \text{for } i = 1 \ldots N-1 \tag{2.21}$$

and then the correlation between two sensors can be found with [13]

$$\rho(d,\theta,R,D) = \frac{1}{N}\sum_{i=0}^{N-1}\exp\left(-j2\pi d\cos(\theta+\theta_i)\right) \tag{2.22}$$

where d is the distance between the two sensors, and θ is defined in figure 2-4 (a).

The modified Lee's model gives the ring of scatterers a rotational velocity around the mobile station in order to introduce a Doppler spread in the received signal.

The typical urban and bad urban are special discrete cases of the circular model, of section (2.3.1.2). The typical urban model places 120 scatterers randomly within a 1km radius of the mobile. The position of the scatterers is held fixed while the mobile moves five meters, after the five meters the scatterers are returned to their original positions relative to the mobile. Random phase and shadowing effects are assigned to the scatterers every five meters. The received signal is determined through brute force from the locations of the scatterers. Simulations have shown that this model yields very similar results to the GSM-typical urban model. The bad urban model is the same as the typical urban model except a second circular scatterer cluster is added. The cluster's position is offset from the first by forty-five degrees and the scatterers in it are assigned 5dB less average power than the original cluster.

The uniform distribution places scatterers in discrete positions uniformly along a line. This line is placed perpendicular to the line joining the mobile station to the base station. This model also causes the correlation to decrease with distance more, as compared to Lee's model.

It has been found [13] that the joint AOA and TOA information generated from these models are not very accurate when compared to measured results.

2.3.1.2 Geometric Models Using Distributed Scatterers

Models where the scatterers are distributed in space with a continuous spatial scatterer density function are more useful where joint AOA-TOA statistics are required, as these properties can be directly computed. Examples of these include: circular, elliptical, elliptical sub-region, and uniform sectored [13], [24].

The distributed circular model, figure 2-4 (c), has the same geometry as Lee's except the scatterers are uniformly distributed throughout the circular region. It is used to model macrocell environments where it is assumed there is no signal scattering from objects near the base station.

The elliptical model places the base station and mobile station at the two foci of an ellipse, where the ellipse contains a uniform distribution of scatterers. The elliptical models are more useful for modelling microcell environments where scattering near the base station is as likely as scattering near the mobile station.

The elliptical sub-region technique fills each elliptical sub-region uniformly with scatterers. The resulting arrival times of multipaths from each sub-region have an exponential probability distribution function (pdf), and there is a Gaussian AOA pdf generated by each cluster. The elliptical sub-region technique can be modified to model a macrocell environment by removing the scatterers inside a circle that is centred on the base station.

2.3.2 Statistical Vector Channel Models

The statistical models do not specify any positions of scatterers or mobile stations, but rather directly assign statistical distributions to the AOA and TOA information. Examples of statistical channel models include the Gaussian Wide Sense Stationary Uncorrelated Scattering (GWSSUS) model, the Gaussian Angle of Arrival (GAA) model, Raleigh's model and the modified Saleh-Valenzuela model, [13], [24], [26].

The GWSSUS model places a number of scatterers in a cluster; the cluster is placed in space, away from the base station and has a mean AOA. The resulting multipaths arriving at the base station from the scatterers are not time resolvable. When the number of scatterers is large (ten or more, [26]) the central limit theorem can be applied to the superposition of the multipaths arising from the cluster, and hence a multivariate Gaussian distribution with an associated

covariance matrix can characterise the cluster. The GWSSUS model was mainly developed with the aim in mind to produce a general result for the form of the array covariance matrix. The GWSSUS model is useful for modelling frequency flat fading, but by having more than one cluster it is also possible to model a frequency selective fading channel.

The GAA model is a specific form of the GWSSUS model where only a single cluster is considered. This only makes it applicable to frequency flat fading channels. Once again there is a mean AOA to the base station, but the AOA's from the scatterers have a Gaussian distribution about this mean. A useful expression exits for the covariance matrix when a ULA is considered and is given in [13].

Raleigh's model is a time varying model that is characterised by local scatterers around the mobile and has L dominant reflectors, whose numbers can change with time. This configuration models a frequency selective/multipath-fading channel. Raleigh's model takes into account both log-normal fading and the multipath intensity profile of the channel, which the other channel models do not consider. The resulting complex amplitude of the received wave, $\beta(t)$, has a complex Gaussian distribution, in all directions away from the mobile.

The modified Saleh-Valenzuela model [26] is useful for modelling indoor environments. It assumes that the TOA and AOA statistics are independent. Multipath components arrive at the antenna array in clusters in both space and time. The mean AOA from a cluster is uniformly distributed on $[0,2\pi]$ and the AOA within a cluster is modelled as a zero mean Laplacian[2] distributed random variable with standard deviation σ.

2.3.3 Measurement based

Measurement based models characterise the vector impulse response with values gathered and computed from experimental readings and results. The time variant impulse response generally takes the form [13],

$$h(\tau,t) = \int_0^{2\pi} \upsilon(\tau,t,\theta) * g(\tau,t) * f(\tau) d\theta \tag{2.23}$$

where $\upsilon(\tau,t,\theta)$ is the time variant directional distribution of the channel impulse response, which corresponds to a particular set of measurements. The base station antenna characteristics

[2] $f(\theta) = \frac{1}{\sqrt{2}\sigma} \exp\left(-\left| \frac{\sqrt{2}\theta}{\sigma} \right| \right)$

are contained in $g(\tau,\theta)$, and $f(\tau)$ is the joint transfer function of the radio system components on the send and receive side.

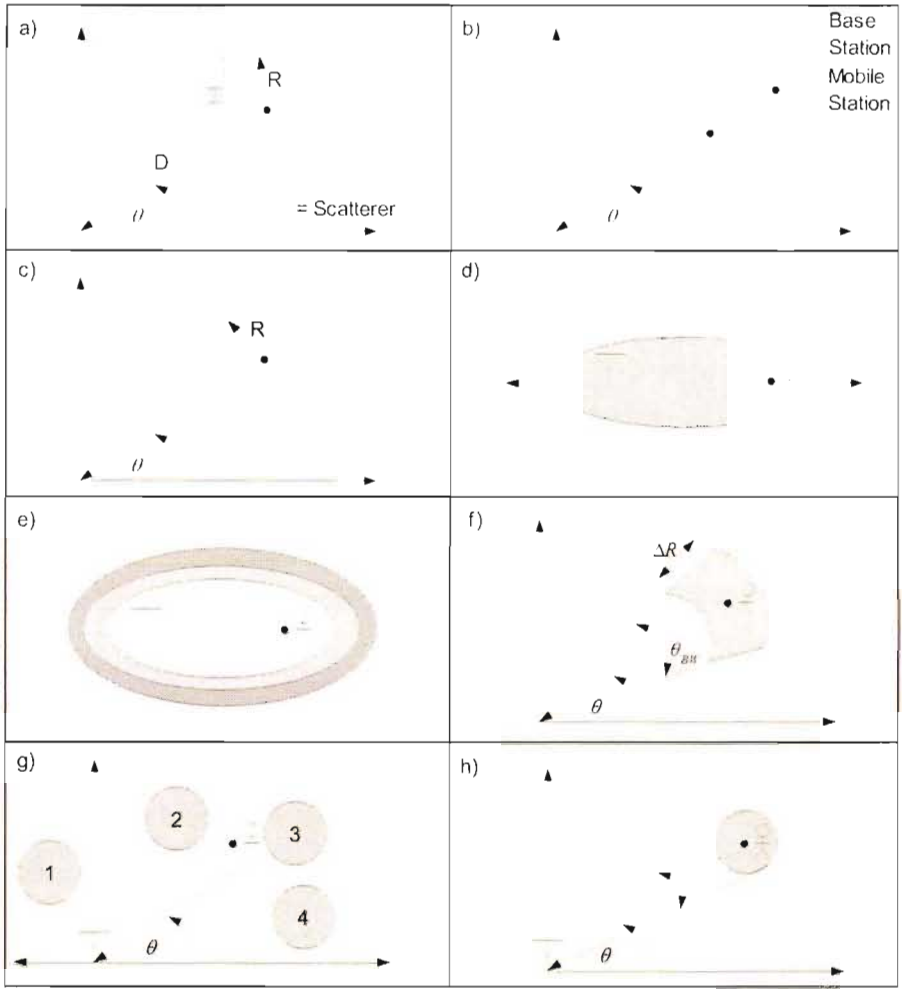

Figure 2-4 Summary of geometrically and statistically based vector channel models: (a) Lee's Model, (b) Discrete Uniform Distribution, (c) Geometrically Based Single Bounce Circular Model, (d) Geometrically Based Single Bounce Elliptical Model, (e) Elliptical Sub-Region Model, (f) Uniform Sectored Distribution Model, (g) Gaussian Wide Sense Stationary Uncorrelated Scattering Model and (h) Gaussian Angle of Arrival Model.

2.4 Fading Correlation

The geometrically based vector channel models have the advantage that they are simple to implement and they provide physical insights into the propagation mechanisms. This is offset by the fact that they are often less flexible and they require the single bounce assumption to hold. The statistically based vector channel models have the advantage that they offer maximum flexibility and are analytically more tractable. This is offset by the fact that they require more input parameters and are harder to implement. More sophisticated models need to take into account such factors as polarisation, antenna elevation and antenna down tilt. A larger body of

measurements needs to be collected, so that the vector channel models can be validated against them and their relative relevancy or accuracy plotted.

The space model that is used in the simulation and analysis of the ST-MUD system described in this dissertation, is based on a model proposed by [27], it was thoroughly analysed in [28] and has subsequently been used in such papers as [29], [30], [31]. It falls under the category of statistically based vector channel models, and is provides a mechanism to predict the fading correlation between the antenna elements of the ST-MUD. In [28] it is shown that this model does correspond closely with measurement data.

2.4.1 Space model

The space model looks at a scattering model where there are a few dominant scatterers placed near the mobile. Each of the dominant scatterers produces a set of multipaths with a mean AOA, θ, that arrive with a uniform distribution within an angle spread of 2Δ around the mean. From a single sensor point of view, it would seem as if each scatterer has produced a time resolvable Rayleigh fading multipath.

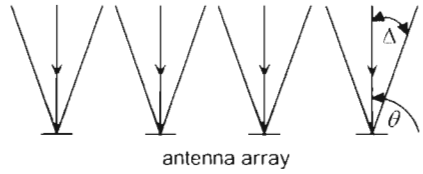

Figure 2-5 Antenna Array showing mean AOA (θ) with uniformly distributed AOA's within $\pm\Delta$ of the mean.

The fading correlation across the antenna array of one of these dominant paths is a function of its mean angle of arrival and the angle spread. It was shown in [28] that for a ULA, the real and imaginary parts of the fading correlation between antenna elements *m* and *n* is given by

$$\mathrm{Re}\left\{\mathbf{R}_s(m,n)\right\} = J_0(z_{mn}) + 2\sum_{l=1}^{\infty} J_{2l}(z_{mn})\cos(2l\theta_{mn})\mathrm{sinc}(2l\Delta) \tag{2.24}$$

$$\mathrm{Im}\left\{\mathbf{R}_s(m,n)\right\} = 2\sum_{l=0}^{\infty} J_{2l+1}(z_{mn})\sin\left((2l+1)\theta_{mn}\right)\mathrm{sinc}\left((2l+1)\Delta\right) \tag{2.25}$$

where $J_l(.)$ is the Bessel function[3] of the first kind of order *l*, and $z_{mn} = 2\pi(d_m - d_n)$, where d_m is the distance between the first antenna and antenna *m*, in wavelengths.

[3] $J_l(x) = \sum_{k=0}^{\infty} \frac{(-1)^k}{\Gamma(k+l+1)k!}\left(\frac{x}{2}\right)^{2k+l}$

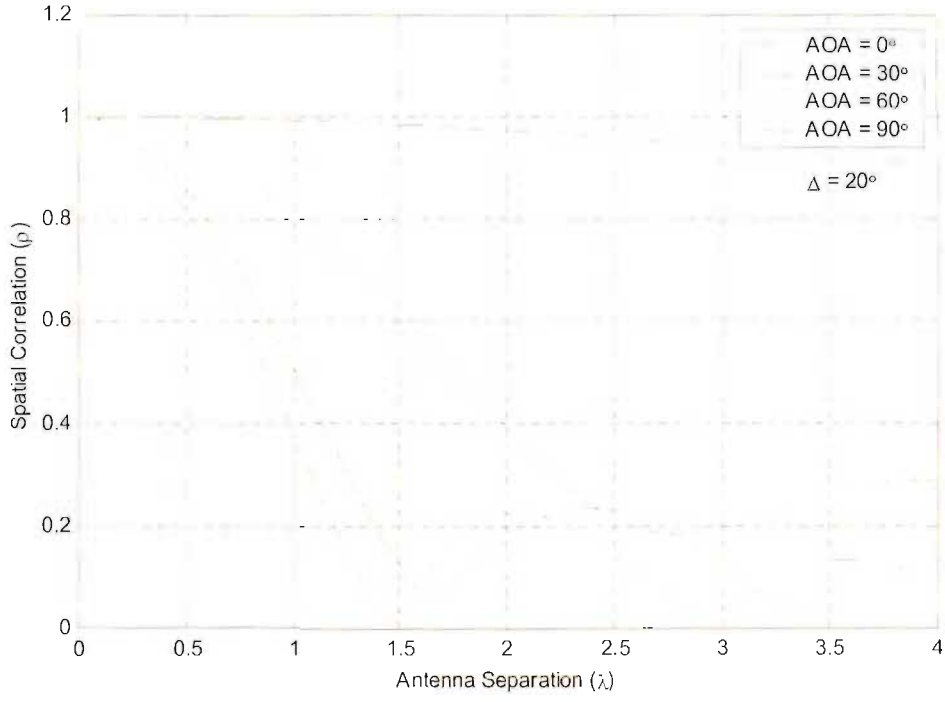

Figure 2-6 Spatial correlation function with different mean angles of arrival, as a function of antenna separation in terms of the wavelength λ. The angle spread Δ is set constant to 20°. $\rho = |\mathbf{R}_{,}(m,n)|$.

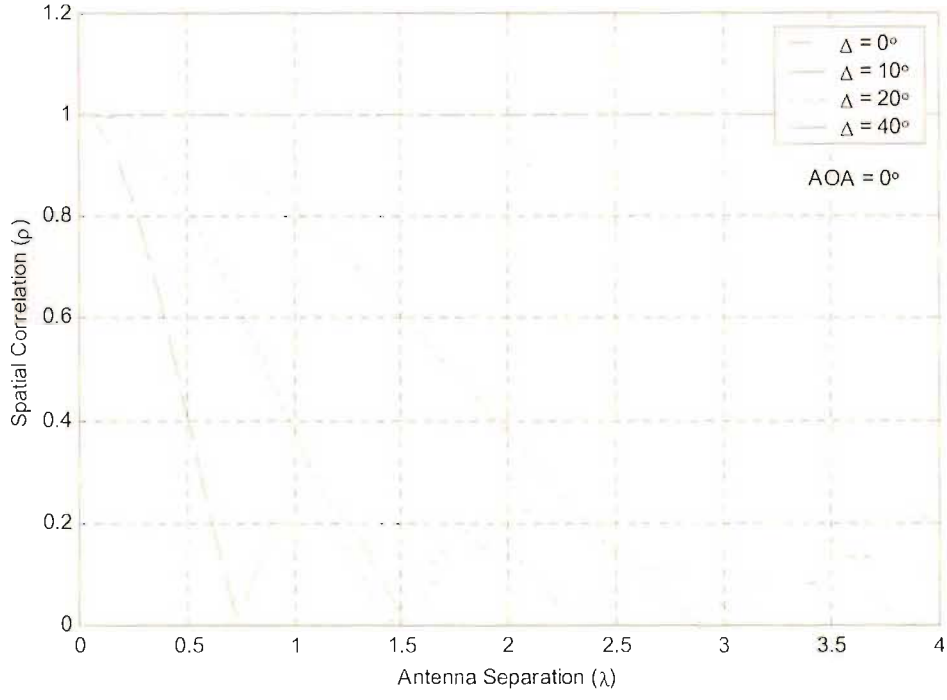

Figure 2-7 Spatial correlation function with different amounts of angle spread, as a function of antenna separation in terms of the wavelength λ. The mean AOA is set constant to 0°. $\rho = |\mathbf{R}_{,}(m,n)|$

2.4.2 Joint Space-Frequency Model

The joint space-frequency correlation matrix is computed directly from

$$\mathbf{R}_{sf}(\Delta f, \Delta d) = \mathbf{R}_f(\Delta f) \times \mathbf{R}_s(d_1, d_2) \tag{2.26}$$

This model allows one to predict the fading correlation as a function of frequency and space offset, which is useful in the context of the ST-MUD for MC-DS-CDMA as it directly relates to the fading correlation between subcarriers and antenna elements.

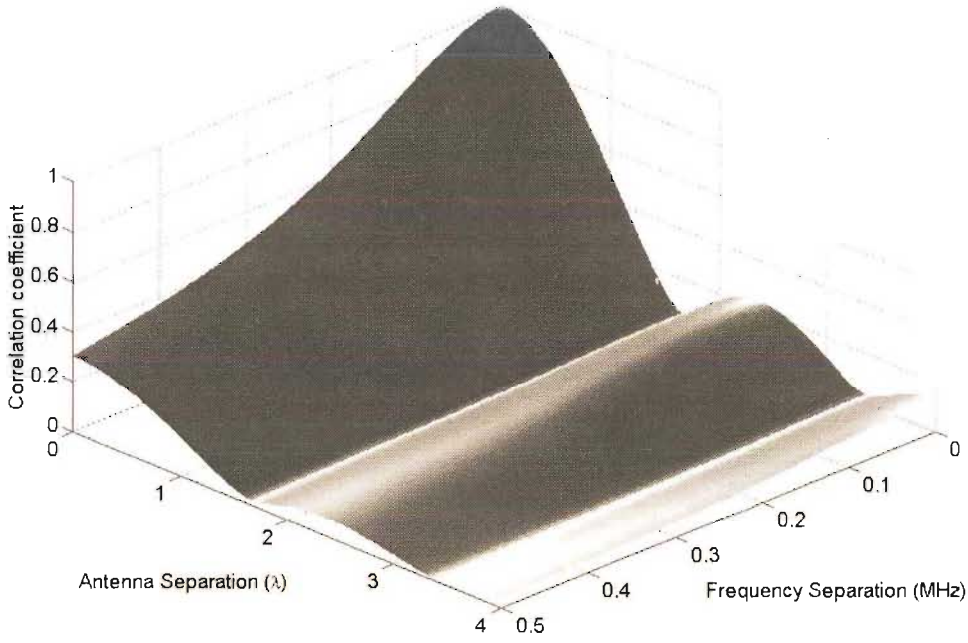

Figure 2-8 Surface plot of the space-frequency correlation function, as a function of antenna separation and frequency separation. The mean AOA is 30° and the angle spread is 20°, the standard deviation of the multipath delays is 1μs, for computing the frequency correlation function.

The elements of the space-frequency correlation matrix are given with the block matrix notation

$$\mathbf{R}_{sf} = \begin{bmatrix} \mathbf{R}_s(1,1) \times \mathbf{R}_f & \cdots & \mathbf{R}_s(1,P) \times \mathbf{R}_f \\ \vdots & \ddots & \vdots \\ \mathbf{R}_s(P,1) \times \mathbf{R}_f & \cdots & \mathbf{R}_s(P,P) \times \mathbf{R}_f \end{bmatrix} \tag{2.27}$$

where

$$\mathbf{R}_s(m,n) \times \mathbf{R}_f = \begin{bmatrix} \mathbf{R}_s(m,n) \times \mathbf{R}_f(1,1) & \cdots & \mathbf{R}_s(m,n) \times \mathbf{R}_f(1,M) \\ \vdots & \ddots & \vdots \\ \mathbf{R}_s(m,n) \times \mathbf{R}_f(M,1) & \cdots & \mathbf{R}_s(m,n) \times \mathbf{R}_f(M,M) \end{bmatrix} \tag{2.28}$$

2.5 Summary

Wireless communications channel models were reviewed and the factors limiting the performance of the mobile radio channel were investigated. Propagation models illustrated the macro scale effects, such as path loss as a function of distance. On a smaller scale, log-normal shadowing effects were shown to cause fluctuations in the mean signal level. Finally, multipath fading phenomena were discussed, and common statistical models were given. A model that computes the fading correlation coefficient as a function of frequency separation was also presented.

The concept of receiving a radio signal with an array of sensors was introduced along with a mathematical and geometrical framework for computing the spatial signature that the antenna array imparts on the received signal. The array response vector and covariance matrix was defined. An outline of vector channel models was presented along with applications. The spatial vector channel model used in this dissertation was also computed for various scenarios. The vector channel concept was extended to the frequency domain to define a space-frequency correlation matrix. This space-frequency correlation matrix had a block matrix form and allowed the modelling of the fading correlation between the subcarriers and antenna elements of the ST-MUD receiver in chapters 5 and 6.

Chapter 3 Smart Antennas

3.1 Introduction

The field of smart antennas (and adaptive antenna arrays) is expansive and its beginnings can be traced to the emergence of digital signal processing in the 1960's. The term "adaptive array" was first used in [32] to describe a self-phasing antenna system that reradiates a signal in the direction from which it was received. By combining time varying filters and antenna elements dispersed in space, adaptive antennas were born [33]. The ability to control antenna directivity and suppress interference spawned a huge body of research, of which [34] provides a summary.

Space-time processing [8], [35] is a branch of smart antenna technology, and was first introduced in 1973 by Brennan and Reed [36] for use in adaptive radar systems.

A smart antenna system consists of multiple antenna elements coupled with a signal processor that is capable of optimising the radiation and/or reception pattern, automatically, in response to the signal environment, as is illustrated in figure (3-1).

Smart antennas are seen to play a major role in the upcoming third generation cellular communication systems as they boost system performance through the following major features:

- Signal Gain

  Smart antennas have higher antenna gains than conventional antennas. This has the advantage of increasing the base station coverage (range) or reducing the power requirements of the mobile stations, which increases their battery life.

- Interference Suppression

Through null steering and beamforming, it is possible to increase the signal-to-interference ratio of the desired user. The capacity of the cell is, since CDMA networks are essentially interference limited.

- Spatial Diversity

Antenna arrays can take advantage of diversity in the space domain and reduce the negative effects of multipath propagation, ie. by reducing the likelihood of deep fades one increases the capacity of the channel.

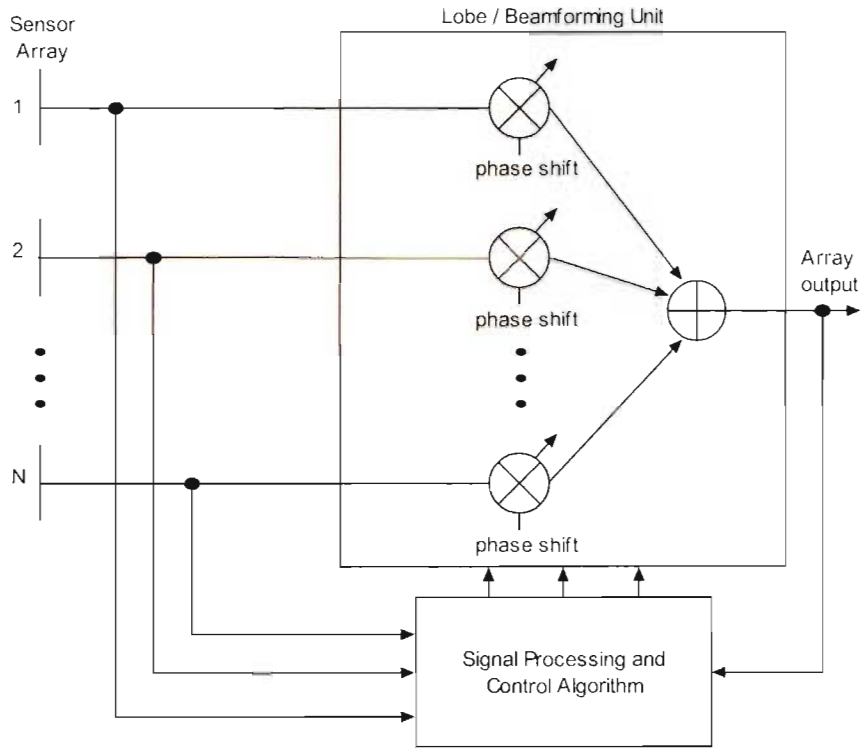

Figure 3-1 Main components of Adaptive Antenna Array.

This chapter introduces the concept of smart antennas to provide a framework and a context for space-time multiuser detection. Smart antenna techniques can be grouped into four categories, namely: diversity, sectorisation, switched beam and beamforming. Under the beamforming category, one can group the smart antennas that do both space and time processing. These smart antennas use algorithms that take into account the time structure of the signal. Smart antennas that perform joint space and time equalisation/processing are often grouped in a category known as space-time processors [8]. Both the equations for diversity gain (3.1) and beam patterns (3.5) are computed to illustrate the performance enhancing effects of increasing the number of antenna elements, through maximal ratio combing and narrower beamwidths respectively (figures 3-2, and 3-6).

3.2 Diversity

Smart antennas at a base station can provide diversity for both the downlink (transmit diversity) and the uplink (receive diversity) [19]. Transmit diversity is achieved by transmitting the same information from two (or more antennas) which are separated in space. When the antennas are far enough apart, there is independent fading on the transmit paths. The received composite signal therefore suffers less severe multipath fading. Transmit diversity can also make use of advanced coding techniques called space-time coding [21], to further improve performance. This section focuses on receive diversity.

Receive diversity is the converse of transmit diversity, where multiple receive antennas (normally on the uplink) are separated in space, such that the received signal at each antenna element suffers from independent (or uncorrelated) fading. Unlike beamforming, diversity combining does not take place at the RF (radio frequency) level, but rather at the IF (intermediate frequency) or baseband level. The actual radiation pattern of the antenna array is unmodified, but by carefully combining the signals at the different antenna elements, it is possible to increase the SINR of the desired user's signal. The signal processor, or receiver circuitry, consequently employs a particular combining strategy for optimal use of the signal received at each antenna element. The three major combining strategies are: maximal ratio combining, equal gain combining, and selection diversity combining. If there are L antenna elements, then there is Lth order diversity.

3.2.1 Equal Gain Combining

An equal gain combiner combines the signals of the desired user at the different antenna elements with an equal weight. This strategy produces the lowest outage probability.

3.2.2 Selection Diversity Combining

A selection diversity scheme will choose to receive only the signal from one of the antenna elements according to a particular criterion. That selection criterion could choose the antenna element with either the highest SNR, power of the desired user, total power, or SINR. When the SINR criterion is used, this technique becomes most effective for combating multi-access interference.

3.2.3 Maximal Ratio Combining

Maximal ratio combining combines the signals of the desired user with a weighting factor proportional to the SNR at each antenna element. For Lth order diversity, the probability of receiving a bit in error using binary PSK has a well-known result [19], and is given by

$$P_e = \left[\tfrac{1}{2}(1-\mu)\right]^L \sum_{k=0}^{L-1} \binom{L-1+k}{k} \left[\tfrac{1}{2}(1+\mu)\right]^k \tag{3.1}$$

where

$$\mu = \sqrt{\frac{\bar{\gamma}_c}{1+\bar{\gamma}_c}} \tag{3.2}$$

and $\bar{\gamma}_c$ is the average SNR per bit per branch. A plot of equation (3.1), with varying amounts of diversity L, is made in figure (3-2). It is noted that as the number of diversity branches, L, tends towards infinity, the probability of error tends towards that of the AWGN channel, thus completely mitigating the effects of fading.

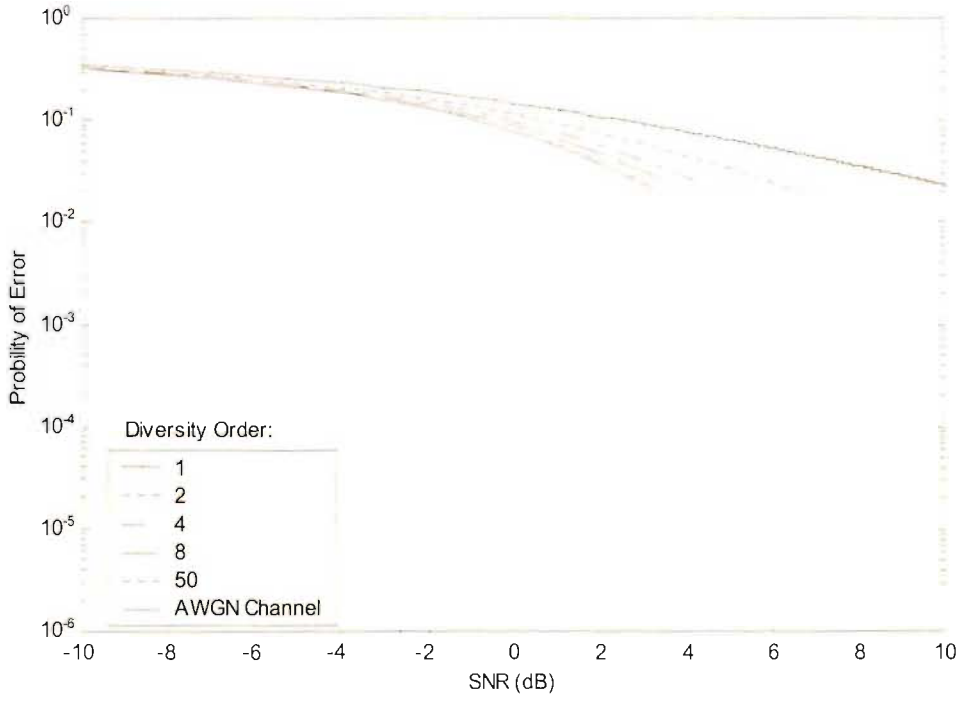

Figure 3-2 Maximal ratio combiner performance in Rayleigh fading.

3.3 Sectorisation

Sectorisation is a standard technique that is used to improve the spectral efficiency of a cell. For example, it is widely used in GSM networks where a base station commonly uses a three-sectored antenna, which splits each cell into three 120° sectors. Each sector only sees a third of the interference that an omni-directional antenna at the base station would normally experience. This effectively increases the capacity of the cell by approximately three times.

Antenna arrays make it is possible to split up a cell into narrow sectors, using beamforming techniques. These sectors are much finer than those possible with conventional directional antennas. The output of each mini-sector is fed into a dedicated radio channel unit (RCU), which calculates that particular mini-sector's SNR. When another mini-sector has a higher SNR, hand-off between sectors can occur. With this structure each mini-sector has dedicated radio channels, and the choice of mini-sector is taken after the RCU on each mini-sector.

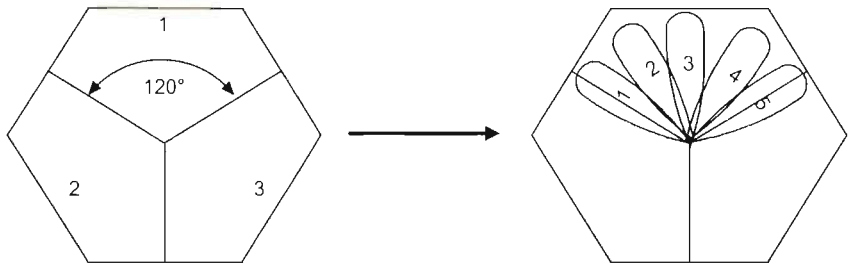

Figure 3-3 Traditional 3-sector sectorisation (left) versus the narrower sectors possible using an antenna array (right).

3.4 Switched beam

The switched beam approach is similar in concept to sectorisation, except that the decision making process as to which mini-sector a user is in, is taken at a higher level, before the RCU's. The antenna array has a set of predefined narrow beams and the signal processing unit continually monitors the power output of each beam. It selects the beam with the highest power output or SINR of the desired user, as he moves around the cell. The Base station resources are reduced since there does not have to be an RTU dedicated to every beam. There is also no need for a radio channel to be dedicated to each mini-sector; therefore, every radio channel assigned to the base station is usable at any specific time, which increases spectral efficiency.

A variation of the switched beam technique exists which is called "tracking-beam". The narrow beam, formed by the antenna array, constantly tracks the position of the desired user as he moves in the cell. A comparison of tracking-beam and switched beam can be found in [22].

3.5 Beamforming

Optimal array processing, or optimal beamforming, is the most complex technique, yet it yields the best results in terms of the performance of individual users. The signal processing unit continually adjusts the radiation pattern of the antenna array to maximise some performance measure (eg. the SINR of the desired user). This involves pointing the main lobe(s) of the antenna array at the angle of arrival (AOA) of the desired user's signal, or multipaths, and placing the nulls at AOA's of the interference. This is an optimisation problem for which many solutions have been devised. A thorough treatment of this field can be found in [39].

Beamforming relies on the fact that there is a phase shift of the received signal between the different antenna elements, and this phase shift is a function of the AOA of the desired signal, as shown in (3.3). Adjusting the phase shift (or complex weights) on each antenna element, (as in figure (3-1), modifies the radiation or beam pattern of the antenna array. A digital signal processor can add the output of the antenna elements in the complex domain, which is the equivalent to using a bank of phase shifters and amplifiers.

3.5.1 Beamforming array geometries

Any arrangement of the array elements in space can be used, but the most common geometries are the uniform linear array (ULA), uniform circular array (UCA) and two-dimensional planar arrays. Three-dimensional arrays are also possible.

The most common of these is the ULA, which consists of equally spaced antenna elements along a line, usually separated by one half wavelength. This is the most convenient spacing because as the antenna element spacing becomes smaller, so the radiation pattern approaches that of a single antenna element, thus making any spacing that is less than a half wavelength very inefficient. In addition, below a particular threshold, the beam pattern has no exact nulls [39]. When the spacing increases an interferometer pattern appears, grating lobes are produced, and the overall physical dimensions are increased. A spacing of one wavelength produces undesirable side lobes at $\pm 90^{\circ}$ with the same gain as the main lobe, hence a spacing of $\lambda/2$ provides a trade off and is commonly used.

The UCA has equally spaced elements along a circle in the azimuth plane. UCA are useful when angular symmetry is desired in a two-dimensional operation [39]. Planar arrays generally have more degrees of freedom, lower side lobe levels and generate more symmetric patterns [24]. Arrays with a non-uniform spacing are know as "thinned arrays".

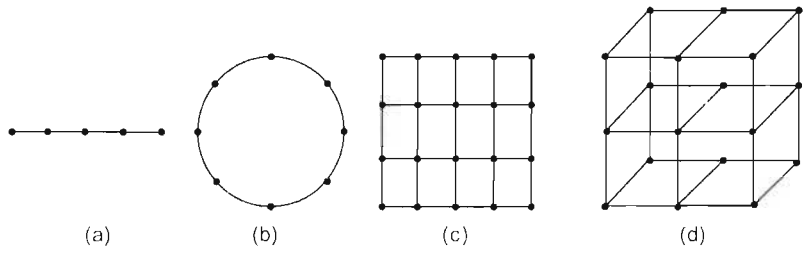

Figure 3-4 Antenna array geometries: (a) uniform linear array (ULA), (b) uniform circular array (UCA), (c) planar grid array, (d) three dimensional grid array.

3.5.1.1 Array Response

A ULA is considered to illustrate the functionality of a phased array. The geometry associated with the problem is illustrated in figure (3-5).

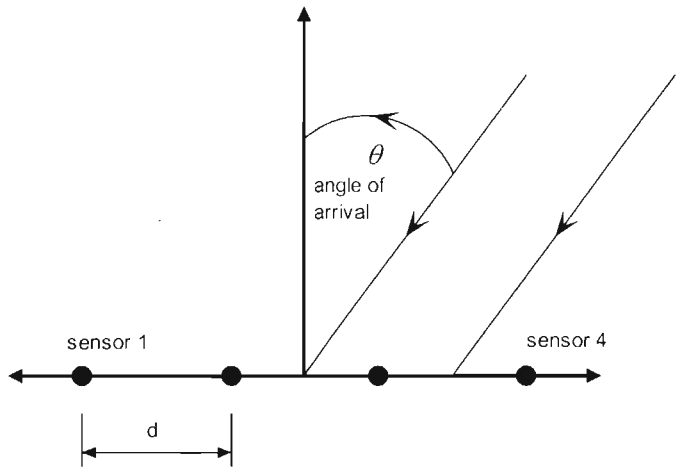

Figure 3-5 Array geometry showing an incident wave with AOA θ and inter-element spacing d.

The phase shift between two antenna elements is a function of the AOA and the distance between the sensors d, and it is

$$\psi = \frac{2\pi}{\lambda} d \sin(\theta) \tag{3.3}$$

where λ is the centre frequency of the transmitted signal. The output of an antenna array (without using phase shifts) is simply the sum of all the complex signal contributions arriving at the individual antenna elements. For an N-element ULA, the resultant phasor arising from the summation of all the individual antenna element contributions, where there is an AOA of θ, is given by

$$A(\theta) = \sum_{i=1}^{N} e^{j(i-1)\psi} \tag{3.4}$$

The normalised radiation beam/ directional pattern is then [39]

$$G(\theta) = 10\log_{10}\left\{\frac{|A(\theta)|^2}{N^2}\right\} \tag{3.5}$$

Figure (3-6) is a composite plot of the resulting beam patterns that arise with different numbers of antenna elements, and was computed using equation (3.5). When a phase shift $(n-1)\delta$ is introduced at the nth-antenna element, it is possible to shift the main lobe by

$$\theta = \arcsin\left(\frac{1}{2}\left(\frac{\lambda}{d}\right)\delta\right) \tag{3.6}$$

degrees. This is useful for direction-of-arrival (DOA) based beamforming, where one wishes to point the main lobe of the antenna array in the direction of the desired user for enhanced signal reception.

3.5.1.2 Beam patterns

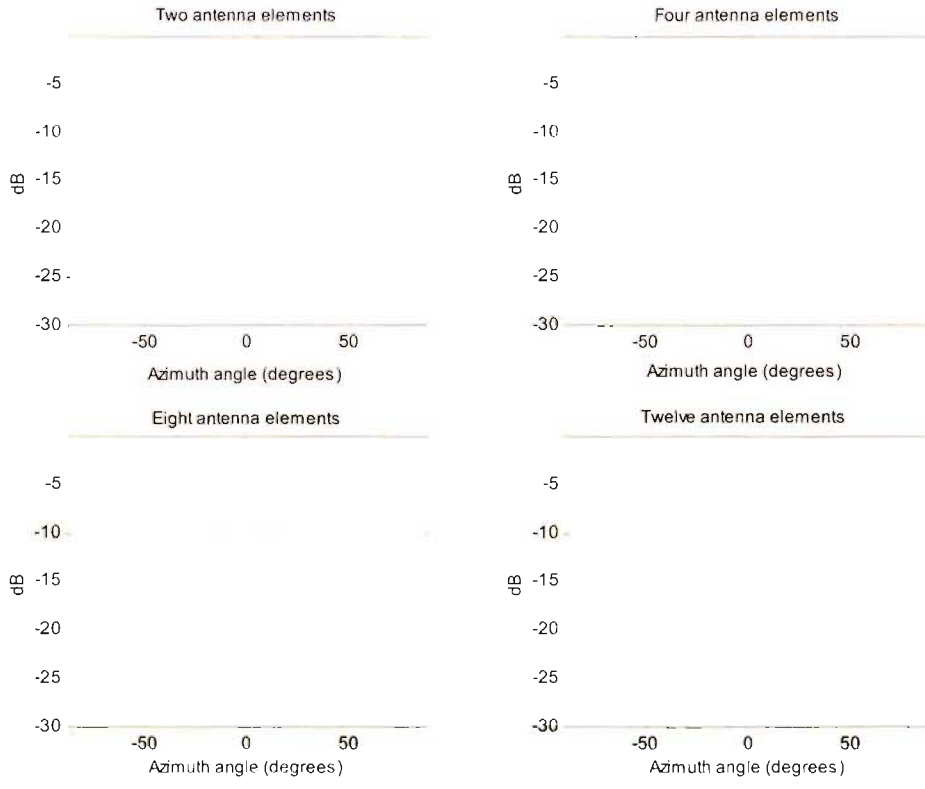

Figure 3-6 Beam patterns generated by ULA's over a 180° arc broadside to the array.

3.5.2 Array Performance Criteria

It is possible to increase both the sensitivity and resolution of an antenna array far beyond that of a single sensor system. There is a trade off in antenna array processing and design, because as one introduces a null to suppress interference, one may reduce the array's sensitivity in the desired direction. To compensate for this, one increases the number of antenna elements, but this adds size, complexity, extra signal processing burden and hence cost. In summation, as one increases the number of antenna elements one achieves a higher resolution capability (narrower beamwidth), lower side lobe levels, and more degrees of freedom, as per figure (3-6). With a ULA, the null beamwidth is inversely proportional to both the element spacing and the sine of the angle of interference signal location.

Non-uniform arrays (or "thinned-arrays"), where the antenna element spacing is random, are used to prevent the grating effect that exists when wide antenna element spacing is employed. The theory for such arrays was developed in [37], and using these designs, it is possible to have high-resolution antenna arrays with moderate side lobe levels, and a very wide bandwidth, whilst using fewer antenna elements than conventional arrays [39].

Other factors that can limit performance include the signal propagation delay across the array aperture and the mutual coupling effect between antenna elements.

3.5.3 Optimal Processing and the Wiener Solution

Most adaptive algorithms attempt to converge on the optimal solution, or weight vector, whether their criterion is the minimum mean square error (MMSE), maximum SNR, or maximum likelihood. It can be shown [39] that these criteria are merely scaled or factored versions of the optimal Wiener solution. The Wiener solution as such is a useful analytical tool and is given by

$$\mathbf{w}_{opt} = \mathbf{R}_{xx}^{-1}\mathbf{r}_{xd} \tag{3.7}$$

where $\mathbf{w}_{opt}$ is the optimal weight vector, $\mathbf{R}_{xx}$ is the autocorrelation matrix of the received signal and $\mathbf{r}_{xd}$ is the cross correlation vector between the received signal vector and the reference signal. The resulting minimum MSE[4] is given by

$$\overline{\varepsilon_{\min}^2} = \overline{d^2(t)} - \mathbf{r}_{xd}^T \mathbf{R}_{xx}^{-1}\mathbf{r}_{xd} \tag{3.8}$$

[4] $\overline{d^2(t)}$ denotes $E\{d^2(t)\}$

where $d(t)$ is the reference signal, and so $\overline{d^2(t)}$ equates to the total signal power.

3.5.4 Beamforming Algorithms

Beamforming techniques commonly make use of adaptive algorithms, because the alternative one-shot techniques are not numerically tractable, and require excessive amounts of processing power. The compromise in adaptive algorithm performance therefore also applies to AAA performance, and that is one of speed versus accuracy of adaptation. There is a trade off between the rate of convergence, and how closely or accurately the adaptive algorithm tracks the time changing environment. There is also a trade off between the complexity of the algorithm and its performance. The robustness of the algorithm also needs to be taken into account, that is, the performance of the algorithm with ill conditioned input data.

The main beamforming algorithms are categorised in table 2. They are divided into either one-shot [24], or adaptive algorithms. These two groups are then further subdivided into either blind or non-blind techniques. One-shot encompasses all those techniques that directly solve the solution to the beamforming weights, through a straight (one-shot) computation. These generally require a direct matrix inversion and as such are not widely employed due to the resulting computational complexity, as already mentioned. It also puts the constraint on to the system that the matrix (usually the sample covariance matrix) needs to be invertible. Numerical problems arise when the input data is ill conditioned and the matrix is no longer invertible (or has a high condition number [38]).

Algorithms that do not make use of either a pilot channel or a training sequence are known as blind algorithms. They mostly fall into the category of the property-restoral algorithms. These make use of the finite alphabet property of digital signals. The constant modulus algorithm (CMA) is an example of this type of algorithm, CMA and its derivatives are listed in table 2. Non-blind algorithms are numerous and are also listed in the table. For a review of integrated algorithms for CDMA signalling, refer to [24].

One-shot	Adaptive Algorithms						
Non-blind	Blind	Non-blind					
Direct Matrix Inversion	Property Restoral	Gradient Based	Recursive methods	Random search algorithms	Direction of arrival based	2-D Rake	Other
MMSE † (Wiener solution*), Maximise: SNR, received power, SINR‡. Maximum likelihood criterion, Minimum noise variance	Constant Modulus (CMA) †‡ :Least squares †, Linearly constrained †, Marquardt method †, Multistage CMA beamformer †, Orthoganilised †, Recursive †, Iterative least squares †	LMS*, differential* steepest decent*, accelerated* gradient approach*, gradient algorithm with constraints*	weighted Least-Squares error processor*, updated covariance matrix inverse*, Kalman filter methods*, minimum variance processor*	Linear Random Search*, Accelerated Random search*, Guided Accelerated Random search*	MUSIC †, ESPRIT †, Maximisation of SINR beamformer‡, Maximum likelihood beamformer ‡, MMSE beamformer ‡	Space-time matched filter †‡	Decision directed †, Code filtering †, Cascade Preprocessors*, Howells-Applebaum adaptive processor*

Table 2 Adaptive beamforming algorithms.

For more detail see:	
*	[39]
†	[24]
‡	[28]

3.6 Combined Space-time Processing

Space-time processors make it possible to exploit signal diversity or structure, in both the time and space domains. There has been much research into adaptive algorithms for space-time processing with applications in radar, sonar, and communications, because space-time adaptive processing (STAP) holds great potential for improving adaptive array performance [40]. Adaptive techniques are also more feasible for implementation purposes. A comprehensive overview of space-time processing for CDMA communications systems can be found in [24], and recent advances in STAP can be found in [40, 8].

The value of diversity has already been discussed in terms of diversity reception with multiple antenna elements; another potential source of diversity is through multipath propagation. When multipaths are separated in time by less than a chip interval, then they are not time resolvable, however if they arrive at the antenna array at different angles, they may be resolvable in space. A Two dimensional RAKE receiver (space-time processor) is capable of optimally combining these multipaths in both the space and time domains. Optimal space-time matched filters and receiver structures have been developed for CDMA applications, as in [28], [42].

A beamformer-RAKE structure is presented in [28], which consists of a spatial beamformer concatenated with a conventional temporal RAKE combiner. It can be considered as a type of space-time processor since it combines the space dimension (antenna array) with the time dimension (RAKE fingers). It, however, yields lower performance results compared to the joint space-time solution.

The space-time matched filter receiver for vector multipath signals over AWGN is also derived in [28].

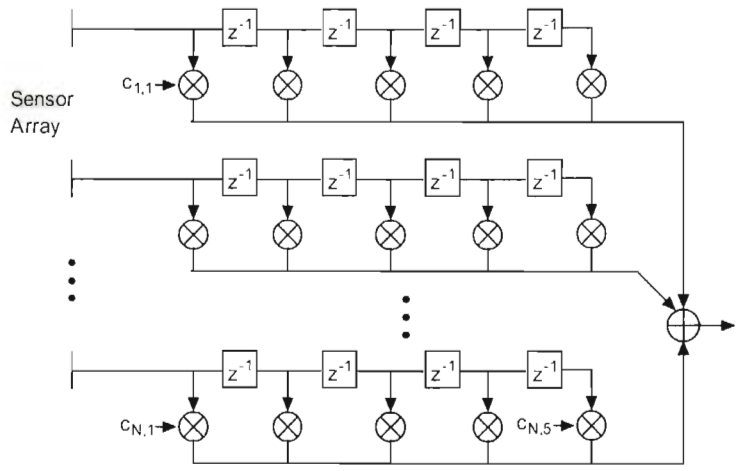

Figure 3-7 Space-time processor architecture with an *N*-element antenna array and five different time bins.

3.7 Summary

Smart antennas are powerful tools for optimising and enhancing the performance of CDMA based cellular networks. Smart antennas can be can be split into two categories, depending on whether or not they use a diversity or a beamforming model. Diversity techniques were discussed and their ability to combat multipath fading was illustrated. This important capability of multiple antenna systems is exploited in chapters 5 and 6 by the ST-MUD architecture. Through the use of switched beam or sectorised antenna arrays, it is possible to increase the SINR of individual users and have tighter frequency reuse patterns, which yields higher spectral efficiencies. The concept of the radiation pattern of an antenna array was illustrated, and it was shown how this pattern could be manipulated electronically through the use of a digital signal processor. It was also shown how the radiation pattern could be optimised for a variety of criteria. The radiation pattern was computed for a ULA to demonstrate the effect the number of antenna elements has on the system. Adaptive algorithms for smart antenna applications were also reviewed, as well as the limiting criteria of array performance.

Chapter 4 Multiuser Detection

4.1 Introduction

Multiuser detection (MUD), also known as Co-channel Interference Suppression, is a useful technique that can be used to greatly improve the performance of a CDMA communications system. MUD is a demodulation technique used when there are mutually interfering streams of digital information. In DS-CDMA all users occupy the same bandwidth at the same time, which lends itself to be greatly exploitable by MUD. When the different users' codes are not completely orthogonal, a conventional single-user-receiver's output contains some of the signal energy (or information) belonging to the other users. As the number of users increases, the amount of energy in the desired user's signal, which constitutes interference, also increases. The other users' signals act like noise to the desired signal and this corrupting influence is referred to as multiaccess interference (MAI). With MUD, it is possible to filter out, subtract or find the most likely combination of transmitted bits knowing the output of all these single-user-receivers (single user matched filters). The capacity (in terms of users or data rates) is thereby enhanced since the MAI, the previous limiting factor, is now either reduced or completely eliminated.

There has been extensive research in MUD since 1986, when Verdú first formulated the optimal MUD for the additive white Gaussian noise (AWGN) channel [43]. Other advances include the formulation of blind adaptive MUD [44]. Adaptive MUD is more viable for implementation purposes, compared to optimal MUD, but has the draw back of requiring a training sequence or pilot channel. Blind adaptation does not require any training sequence, but rather makes use of the digital signal structure and waveform induced by the spreading operation. The performance of blind MUD with multipath was developed in [45]. Other recent works in blind MUD and limited-complexity techniques, along with applications of MUD, are contained in [46].

A common criterion of adaptive schemes is the minimum mean square error (MMSE), therefore, the performance of MMSE MUD has been thoroughly scrutinised [47], [48]. The performance of MMSE MUD was also extended to frequency selective fading channels in [49].

Another important step in the MUD literature was the development of subspace techniques for MUD [50]. MUD for MC-DS-CDMA was also developed [51], [52], followed by subspace techniques for MUD of MC-DS-CDMA [80]. Various other performance analyses of MUD, using different techniques and under varying conditions, have been completed in [54], [55], [56], [57] and [58].

In this chapter, a synchronous and an asynchronous DS-CDMA model is presented. Some of the important performance measures of MUD's are discussed and then the form of the optimal MUD is explained. The performance of the optimal MUD is quantified in order to provide a benchmark for the performance of other MUD techniques. Two types of Linear MUD are reviewed, namely the decorrelating detector and the MMSE MUD. The decorrelating detector is investigated because some of its performance characteristics match that of the MMSE MUD. Interference cancelling techniques are also covered. An insight into the performance enhancing effects of MUD and the structure and performance of MMSE MUD specifically, enables one to motivate its use in the receiver design presented in this dissertation.

4.2 DS-CDMA Model

An asynchronous DS-CDMA transmitter model for the uplink of a mobile radio network is considered. The baseband representation of the kth user's transmitted signal is given by

$$x_k(t) = A_k \sum_{i=-\infty}^{\infty} b_k(i) s_k(t - iT - \tau'_k), \quad k = 1, \ \ldots, \ K \tag{4.1}$$

where A_k and s_k denote the amplitude and normalised spreading waveform of the kth user respectively, T is the data symbol duration, τ'_k is the start time of user k. The kth user's ith transmitted symbol $b_k(i)$ takes on the values $\{+1, -1\}$ with equal probability. The synchronous model is identical, except $\tau'_k = 0$ for all values of k. The spreading waveform takes the form

$$s_k(t) = \sum_{n=0}^{N-1} c_k(j) \psi(t - nT_c), \quad 0 \le t \le T_c \tag{4.2}$$

where N is the processing gain and c_k is the kth user's spreading code, $\psi(t)$ is the chip pulse shape; for a single carrier (SC) DS-CDMA system the chip duration is defined as T_c. It is shown that $s_k(t)$ only takes on values in the interval $[0, T_c]$, and has unit energy

$$\int_0^{T_c} s_k^2(t) dt = 1 \tag{4.3}$$

The cross correlation between user i and j is defined as

$$\rho_{ij} = \int_0^T s_i(t)s_j(t)dt \tag{4.4}$$

The cross correlation matrix is defined as the matrix $\mathbf{R}$ whose $\{i,j\}$ element is defined as

$$[\mathbf{R}]_{i,j} = \rho_{ij} \tag{4.5}$$

The output of a bank of matched filters, each with the respective knowledge of the correct timing, phase and spreading sequence of all the users is a sufficient statistic to perform optimal MUD [43], [10] and as such it is convenient to write the vector $\mathbf{r}$ of these values in the form

$$\mathbf{r} = \mathbf{RAb} + \mathbf{n} \tag{4.6}$$

where

$$\mathbf{A} = \begin{bmatrix} A_1 & \dots & A_K \end{bmatrix}^T \tag{4.7}$$

$$\mathbf{b} = \begin{bmatrix} b_1 & \dots & b_K \end{bmatrix}^T \tag{4.8}$$

$$\mathbf{n} = \begin{bmatrix} n_1 & \dots & n_K \end{bmatrix}^T \tag{4.9}$$

The noise vector $\mathbf{n}$ is made up of independent and identically distributed (i.i.d.) zero mean Gaussian random variables, with covariance matrix $\sigma^2\mathbf{I}$ where σ^2 is the noise variance with power spectral density equal to $\frac{1}{2}N_0$.

4.3 Performance Measures

Bit error rate (BER) is typically used to quantify the performance of receivers, but is not the most suitable quantity for comparing the relative efficiency or effectiveness of MUD algorithms. The output signal-to-interference-plus-noise-ratio (SINR) is more useful because it gives a measure of how much the interference has been reduced, and is defined as

$$SINR \triangleq \frac{A_k^2}{\sigma^2 + \sum_{j \neq k} A_j^2 \rho_{jk}^2} \tag{4.10}$$

where A_k is the transmit amplitude of desired user k, σ^2 is the variance of the noise term and ρ_{jk} is the crosscorrelation coefficient between user j and k. This formula can be used to compute BER's, and is also useful in the assessment of error control codes [10].

Another method of presenting the information contained in the BER is to calculate a quantity known as the effective energy of user k. The effective energy of user k, $e_k(\sigma)$, is the amount of

energy required to achieve the same bit error rate if there were no interfering users, ie. it is the portion of energy that is used to overcome the effects of the AWGN.

The multiuser efficiency ratio is then defined as the ratio of the effective energy to the actual energy.

$$\kappa_k = \frac{e_k(\sigma)}{A_k^2} \tag{4.11}$$

When the MUD performs very well, the effective energy is very close to the actual transmitted energy, and therefore the multiuser efficiency ratio approaches one. When the MUD performs badly, it indicates that the transmitter has to transmit at a very high level to achieve the required BER. Under these conditions the actual energy, A_k^2, is very high and the effective energy, $e_k(\sigma)$, is very low, and the multiuser efficiency ratio tends to zero. On a log scale (dB's) this range translates to $[-\infty, 0]$. The multiuser efficiency ratio quantifies the performance loss due to the presence of other users, and hence the reciprocal (in dB's) of the multiuser efficiency ratio, is a positive value and is often referred to as the degradation factor.

The asymptotic multiuser efficiency is defined as

$$\eta_k = \lim_{\sigma \to 0} \frac{e_k(\sigma)}{A_k^2} \tag{4.12}$$

and measures the slope with which the BER function approaches zero, on a logarithmic scale, as the SNR goes to infinity. The asymptotic multiuser efficiency is a very important analytical tool to quantify the performance of a MUD scheme, namely:

- if the asymptotic multiuser efficiency = 0, the BER does not go to zero as SNR goes to infinity
- if the asymptotic multiuser efficiency is positive, the BER decreases exponentially with the SNR.

Near-far resistance is defined in [10] as the asymptotic multiuser efficiency minimised over the received energies of all the other users, and is

$$\overline{\eta}_k = \inf_{\substack{A_j > 0 \\ j \neq k}} \eta_k \tag{4.13}$$

The near-far resistance is useful for calculating how effectively a receiver can overcome the near-far problem. A conventional matched filter receiver's near-far resistance is zero when non-

orthogonal codes are used [10], and subsequently cannot combat the near-far problem under such conditions.

Spectral efficiency is another measure used to quantify the relative performance of MUD algorithms. Spectral efficiency is defined as the data rate per unit bandwidth $\left(bits.s^{-1}.Hz^{-1}\right)$. In DS-CDMA systems the spreading rate (or processing gain) is directly proportional to the bandwidth, consequently, another interpretation of spectral efficiency would be the number of bits per chip that can be reliably transmitted $\left(bits.chip^{-1}\right)$. The increase in spectral efficiency of the channel can thus be used to rate the relative performance of MUD techniques.

4.4 Types of Multiuser Detection

Optimal MUD grows exponentially in complexity with the number of users in the system. This is the driving force to develop suboptimum techniques. Various one-shot and iterative approaches have been developed, and with the use of short spreading codes, it is possible to implement some of these schemes adaptively. MUD techniques can be divided into three broad categories: optimum, linear and interference cancellation techniques. Two of the most widely used linear techniques are the MMSE and the decorrelating detector. The Interference cancelling group can further be divided into linear and non-linear interference techniques.

4.4.1 Optimum Multiuser Detection

An optimal MUD architecture consists of a bank of matched filters, where there is one per user, and each matched filter is decoding *1* of the total *K* users in the system. A linear programming algorithm, like the Viterbi algorithm, is then employed to estimate the most likely set of bits transmitted by the users. This set of bits is the output of the receiver, as in Figure (4-1), and for convenience, is written as a vector. The optimal MUD algorithm's task is therefore to select the vector $\mathbf{b}_{\max} = \left[\hat{b}_1 \ldots \hat{b}_K\right]^T$ that maximises the probability of receiving the signal **r** given the actual vector of transmitted bits **b**

$$\mathbf{b}_{\max} = \arg \max_{\mathbf{b}\in\{-1,1\}^K} P\left(\mathbf{r} \mid \mathbf{b}\right) \tag{4.14}$$

To reiterate, the optimum receiver must find the vector of transmitted bits which minimises the log-likelihood function

$$\Omega(\mathbf{b}) = \int_0^T \left[r(t) - \sum_{j=1}^{K} A_j b_j s_j(t) \right]^2 dt \tag{4.15}$$

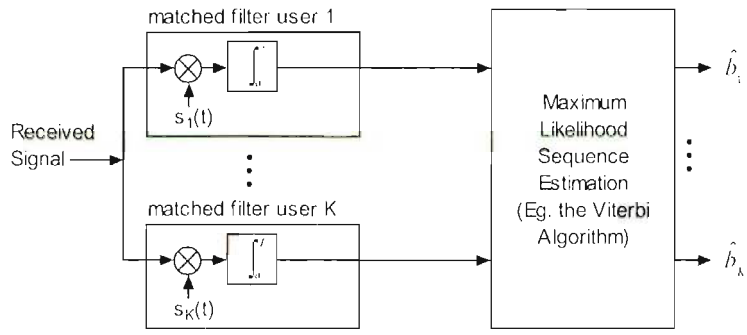

Figure 4-1 Optimal MUD Architecture.

For a K user system, where the transmitted bits take on the values $\{-1,1\}$ with equal probability, it is easy to see there are 2^K different combinations of $\mathbf{b}$, and only an exhaustive search through all combinations will ensure a global minimum. This type of problem is known as a combinatorial optimisation problem, and as such grows exponentially in the number of users. A derivation of the recursive metric to perform maximum likelihood sequence detection (eg. using the Viterbi Algorithm) can be found in [24].

It is interesting to analyse the optimum solution since it yields the optimum bit error rate (BER), optimum asymptotic multiuser efficiency and the optimum near-far resistance values which serve as a comparison for the suboptimum detectors. The lower bound on the BER of the optimum MUD is given by [10]

$$P_k(\sigma) \geq 2^{1-w_{k,\min}} Q\left(\frac{d_{k,\min}}{\sigma}\right) \tag{4.16}$$

where $w_{k,\min}$ is the smallest weight of all the error vectors $\left(\boldsymbol{\varepsilon} = \mathbf{b} - \hat{\mathbf{b}}\right)$, $Q(.)$ is the Q-function, and $d_{k,\min}$ is one half of the minimum distance between two multiuser signals that differ in the kth bit. The optimal MUD upper bound is given in [10].

The optimum asymptotic multiuser efficiency is given by

$$\eta_k = \min_{\substack{\boldsymbol{\varepsilon}\in\{-1,0,1\}^K \\ \varepsilon_k = 1}} \frac{1}{A_k^2} \boldsymbol{\varepsilon}^T \mathbf{ARA}\boldsymbol{\varepsilon} \tag{4.17}$$

where $\boldsymbol{\varepsilon}$ is error vector of length K which is the normalised difference between any pair of distinct transmitted vectors, and hence the elements of $\boldsymbol{\varepsilon}$ may take on the values $\{-1,0,1\}$. In the same fashion as finding the optimum solution to (4.14), there is no polynomial-in-K solution to

the optimum asymptotic multiuser efficiency, because it is a combinatorial optimisation problem.

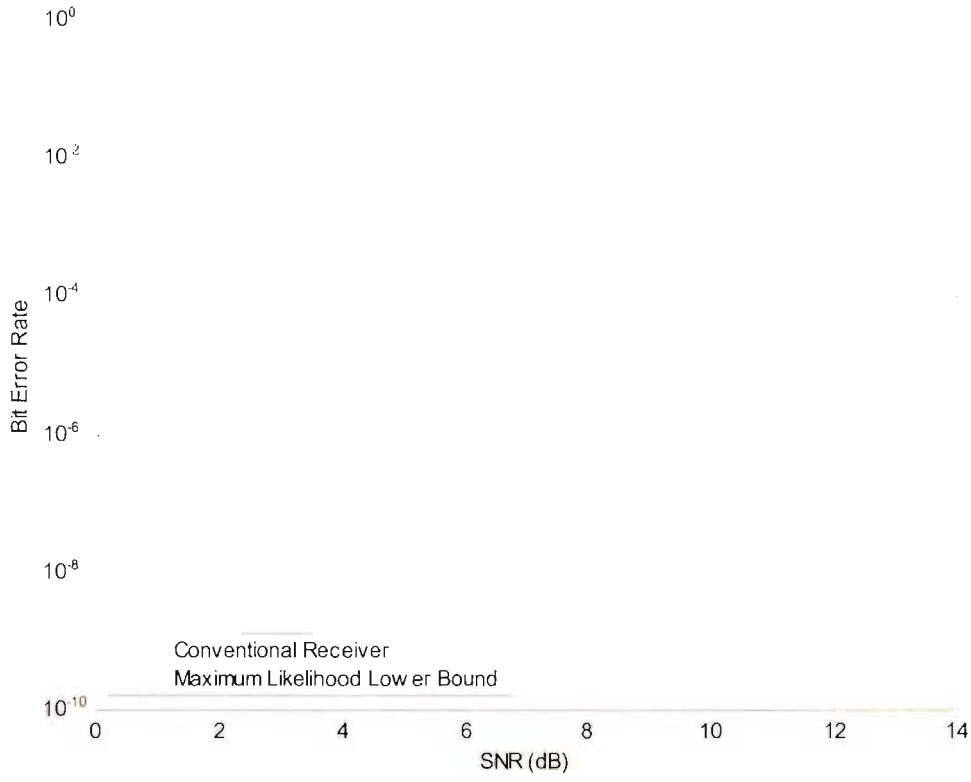

Figure 4-2 Performance comparison of conventional receiver and the lower bound (4.16) of the maximum likelihood MUD in a 15 user (synchronous) channel with a crosscorrelation ρ , between users of 0.09, as in [10].

The average optimum near-far resistance with random spreading sequences, provides a simple lower bound on performance in a synchronous DS-CDMA system, as a function of the number of users and spreading factor. It is given by

$$E[\bar{\eta}_k] = \left[1 - \frac{K-1}{N}\right]^{+} \tag{4.18}$$

and in a symbol-asynchronous, chip-synchronous system, the average optimum near-far resistance satisfies

$$E[\bar{\eta}_k] \geq \left[1 - \frac{2K-2}{N}\right]^{+} \tag{4.19}$$

Equations (4.18) and (4.19) provide intuitive results based on only the number of users, K, and the processing gain, N.

4.4.2 Linear Multiuser Detection

Linear MUD techniques apply a linear transformation on the received vector of samples (the output of the chip matched filters). They fall under the category of the one-shot detectors, although some linear techniques, like the MMSE can be implemented adaptively. Linear MUD's have the general structure as seen in figure (4-3).

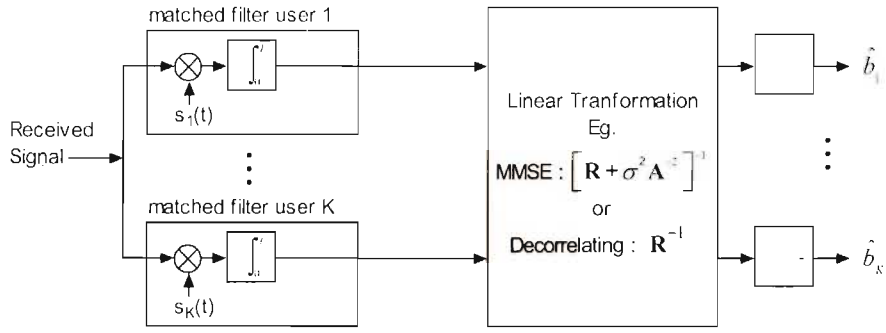

Figure 4-3 Linear MUD receiver structure.

Linear MUD schemes also have the advantage that they can be implemented in a decentralised manner, that means that only the desired user needs be detected, and not all the users in the system. A transversal/FIR filter [62] can then be used to implement the single user detector, as illustrated in figure (4-4).

4.4.2.1 Optimum Linear Multiuser Detection

The optimum linear MUD, in the sense of maximising the asymptotic multiuser efficiency or minimising the BER, is prohibitively complex to compute for the K-user case [10], as it requires the solution to a non-linear optimisation problem that does not have a closed-form solution. The maximum asymptotic multiuser efficiency that a linear transformation can achieve in a 2-user scenario was plotted in figure (4-5) using

$$\eta_k = \begin{cases} 1+\frac{A_1}{A_2}-2|\rho|\frac{A_1}{A_2}, & \text{if } \frac{A_1}{A_2} < |\rho| \\ 1-\rho^2, & \text{otherwise.} \end{cases} \tag{4.20}$$

4.4.2.2 Decorrelating Detector

The decorrelating detector uses the inverse of the crosscorrelation matrix, $\mathbf{R}^{-1}$, as the linear transformation. If (4.6) is rewritten without the noise term,

$$\mathbf{r} = \mathbf{RAb} \tag{4.21}$$

then it is easy to show that the decorrelating detector correctly decodes the desired users' bits in the absence of noise,

$$\begin{aligned}\hat{\mathbf{b}} &= \operatorname{sgn}\left(\mathbf{R}^{-1}\mathbf{r}\right) \\ &= \operatorname{sgn}\left(\mathbf{R}^{-1}\mathbf{RAb}\right) \\ &= \operatorname{sgn}\left(\mathbf{Ab}\right) \\ &= \mathbf{b}\end{aligned} \tag{4.22}$$

The requirement of the system, though, is that the signature waveforms of the users be independent, which in turn ensures that $\mathbf{R}$ is invertible.

When background noise is taken into consideration, it is possible that the decorrelating detector actually performs worse than the matched filter in low SNR conditions since the AWGN can be amplified by the $\mathbf{R}^{-1}$ term,

$$\begin{aligned}\mathbf{R}^{-1}\mathbf{r} &= \mathbf{Ab} + \mathbf{R}^{-1}\mathbf{n} \\ &= \mathbf{Ab} + \hat{\mathbf{n}}\end{aligned} \tag{4.23}$$

where the variance of the new noise term is

$$E\left\{\hat{\mathbf{n}}\hat{\mathbf{n}}^{T}\right\} = \sigma^{2}\mathbf{R}^{-1} \tag{4.24}$$

When the received amplitudes of all the users in the system are unknown, the decorrelating detector is a good choice to make, because under this condition the decorrelating detector is optimal in terms of near-far resistance and maximum likelihood [10]. The near-far resistance is given by

$$\overline{\eta}_{k} = \frac{1}{\left(1-\mathbf{a}_{k}^{T}\mathbf{R}_{k}^{-1}\mathbf{a}_{k}\right)} \tag{4.25}$$

where $\mathbf{a}_{k}$ is the kth column of $\mathbf{R}$ without the diagonal element, and $\mathbf{R}_{k}$ is the $(K-1)\times(K-1)$ matrix that results from striking out the kth row and kth column of $\mathbf{R}$. It is important to note that the decorrelating detector completely decorrelates $\mathbf{r}$. This means that its performance is completely independent of the power ratios of the users in the system, ie. equation (4.25) is not a function of A_2/A_1 and the decision statistic at the output of the receiver is independent of the interfering amplitudes. The decorrelating detector achieves maximum near-far resistance with very little complexity increase over a conventional matched filter receiver.

4.4.2.3 MMSE Multiuser Detection

The MMSE solution takes into account the SNR of the different users in the system, and produces a solution that is superior to the decorrelating detector's. The output of the linear MUD is

$$\hat{\mathbf{b}} = \mathbf{M}^T \mathbf{r} \tag{4.26}$$

The problem is to find the linear transformation $\mathbf{M}$ that minimises the mean square error

$$MSE_{\min} = \min_{\mathbf{M} \in \mathbb{R}^{K \times K}} E\left\{ \left\| \mathbf{b} - \mathbf{M}^T \mathbf{r} \right\|^2 \right\} \tag{4.27}$$

This solution is given by [10]

$$\mathbf{M}_{MSE} = \left[\mathbf{R} + \sigma^2 \mathbf{A}^{-2} \right]^{-1} \tag{4.28}$$

where

$$\sigma^2 \mathbf{A}^{-1} = diag\left\{ \frac{\sigma^2}{A_1^2}, \ \ldots, \ \frac{\sigma^2}{A_K^2} \right\} \tag{4.29}$$

The MMSE solution has the important property that it can be implemented in a decentralised manner. To receive just user k one uses the kth column of $\mathbf{M}$, which is given by [9] as

$$\mathbf{m}_k = \tilde{\mathbf{R}}^{-1} \boldsymbol{\alpha}_k \tag{4.30}$$

where $\tilde{\mathbf{R}}$ is the input covariance matrix,

$$\tilde{\mathbf{R}} = E\left\{ \mathbf{r}\mathbf{r}^T \right\} \tag{4.31}$$

and $\boldsymbol{\alpha}_k$ is the crosscorrelation of the desired user's transmitted bit with the received vector of samples

$$\boldsymbol{\alpha}_k = E\left\{ b_k \mathbf{r} \right\} \tag{4.32}$$

This formulation of the solution is commonly referred to as the Wiener solution.

Another important advantage of the MMSE technique is the ease with which it can be implemented adaptively [9]. When implemented adaptively, the MMSE MUD suppresses all interference regardless of whether it originated in cell (intra-cell interference) or out of cell (inter-cell interference). Adaptive implementation requires the use of training symbols and/or pilot channel to correctly adapt the filter coefficients.

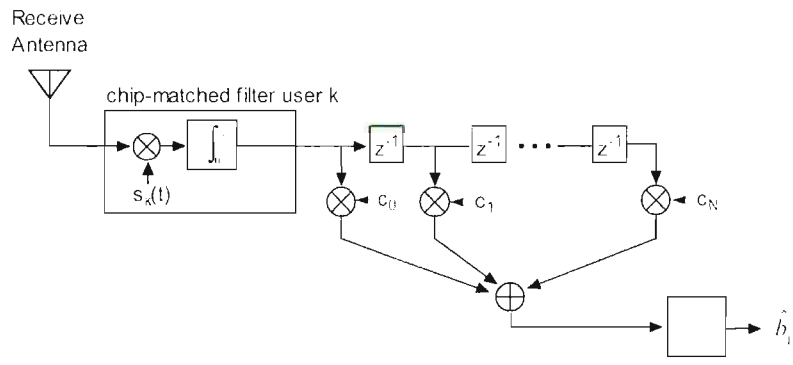

Figure 4-4 Decentralised implementation of a MMSE MUD, using a FIR filter.

MMSE Performance Analysis

In low SNR conditions the MMSE solution converges towards the matched filter receiver, and consequently outperforms the decorrelating detector in this region. This is attributed to the noise amplification the decorrelating detector tends to perform, as it was shown in (4.23). In high SNR conditions the MMSE solution converges towards the decorrelating solution, thus it is near-far resistant in this region. The near-far resistance and the asymptotic multiuser efficiency of the MMSE solution is, therefore, the same as that of the decorrelating detector (4.25).

The MMSE solution yields the maximum SINR of any linear transformation. The SINR can be expressed as

$$SINR_k = A_k^2 \mathbf{s}_k^T \boldsymbol{\Sigma}^{-1} \mathbf{s}_k \tag{4.33}$$

where $\boldsymbol{\Sigma}$ is the interference covariance matrix, defined as

$$\boldsymbol{\Sigma} \triangleq \sigma^2 \mathbf{I} + \sum_{k=2}^{K} A_k^2 \mathbf{s}_k \mathbf{s}_k^T \tag{4.34}$$

The output of the MMSE transformation can be written as [10]

$$\left(\mathbf{M}^T \mathbf{r}\right)_1 = B_1 \left(b_1 + \sum_{k=2}^{K} \beta_k b_k \right) + \sigma \tilde{n}_1 \tag{4.35}$$

where

$$\beta_k = \frac{B_k}{B_1} \tag{4.36}$$

$$B_k = A_k \left(\mathbf{M}^T \mathbf{R}\right)_{1k} \tag{4.37}$$

$$\tilde{n}_1 \sim N\left(0, \left(\mathbf{M}^T \mathbf{R} \mathbf{M}^T\right)\right) \tag{4.38}$$

The leakage coefficient β_k is the contribution of the kth user to the decision statistic of user 1. The probability of error can be expressed using

$$P_e = Q\left(\sqrt{SINR}\right) \tag{4.39}$$

From the previous formulations, it is possible to compute the probability of error as [10]

$$P_1^{(m)}(\sigma) = 2^{1-K} \sum_{b_2,\ldots,b_K \in \{-1,1\}^{K-1}} Q\left(\frac{A_1}{\sigma}\frac{\left(\mathbf{M}^T\mathbf{R}\right)_{11}}{\sqrt{\left(\mathbf{M}^T\mathbf{R}\mathbf{M}^T\right)_{11}}}\left(1+\sum_{k=2}^{K}\beta_k b_k\right)\right) \tag{4.40}$$

This equation becomes exponentially complex in the number of users to compute. A valid approximation [47] is to substitute the multiaccess interference term with a Gaussian random variable that has the same mean and variance. The mean of the substituted Gaussian random variable is

$$\mu = \frac{A_1}{\sigma}\frac{\left(\mathbf{M}^T\mathbf{R}\right)_{11}}{\sqrt{\left(\mathbf{M}^T\mathbf{R}\mathbf{M}^T\right)_{11}}} \tag{4.41}$$

with variance

$$\lambda^2 = \mu^2 \sum_{k=2}^{K} \beta_k^2 \tag{4.42}$$

and so the probability of error is given by

$$\begin{aligned} P_e &= E\left\{Q(\mu + \lambda X)\right\} \\ &= Q\left(\frac{\mu}{\sqrt{1+\lambda^2}}\right) \end{aligned} \tag{4.43}$$

where X is a unit normal random vector. The performance of the MMSE MUD degrades gracefully with the number of users. The MMSE receiver can effectively suppress N-1 interferers in a synchronous system and $\lfloor (N-1)/2 \rfloor$ interferers in an asynchronous system, when the digital filter spans one symbol interval [9]. The linear MMSE receiver is also nearly optimal for a wide range of loads $(K/N < 70\%)$ [9].

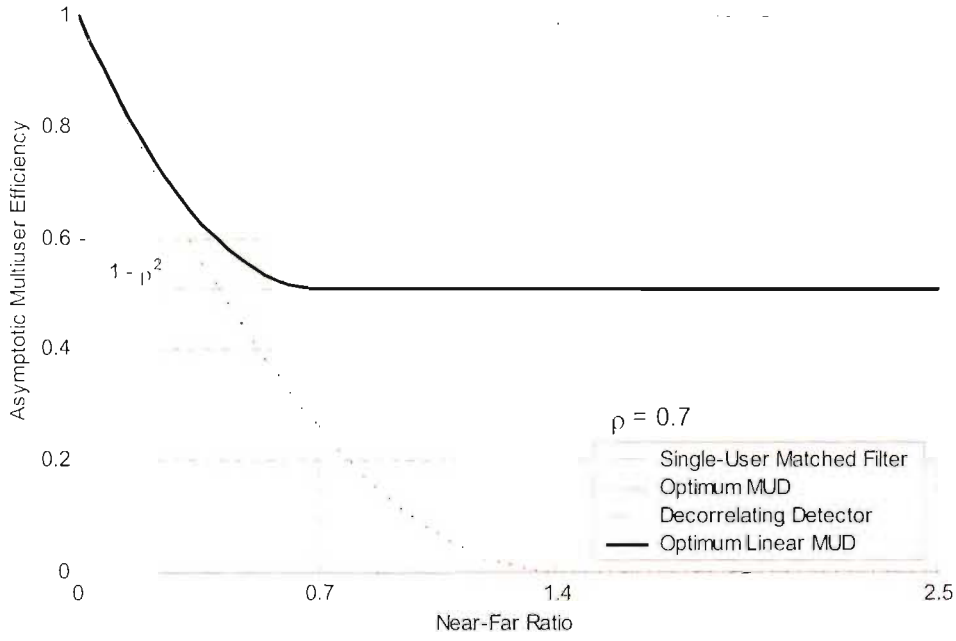

Figure 4-5 Comparison of asymptotic multiuser efficiency for a two user scenario, where the cross correlation (ρ) is equal to 0.7.

4.4.3 Interference Cancellation

Interference cancelling schemes provide an alternative to optimal, or maximal likelihood, detection and still offer the capability of removing the MAI. Iterative interference cancellers re-spread the interfering users' transmitted bits and subtract these from the desired user's spread signal. After each iteration, a better estimate of the users' bits enables better interference cancellation. These techniques generally require a reliable first estimate to be effective, otherwise errors propagate through each iteration and convergence is not assured.

The interference cancelling schemes are grouped into either parallel or successive categories. This field is treated thoroughly in [10], [24].

4.4.3.1 Linear Interference Cancellation

The linear interference cancellation techniques are comparable to iterative techniques for evaluating $\mathbf{R}^{-1}$, these being namely the Jacobi and Gauss-Seidel iterations [38]. No hard decisions of the transmitted bits are made after each iteration, but rather tentative soft decisions. The Jacobi iteration corresponds to parallel interference cancellation. It has the feature that it can be implemented on parallel processors. The Gauss-Seidel iteration corresponds to

successive interference cancellation, each iteration makes use of more of the available information and consequently converges quicker. It, however, could not be implemented on parallel processors.

4.4.3.2 Non-Linear Interference Cancellation

Non-linear interference cancellation techniques make hard decisions on the transmitted bit values which are used at each iteration. They are often, therefore, referred to as decision driven non-linear feedback techniques, and are particularly suited to high SNR scenarios where there are large power imbalances. The high SNR ensures a fairly reliable initial estimate of the transmitted bits, which stops errors propagating through the iterations.

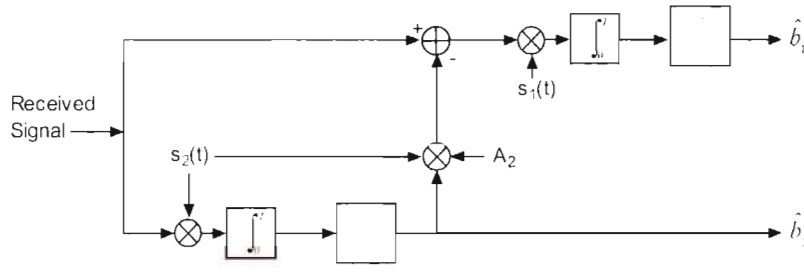

Figure 4-6 Two user, successive interference canceller (from [10]).

4.5 Summary

This chapter has provided an insight into the performance of MUD's and motivated their use through their capabilities in the reduction of MAI and their near-far resistance. A synchronous and an asynchronous DS-CDMA model were developed. MUD schemes were divided into either optimal or sub optimal categories. The sub optimal schemes were further subdivided into either linear techniques or interference cancelling techniques. Optimal MUD was shown to be too complex to implement, thus necessitating the need for sub-optimal linear and interference-cancelling techniques. The structure of optimal MUD and linear MUD schemes was illustrated.

The BER of optimal MUD was plotted along side that of the conventional receiver, which gave a graphical representation of the performance improvement possible with MUD. The asymptotic multiuser efficiency was shown to be a useful metric for the comparison of the performance of various MUD schemes. The asymptotic multiuser efficiency of four different MUD schemes was computed and plotted together for comparative purposes. Different types of MUD schemes were shown to have a varying capability to combat the near-far problem. This capability was quantified using the near-far resistance metric.

An abbreviated performance analysis was completed on the MMSE technique since it provides insight into the expected behaviour of the MMSE ST-MUD detector. It was shown how the MMSE MUD could be implemented in a decentralised manner, in the form of a digital FIR filter, and how it could be implemented adaptively. These properties motivate the investigation of the MMSE scheme for ST-MUD, as the FIR structure creates a viable implementation possibility for MMSE ST-MUD.

Chapter 5 Space-Time MUD

5.1 Introduction

Multiaccess interference and multipath channel distortion are two of the performance limiting factors of broadband CDMA systems. The techniques proposed to combat these inhibiting effects fall largely into two categories, namely: space-time processing [8] and MUD [10]. ST-MUD is the combination of these two techniques. Combined MUD and array processing was first discussed in [63] and extended in [64] to include decision feedback and successive interference cancellation techniques. The maximal likelihood ST-MUD structure has only recently been developed [65]. Optimal, linear, and blind adaptive ST-MUD structures for multipath CDMA channels were also devised in [65].

Recently, there has been much interest in multiuser space-time communication [67], and ST-MUD, [68], [69], [70]. A performance analysis of the MMSE space-time detection of synchronous DS-CDMA was also recently performed in [71].

Antenna arrays and MUD are combined in this chapter to perform MMSE Space-time MUD for MC-DS-CDMA. The MC-DS-CDMA transmitter model is presented, and a new ST-MUD receiver structure for MC-DS-CDMA and multipath reception is given. Using techniques developed in the Vector channel model chapter, the received vector of samples of the ST-MUD receiver is derived. A performance analysis is completed, where the MMSE is the combining criterion, and there is any given space-frequency correlation matrix. Analysis results are compared to those from a computer simulation, for verification of the analysis technique. The simulation results were computed using a custom software environment created by the author, using the *C++* programming language.

5.2 MC-DS-CDMA Model

An asynchronous MC-DS-CDMA transmitter model for the uplink of a mobile radio network is considered, similar to that presented in [72]. The MC-DS-CDMA transmitter model is an

extension of the DS-CDMA model presented in (4.1), where the baseband representation of the kth user's transmitted signal is given by

$$x_k(t) = A_k \sum_{i=-\infty}^{\infty} b_k(i) s_k(t - iT - \tau'_k) \sum_{m=1}^{M} \cos(\omega_m t + \theta_{k,m}), \quad k = 1, \ldots, K \tag{5.1}$$

where A_k and s_k denote the amplitude and normalised spreading waveform of the kth user respectively, T is the data symbol duration, and τ'_k is the start time of user k. The kth user's ith transmitted symbol $b_k(i)$ takes on the values $\{+1, -1\}$ with equal probability. The mth subcarrier frequency of user k has random carrier phase $\theta_{k,m}$, and there is a total of M subcarriers. The spreading waveform takes the form

$$s_k(t) = \sum_{j=0}^{N-1} c_k(j) \psi(t - nMT_c), \quad 0 \le t \le MT_c \tag{5.2}$$

where N is the processing gain and c_k is the kth user's spreading code, $\psi(t)$ is the chip pulse shape; for a single carrier (SC) DS-CDMA system the chip duration is defined as T_c, but here the MC-DS-CDMA chip duration is defined as MT_c. It is shown that $s_k(t)$ only takes on values in the interval $[0, MT_c]$.

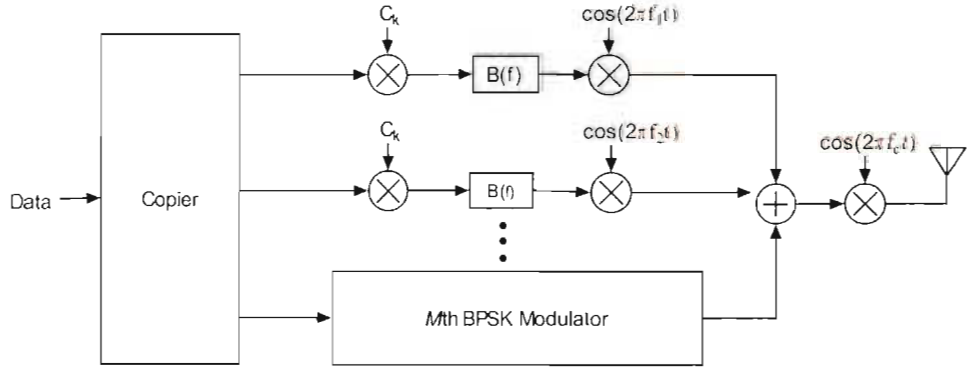

Figure 5-1 Transmitter model for a MC-DS-CDMA system.

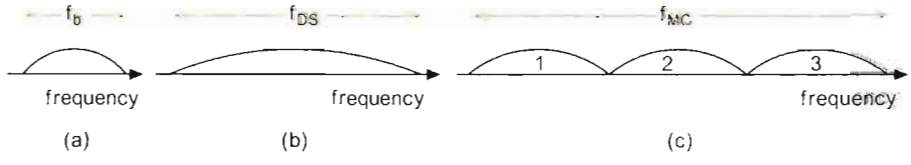

Figure 5-2 Comparison of the frequency expansion from f_b of the baseband signal in (a) to f_{DS} of a DS-CDMA system in (b) and to f_{MC} of a three subcarrier MC-DS-CDMA system in (c).

5.3 Channel Model

The transmitted signal is passed through a frequency selective Rayleigh fading channel. The coherence bandwidth of the channel is such that there is still frequency selectivity in each subcarrier band, which gives rise to L resolvable multipaths per subcarrier. The baseband impulse response of the channel for user k's mth subcarrier is given by

$$\mathbf{h}_{k,m}(t) = \sum_{l=1}^{L} \mathbf{a}_{k,m,l}\mathbf{g}_{k,m,l}\delta(t-\tau_{k,l}) \tag{5.3}$$

where $\mathbf{a}_{k,m,l} = \begin{bmatrix} a_{k,1,m,l} & \cdots & a_{k,P,m,l} \end{bmatrix}^T$ is the kth user's array response vector for multipath l, of subcarrier m. In a similar fashion, the complex fading vector $\mathbf{g}_{k,m,l} = \begin{bmatrix} g_{k,1,m,l} & \cdots & g_{k,P,m,l} \end{bmatrix}^T$ is defined. The transmission delay for user k's lth multipath is $\tau_{k,l}$, and the multipath delay spread of the channel is confined to less than a symbol interval T. The total received signal of all K transmitting users at the antenna array is

$$\mathbf{r}(t) = \sum_{i=-\infty}^{\infty} \sum_{k=1}^{K} A_k b_k(i) \sum_{l=1}^{L} s_k(t-iT-\tau_{k,l}) \sum_{m=1}^{M} \mathbf{a}_{k,m,l} \mathbf{g}_{k,m,l} \cos(\omega_m t + \theta_{km}) + \mathbf{n}(t) \tag{5.4}$$

The additive noise at each antenna element forms the vector $\mathbf{n}(t) = \begin{bmatrix} n_1(t) & \cdots & n_P(t) \end{bmatrix}$, where each term $n_p(t)$ is an independent white Gaussian process with variance σ^2.

The correlation in space is given by (2.24, 2.25), and the correlation in frequency is defined in (2.14).

5.4 MMSE ST-MUD Receiver Model

The receiver, figure (5-3), consists of a P-element antenna array, and on each antenna element there are M chip-matched filters for every user that the receiver wishes to receive. The performance of the single user receiver structure is indicative of the performance of the ST-MUD technique, and so for simplicity, only a single user receiver architecture will be considered. Attached on to each chip-matched filter are L adaptive FIR filters, of length $\bar{N}$. These are essentially the MUD elements of the receiver, as in figure (4-4).

5.4.1 Received Vector of Samples

The received vector of samples is fundamental to the formulation of the joint space-frequency-multipath MMSE solution that the ST-MUD architecture uses. The received vector of samples

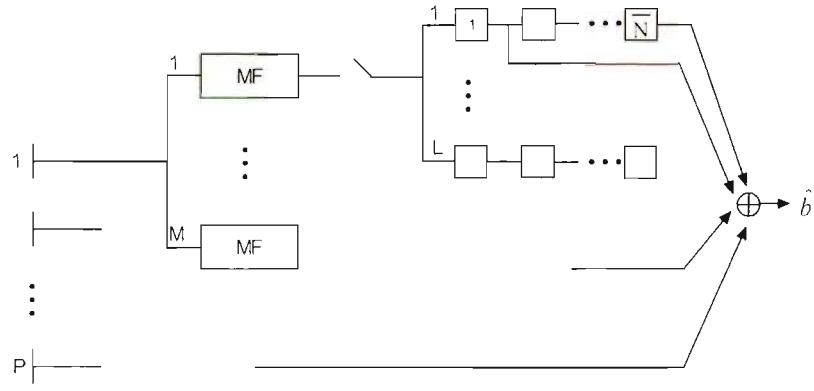

Figure 5-3 Space-time MUD model for MC-DS-CDMA

is the concatenation of the samples of the outputs of all the chip-matched filters. The chip-matched filters are sampled at the chip rate, and the nth output sample of the mth chip-matched filter (on subcarrier m) on antenna element p, which goes into the lth filter, for the detection of user k's ith symbol is given by

$$r_{k,p,m,l,n}(i) = \int_{iT+\tau_{k1}+nMT_c}^{iT+\tau_{k1}+(n+1)MT_c} r_{p,m}(t)\ \psi\left(t - iT - \tau_{kl} - nMT_c\right)\ dt \tag{5.5}$$

The received vector of samples for this multipath filter element is defined as

$$\mathbf{r}_{k,p,m,l}(i) = \left[r_{k,p,m,l,0}(i)\ \ r_{k,p,m,l,1}(i)\ \ \cdots\ \ r_{k,p,m,l,\bar{N}-1}(i)\right]^T \tag{5.6}$$

where the length of this vector is defined as

$$\bar{N} = N + \left\lceil \frac{\tau_{kl} - \tau_{k1}}{MT_c} \right\rceil \tag{5.7}$$

in such a manner that the received vector captures the information from all of user k's multipaths. To simplify the notation assume the desired user is user 1, so that the signal $r_{1,p,m,l}$ is represented by $r_{p,m,l}$. The total received vector of samples $\mathbf{r}$, of dimension $\left(PML\bar{N}\times 1\right)$, is then the concatenation of these received vectors from all the subcarriers and antenna elements,

$$\mathbf{r}_{pm} = \left[\mathbf{r}_{pm1}^T\ \ \cdots\ \ \mathbf{r}_{pmL}^T\right]^T \tag{5.8}$$

$$\mathbf{r}_{p} = \left[\mathbf{r}_{p1}^T\ \ \cdots\ \ \mathbf{r}_{pM}^T\right]^T \tag{5.9}$$

$$\mathbf{r} = \left[\mathbf{r}_{1}^T\ \ \cdots\ \ \mathbf{r}_{P}^T\right]^T \tag{5.10}$$

5.4.2 MMSE Solution

The MMSE algorithm produces a vector of filter coefficients (or weights), **w**, which filters the received vector **r**. These coefficients are derived jointly for the space-frequency-multipath components of the receiver. The output of the MMSE ST-MUD receiver is the decision statistic

$$\hat{b} = \mathrm{sgn}\left(\mathbf{w}^{H}\mathbf{r}\right) \tag{5.11}$$

As already stated, the weights are chosen to minimise the mean square error (MSE),

$$MSE = E\left\{\left(\mathbf{w}^{H}\mathbf{r} - b_1\right)^2\right\} \tag{5.12}$$

The MMSE solution is well known [39], [24], [19] and is (4.30)

$$\mathbf{w}_{opt} = \mathbf{R}^{-1}\boldsymbol{\alpha} \tag{5.13}$$

where the sample covariance matrix is

$$\mathbf{R} = E\left\{\mathbf{r}\mathbf{r}^{H} \mid \mathbf{q}\right\} \tag{5.14}$$

and the crosscorrelation is

$$\boldsymbol{\alpha} = E\left\{b\mathbf{r} \mid \mathbf{q}\right\} \tag{5.15}$$

where $\mathbf{w}_{opt}$ is optimal conditioned on all parameters $\mathbf{q} = \{\mathbf{a}_1, \cdots, \mathbf{a}_K, \mathbf{g}_1, \cdots, \mathbf{g}_K\}$ which are the angles of arrival (AOA) and the fading coefficients of all users.

5.5 Performance Analysis

The performance of the MMSE ST-MUD is calculated through a semi-analytical technique. This technique has been used in recent papers [49] for systems where the random variable does not have a white Gaussian distribution and no closed form solutions easily arise. The analysis derives an expression of the signal-to-interference-plus-noise-ratio (SINR) at the output of the receiver, based on the average interference-plus-noise covariance matrix. The instantaneous bit error rate (BER) can easily be computed knowing the instantaneous SINR (5.39). The average BER is then computed from a sample of SINR values.

The cross correlation term $\boldsymbol{\alpha}$ is useful and can be expressed in terms of the fading parameters and the array response

$$\boldsymbol{\alpha}_{p,m,l} = A_1 a_{1,p,l} g_{1,p,m,l} \mathbf{s}_{1,l} \tag{5.16}$$

The received signal vector $\mathbf{r}$ can be written in terms of the desired signal component and then the inter-symbol interference (ISI) plus multiaccess interference term (MAI) plus noise thus

$$\mathbf{r}(i) = \dot{\mathbf{r}}(i) + \ddot{\mathbf{r}}(i) \tag{5.17}$$

where $\dot{\mathbf{r}}(i)$ is the desired signal component and $\ddot{\mathbf{r}}(i)$ is the ISI plus MAI plus noise term. The exact structure of these terms is detailed in appendix A. The sample covariance matrix $\mathbf{R}$ can be written in terms of its constituent parts

$$\mathbf{R} = \dot{\mathbf{R}} + \ddot{\mathbf{R}} \tag{5.18}$$

where $\dot{\mathbf{R}}$ is the covariance matrix of the desired signal component given by

$$\dot{\mathbf{R}} = E\left\{\dot{\mathbf{r}}\dot{\mathbf{r}}^{H} \mid \mathbf{q}\right\} = \boldsymbol{\alpha}_{pml}\boldsymbol{\alpha}_{pml}^{H} \tag{5.19}$$

and $\ddot{\mathbf{R}}$ is the MAI plus noise covariance matrix (see appendix B for details), given by

$$\ddot{\mathbf{R}} = E\left\{\ddot{\mathbf{r}}\ddot{\mathbf{r}}^{H} \mid \mathbf{q}\right\} \tag{5.20}$$

The output SINR is defined as

$$SINR = \frac{|A|^2}{\tilde{\sigma}^2} \tag{5.21}$$

In order to get some insight into the structure of the SINR term, the decision statistic is rewritten as

$$\hat{b}_1 = \mathbf{w}_{opt}^{H}\mathbf{r} = \left(\mathbf{R}^{-1}\boldsymbol{\alpha}\right)^{H}\left(\dot{\mathbf{r}} + \ddot{\mathbf{r}}\right) \tag{5.22}$$

By recognising the fact that the desired signal $\dot{\mathbf{r}}(i)$ can be rewritten in terms of the cross correlation vector $\boldsymbol{\alpha}$ using (5.16),

$$\dot{\mathbf{r}}_{p,m,l}(i) = A_1 b_1(i) a_{1,p,m,l}\, g_{1,p,m,l}\, \mathbf{s}_{1,l} = \boldsymbol{\alpha}_{p,m,l}\ \ b_1(i) \tag{5.23}$$

then substituting this result into (5.22), the decision statistic can be written as

$$\hat{b}_1 = b_1 \boldsymbol{\alpha}^{H}\mathbf{R}^{-1}\boldsymbol{\alpha} + \ddot{\mathbf{r}}^{H}\mathbf{R}^{-1}\boldsymbol{\alpha} \tag{5.24}$$

The amplitude, A, of the desired signal component at the output of the receiver is therefore $\boldsymbol{\alpha}^{H}\mathbf{R}^{-1}\boldsymbol{\alpha}$, and the residual MAI and noise component is $\ddot{\mathbf{r}}^{H}\mathbf{R}^{-1}\boldsymbol{\alpha}$. The variance of the residual noise plus interference term, $\tilde{\sigma}^2$, is given by

$$\tilde{\sigma}^2 = E\left\{\left|\ddot{\mathbf{r}}^{H}\mathbf{R}^{-1}\boldsymbol{\alpha}\right|^2\right\} \tag{5.25}$$

This expression was shown in [51] to be equal to

$$\tilde{\sigma}^2 = \boldsymbol{\alpha}^{H}\mathbf{R}^{-1}\boldsymbol{\alpha}\left(1-\boldsymbol{\alpha}^{H}\mathbf{R}^{-1}\boldsymbol{\alpha}\right) \tag{5.26}$$

Equation (5.21) can then be written as,

$$SINR = \frac{\left(\boldsymbol{\alpha}^{H}\mathbf{R}^{-1}\boldsymbol{\alpha}\right)^2}{\boldsymbol{\alpha}^{H}\mathbf{R}^{-1}\boldsymbol{\alpha}\left(1-\boldsymbol{\alpha}^{H}\mathbf{R}^{-1}\boldsymbol{\alpha}\right)} \tag{5.27}$$

$$= \frac{\boldsymbol{\alpha}^{H}\mathbf{R}^{-1}\boldsymbol{\alpha}}{1-\boldsymbol{\alpha}^{H}\mathbf{R}^{-1}\boldsymbol{\alpha}} \tag{5.28}$$

The sample covariance matrix can be written in terms of its constituent parts

$$\mathbf{R} = \dot{\mathbf{R}} + \ddot{\mathbf{R}} \tag{5.29}$$

where $\dot{\mathbf{R}}$ is the covariance matrix of the desired signal component given by

$$\dot{\mathbf{R}} = E\left\{\dot{\mathbf{r}}\dot{\mathbf{r}}^{H} \mid \mathbf{q}\right\} = \boldsymbol{\alpha}_{pml}\boldsymbol{\alpha}_{pml}^{H} \tag{5.30}$$

$\mathbf{R}^{-1}$ can be rewritten in terms of (5.29) and (5.30),

$$\mathbf{R}^{-1} = \left(\dot{\mathbf{R}} + \ddot{\mathbf{R}}\right)^{-1} = \left(\boldsymbol{\alpha}\boldsymbol{\alpha}^{H} + \ddot{\mathbf{R}}\right)^{-1} \tag{5.31}$$

The *matrix inversion lemma* [38], also referred to as the Sherman-Morrison Formula or Woodbury's identity, gives the identity

$$\mathbf{B}^{-1} = \left(\mathbf{A} + \mathbf{x}\mathbf{y}^{H}\right)^{-1} = \mathbf{A}^{-1} - \frac{\mathbf{A}^{-1}\mathbf{x}\mathbf{y}^{H}\mathbf{A}^{-1}}{1+\mathbf{y}^{H}\mathbf{A}^{-1}\mathbf{x}} \tag{5.32}$$

If the substitution $\mathbf{A} = \ddot{\mathbf{R}}$ and $\mathbf{x} = \mathbf{y} = \boldsymbol{\alpha}$ is made, (5.31) can be written as

$$\mathbf{R}^{-1} = \left(\boldsymbol{\alpha}\boldsymbol{\alpha}^{H} + \ddot{\mathbf{R}}\right)^{-1} = \ddot{\mathbf{R}}^{-1} - \rho\ddot{\mathbf{R}}^{-1}\boldsymbol{\alpha}\boldsymbol{\alpha}^{H}\ddot{\mathbf{R}}^{-1} \tag{5.33}$$

where

$$\rho = \frac{1}{1+\boldsymbol{\alpha}^{H}\ddot{\mathbf{R}}^{-1}\boldsymbol{\alpha}} \tag{5.34}$$

Expanding $\mathbf{R}^{-1}$ of the amplitude $\boldsymbol{\alpha}^{H}\mathbf{R}^{-1}\boldsymbol{\alpha}$ term, and using the substitution $\boldsymbol{\alpha}^{H}\ddot{\mathbf{R}}^{-1}\boldsymbol{\alpha} = \frac{1-\rho}{\rho}$:

$$\begin{aligned}\boldsymbol{\alpha}^{H}\mathbf{R}^{-1}\boldsymbol{\alpha} &= \boldsymbol{\alpha}^{H}\left(\ddot{\mathbf{R}}^{-1} - \rho\ddot{\mathbf{R}}^{-1}\boldsymbol{\alpha}\boldsymbol{\alpha}^{H}\ddot{\mathbf{R}}^{-1}\right)^{-1}\boldsymbol{\alpha} \\ &= \frac{1-\rho}{\rho} - \frac{\rho(1-\rho)(1-\rho)}{\rho^{2}} \\ &= 1-\rho\end{aligned} \tag{5.35}$$

after simplifying $1-\rho$, the following identities result

$$\begin{aligned}A &= 1-\rho \\ &= \boldsymbol{\alpha}^{H}\mathbf{R}^{-1}\boldsymbol{\alpha} \\ &= \frac{\boldsymbol{\alpha}^{H}\ddot{\mathbf{R}}^{-1}\boldsymbol{\alpha}}{1+\boldsymbol{\alpha}^{H}\ddot{\mathbf{R}}^{-1}\boldsymbol{\alpha}}\end{aligned} \tag{5.36}$$

Using these results, (5.28) may now be written as

$$SINR = \frac{\boldsymbol{\alpha}^{H}\mathbf{R}^{-1}\boldsymbol{\alpha}}{1-\boldsymbol{\alpha}^{H}\mathbf{R}^{-1}\boldsymbol{\alpha}} = \frac{1-\rho}{1-(1-\rho)} = \frac{1-\rho}{\rho} \tag{5.37}$$

This expression for the SINR can be simplified further using (5.34) and (5.36) to give the final result

$$\begin{aligned}SINR &= \frac{1-\rho}{\rho} \\ &= \frac{\boldsymbol{\alpha}^{H}\ddot{\mathbf{R}}^{-1}\boldsymbol{\alpha}}{1+\boldsymbol{\alpha}^{H}\ddot{\mathbf{R}}^{-1}\boldsymbol{\alpha}} \times \frac{1+\boldsymbol{\alpha}^{H}\ddot{\mathbf{R}}^{-1}\boldsymbol{\alpha}}{1} \\ &= \boldsymbol{\alpha}^{H}\ddot{\mathbf{R}}^{-1}\boldsymbol{\alpha}.\end{aligned} \tag{5.38}$$

The bit error rate in terms of the instantaneous SINR is given by [10], [19],

$$P_{e\,SINR} = Q\left(\sqrt{SINR}\right) \tag{5.39}$$

where $Q(.)$ is the Q-function[5]. This conditional probability of error (or BER) is influenced more heavily by the random fluctuations in $\boldsymbol{\alpha}$, rather than the variations in $\ddot{\mathbf{R}}^{-1}$, therefore an appropriate approximation [30] is to use the average interference plus noise covariance matrix,

[5] $Q(x) = \int_{x}^{\infty} \frac{1}{\sqrt{2\pi}} e^{-t^{2}/2}\,dt = \frac{1}{2}erfc\left(\frac{x}{\sqrt{2}}\right)$

$$E\left\{\ddot{\mathbf{R}}\right\}^{-1} = \overline{\ddot{\mathbf{R}}}^{-1} \tag{5.40}$$

the probability of error is now only conditioned on the crosscorrelation vector

$$\begin{aligned} P_{e|\alpha} &= Q\left(\sqrt{SIR \mid \boldsymbol{\alpha}}\right) \\ &= Q\left(\sqrt{\boldsymbol{\alpha}^{H} \overline{\ddot{\mathbf{R}}}^{-1} \boldsymbol{\alpha}}\right) \end{aligned} \tag{5.41}$$

The final unconditional probability of error is derived through a pseudo-simulation technique of generating multiple crosscorrelation vectors with random angles of arrival and fade terms, and calculating the average probability of error from the samples of the SINR values. The number of crosscorrelation vectors to generate is S. The value of S for convergence was found to be in the range of 1000. The final probability of error is then given by

$$P_e = \frac{1}{S} \sum_{i=0}^{S} Q\left(\sqrt{\boldsymbol{\alpha}_i^{H} \overline{\ddot{\mathbf{R}}}^{-1} \boldsymbol{\alpha}_i}\right) \tag{5.42}$$

5.6 Results

The following results section investigates the performance of the MMSE ST-MUD. The simulation results are used to confirm the validity of the analysis technique. The conventional matched filter receiver's performance is shown alongside the performance curves to indicate the performance gain achieved by the ST-MUD scheme, and also to verify the simulation results against a known system. In addition, the theoretical curves in figures (5-6) and (5-7) from equation (3.1) are also used to verify the simulation results.

5.6.1 Reduction of Multiaccess Interference

The performance of the ST-MUD receiver is first analysed, figure 5-4, in the lowest dimension scenario, where there is only 1 antenna element, 1 subcarrier and all the users' signals only travel along 1 Rayleigh fading path. With this configuration the receiver is a conventional MMSE MUD. Length 31 gold codes are used in all simulations, which causes the load in the cell to go from 1/31 to 1, as the number of users vary from 1 to 31. There are 2 error-causing phenomena in the system, AWGN and MAI. The matched filter receiver cannot combat MAI, and because the performance of the MUD is better than that of the matched filter, one concludes that the MUD is in fact reducing the amount of MAI. Figure 5-4 also shows that the receiver can effectively cancel all the MAI (up to 31) when all the users are synchronous. In the asynchronous system, the values of the transmitted bits of the other users change once during the capture of the received vector. The receiver is in fact capturing part of the current bit and

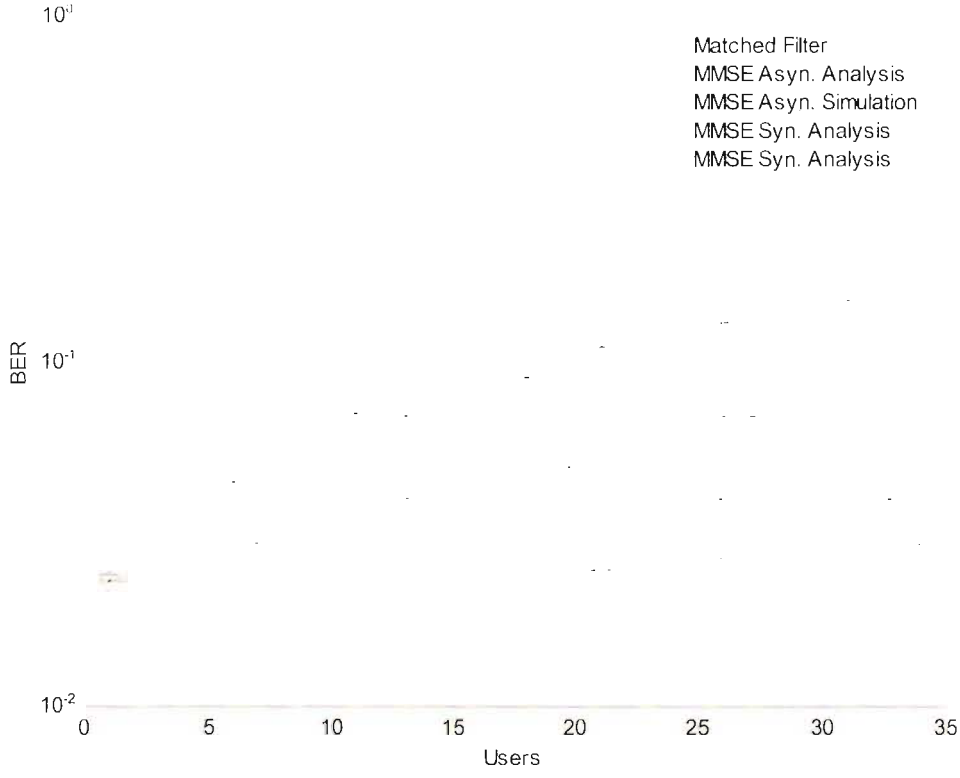

Figure 5-4 Rayleigh fading channel with a mean SNR of 10dB. 1 antenna element, 1 subcarrier and 1 multipath system. (Asyn. – Asynchronous, Syn. – Synchronous).

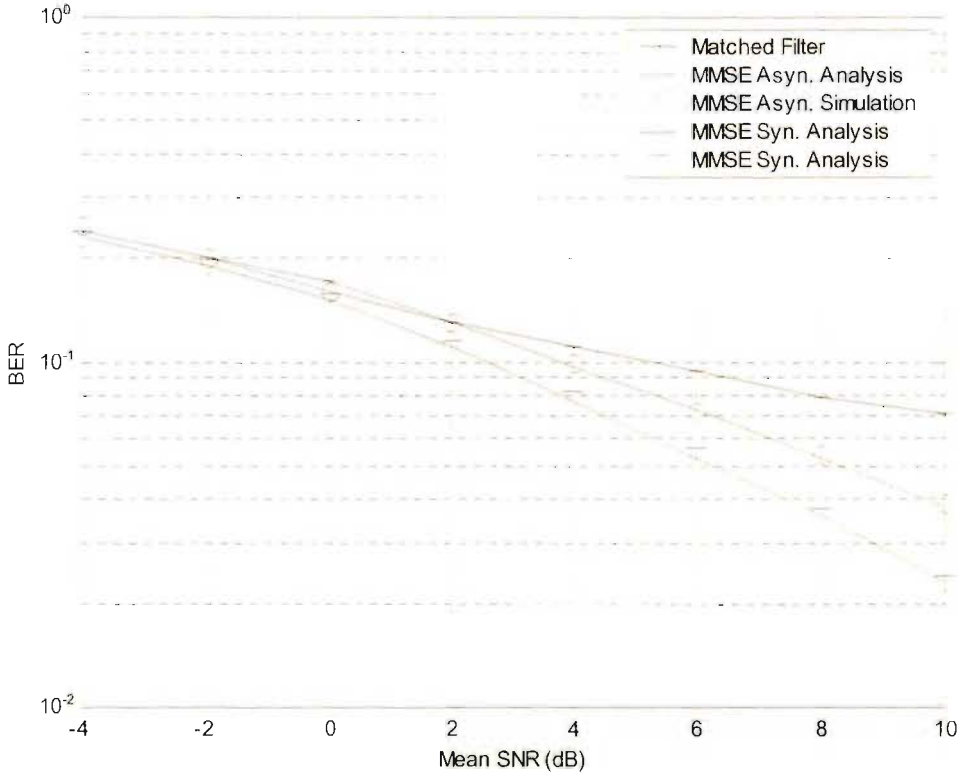

Figure 5-5 10 users, P = M = L = L_{tot} = 1. Rayleigh fading. (Asyn. – Asynchronous, Syn. – Synchronous).

part of the successive bit epoch of the other users in the system. This extra degree of complexity reduces the receiver's ability to cancel out the MAI.

The AWGN and MAI, as already stated, are the two error producing phenomena in the modelled communications channel. In low SNR conditions the AWGN is the dominant error-causing phenomenon. Figure 5-5 shows that in the low SNR region the performance of the MUD converges to that of the conventional matched filter receiver and as the SNR increases it yields a lower BER as more MAI is suppressed. Rayleigh fading has the effect of varying the instantaneous SNR, which reduces the rate at which the BER decreases with increasing mean SNR.

5.6.2 Antenna Effects

The antenna array enhances the performance of the ST-MUD when there is uncorrelated fading by providing diversity. Figure 5-6 shows simulation and analysis results for the single user case with different numbers of antenna elements. These coincide with the theoretical results predicted by (3.1).

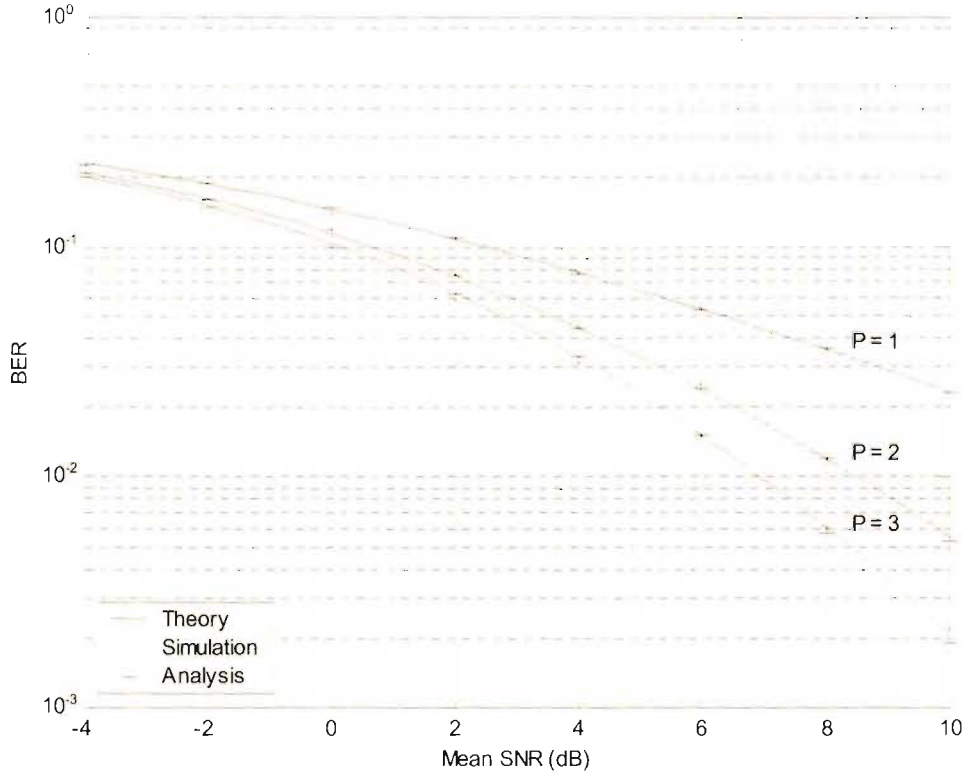

Figure 5-6 BER improvement of the MMSE receiver with increasing diversity, in an uncorrelated Rayleigh fading channel. One user present and P is the number of antenna elements.

Fading correlation reduces the amount of diversity gain. Figure 5-7 illustrates this concept by showing the performance of a 3-antenna system, with correlation, having performance between

that of the single antenna system and the uncorrelated 3-antenna system. With high correlation $(\Delta = 10^\circ)$ the performance approaches that of the single antenna system, and with low correlation $(\Delta = 40^\circ)$ the performance approaches that of the uncorrelated system. The space-frequency correlation matrices are given in (5.43). There are no subcarriers present in this system, and thus the $[\mathbf{R}_{sf}]_{i,j}$ element is equal to the correlation coefficient between antenna element i and j.

$$\mathbf{R}_{sf,\Delta=10} = \begin{bmatrix} 1.0000 & 0.9529 & 0.8197 \\ 0.9529 & 1.0000 & 0.9529 \\ 0.8197 & 0.9529 & 1.0000 \end{bmatrix} \quad \mathbf{R}_{sf,\Delta=20} = \begin{bmatrix} 1.0000 & 0.8226 & 0.4007 \\ 0.8226 & 1.0000 & 0.8226 \\ 0.4007 & 0.8226 & 1.0000 \end{bmatrix}$$

$$\mathbf{R}_{sf,\Delta=40} = \begin{bmatrix} 1.0000 & 0.4311 & 0.2350 \\ 0.4311 & 1.0000 & 0.4311 \\ 0.2350 & 0.4311 & 1.0000 \end{bmatrix} \tag{5.43}$$

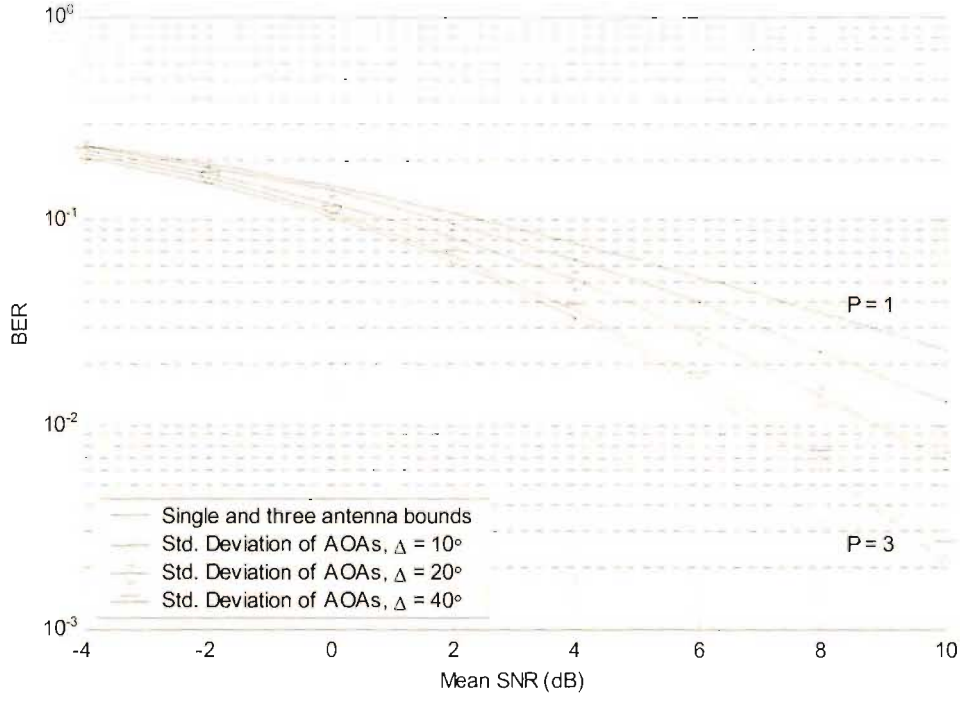

Figure 5-7 Bit error rate of the MMSE receiver with 3 antenna elements, and varying amounts of correlation between the antenna elements. The single user, single antenna and three antenna performance curves in uncorrelated fading are plotted as bounds to the performance. P is equal to the number of antenna elements.

5.6.3 ST-MUD Performance

A common receiver architecture consisting of 3 antenna elements, 3 subcarriers and 3 multipath receivers is used to analyse the performance of the ST-MUD. The channel consists of a total of 3 resolvable multipaths per user $(L_{tot} = 3)$, and a mean SNR of 5 dB. There is correlated fading,

with parameters $\Delta = 40^{\circ}$ and $\sigma_d = 1.0\mu s$. The exact space-frequency correlation matrix is given in appendix C. The number of users in the system is varied from 1 to 31, and they all transmit asynchronously using length 31 Gold codes.

The conventional matched filter receiver, which is used for comparative purposes, only receives the strongest out of the 3 resolvable multipaths. It makes use of only one antenna element and uses equal gain combining on the subcarriers.

The simulation and analysis of the ST-MUD are seen to concur in Figure 5-8, thus validating the analysis technique. The omission of the ISI factor in the analysis had a negligible effect, as predicted. A large performance gain is evident over the conventional system, which can be attributed to the diversity gain of the antenna elements and multipath receivers, MMSE combining of the subcarriers, and the MAI reduction. The ST-MUD, with 31 users, achieves a BER nearly half that of the conventional matched filter receiver when it is operating in a single user environment. This emphasises the advantage the ST-MUD has over the conventional receiver, because of its increased diversity.

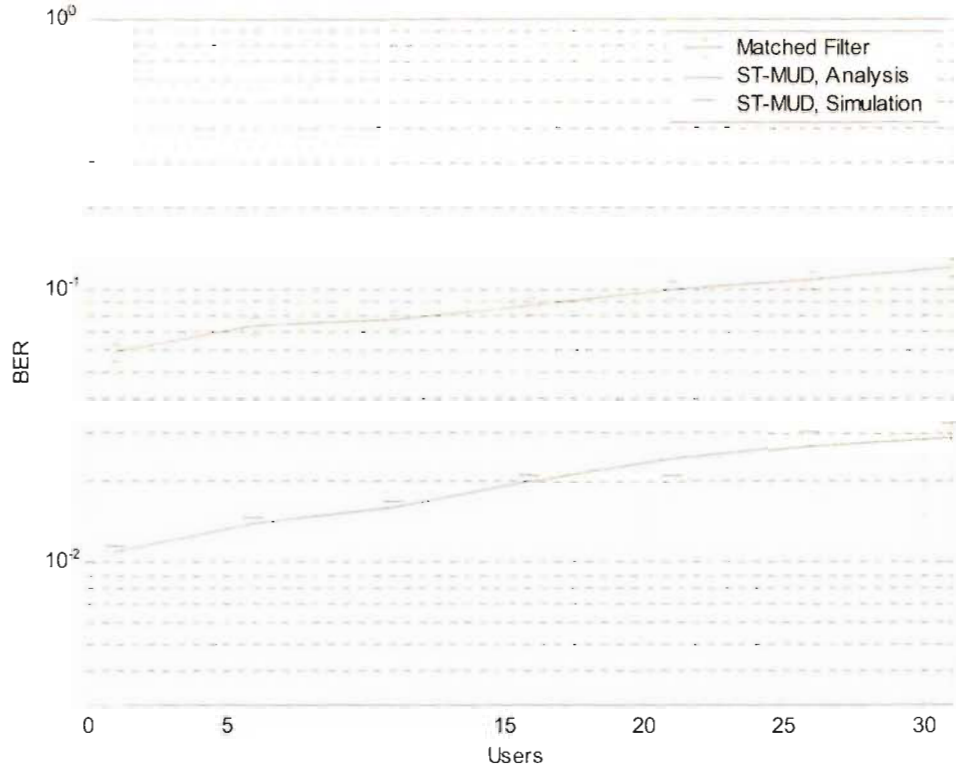

Figure 5-8 Performance comparison of ST-MUD with conventional matched filter receiver. SNR = 5 dB. 3 antenna elements, 3 subcarriers, 3 multipaths receivers and 3 resolvable multipaths in the channel.

The ST-MUD performance gain over the conventional receiver is shown in figure 5-9 as a function of SNR. There are always 10 users transmitting asynchronously. The initial gap in performance is due to the increased diversity induced by the antenna array and multipath receivers of the ST-MUD. At the higher SNR's, more MAI is suppressed and the gap between the MF and the ST-MUD increases, which emphasises the performance gain achieved by reducing MAI. At a BER of 5.5×10^{-2} the ST-MUD has approximately a 5dB gain in performance, which subsequently grows as the mean SNR increases.

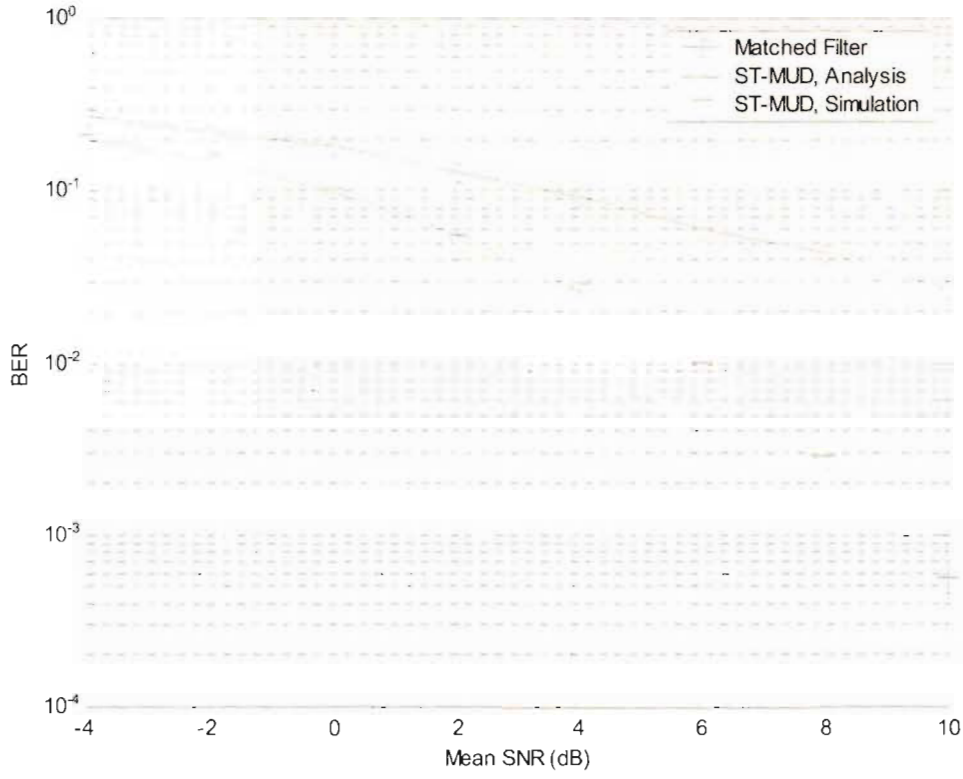

Figure 5-9 Performance gain of ST-MUD architecture over conventional matched filter receiver as SNR increases.

Reducing the number of antenna elements decreases the amount of diversity in the space domain and has an expected negative effect on system performance, as illustrated in figure 5-10. If system capacity is defined as the maximum number of users that the system can support whilst still achieving some minimum BER, then figure 5-10 shows that by increasing the number of antenna elements from 1 to 2, capacity is increased by 7 users. A further antenna element allows another 3 users to transmit, while the same BER (eg. 2.1×10^{-2}) is maintained. This indicates the trend that there are diminishing returns as one increases the number of antenna elements.

Reducing the number of subcarriers, as in figure 5-11, decreases the amount of diversity in the frequency domain and has an expected negative effect on system performance. The performance degradation from reducing the number of subcarriers is slightly more severe than reducing the number of antenna elements. The reason for this is that the correlation between the antenna elements is slightly higher than the correlation between the 3 subcarriers; therefore the diversity provided by 3 antenna elements is slightly lower than that provided by 3 subcarriers. The capacity increase of 10 users (BER of 2.4×10^{-2}) when going from one subcarrier to 2 further illustrates this point. The capacity increase of 6, users when the number of subcarriers is increased from 2 to 3, reiterates the diminishing returns provided by increasing the order of diversity.

The effect of multipath diversity is investigated in figure 5-12. The total number of multipaths (L_{tot}) is set at 3, and as L increases, the receiver exploits more of the transmitted energy that has been dispersed in the time domain. Increasing the number of multipath receivers has the most dramatic effect on the capacity of the system. If the minimum BER required is 3.1×10^{-2}, then a second multipath receiver enables a capacity increase of 31 users. This large capacity improvement occurs as a result of the fading on the resolvable multipaths being completely uncorrelated, therefore, the maximum diversity gain is achieved. Further increasing the number of multipath receivers, though, has the fastest diminishing return, in terms of capacity. A second multipath receiver only increases the capacity by 6 users, and this is attributable to the exponential MIP. The fraction of power contained in the multipaths decreases exponentially with the multipath delay, consequently, adding more multipath receivers provides a diminishing performance gain.

Figure 5-13 demonstrates the performance degradation associated with a frequency selective channel, when multipath receivers are not employed. The number of multipath receivers is fixed at 1, and as the channel becomes frequency selective ($L_{tot}=2$) there is a large reduction in performance. Specifically, if the minimum BER required is 2.9×10^{-2}, system capacity is reduced by 25 users, when the number of resolvable multipaths in the channel is increased to 2. This performance degradation is accounted for by the presence of ISI, which distorts the desired signal, as well as the increased MAI. The added multipath is equivalent to adding another set of slightly lower powered users into the system. They are slightly lower powered because of the exponential MIP, which is also the reason why the capacity degradation going from 2 to 3 multipaths is not as severe. This capacity reduction is only 10 users.

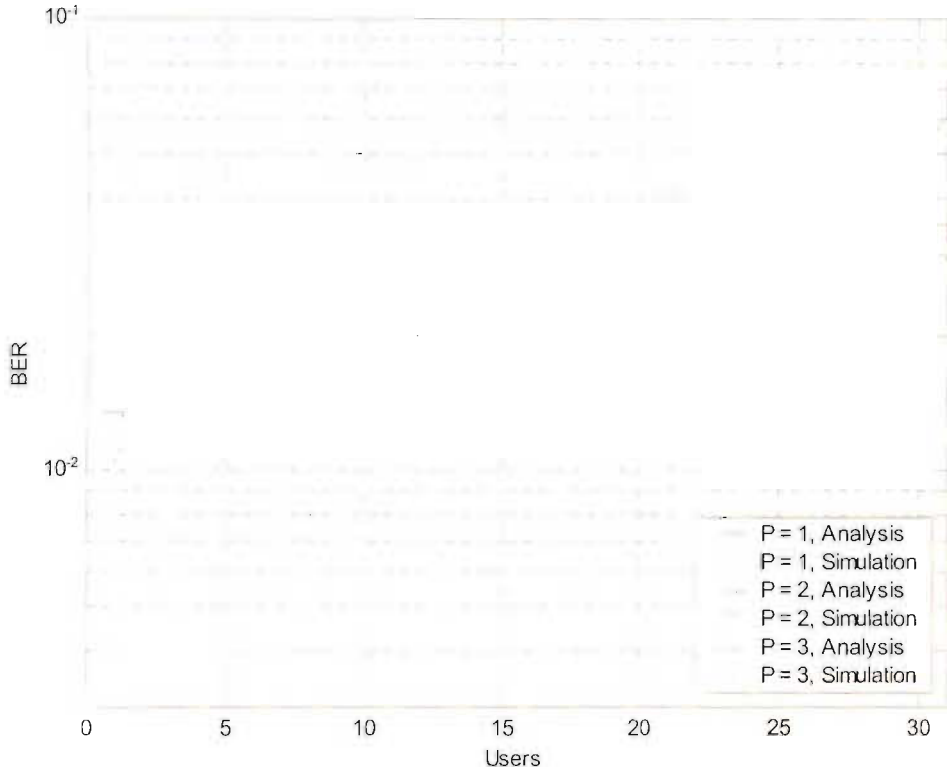

Figure 5-10 Diversity reduction with fewer antenna elements. M = L = L_{tot} = 1. Mean SNR 5dB.

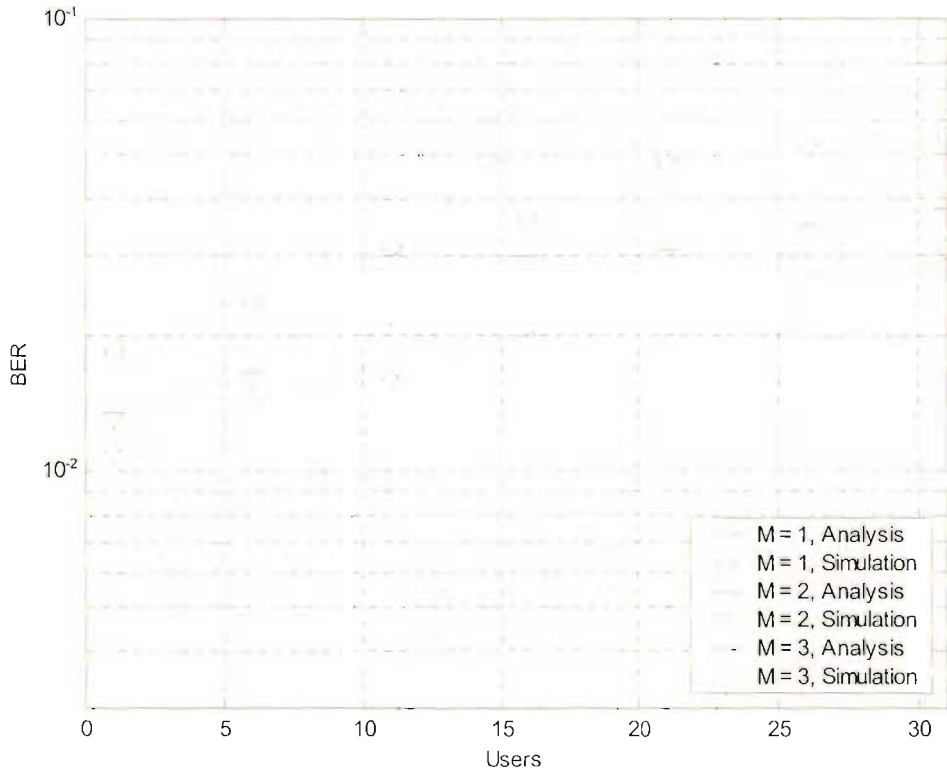

Figure 5-11 Diversity reduction with fewer subcarriers. P = L = L_{tot} = 3. Mean SNR 5dB.

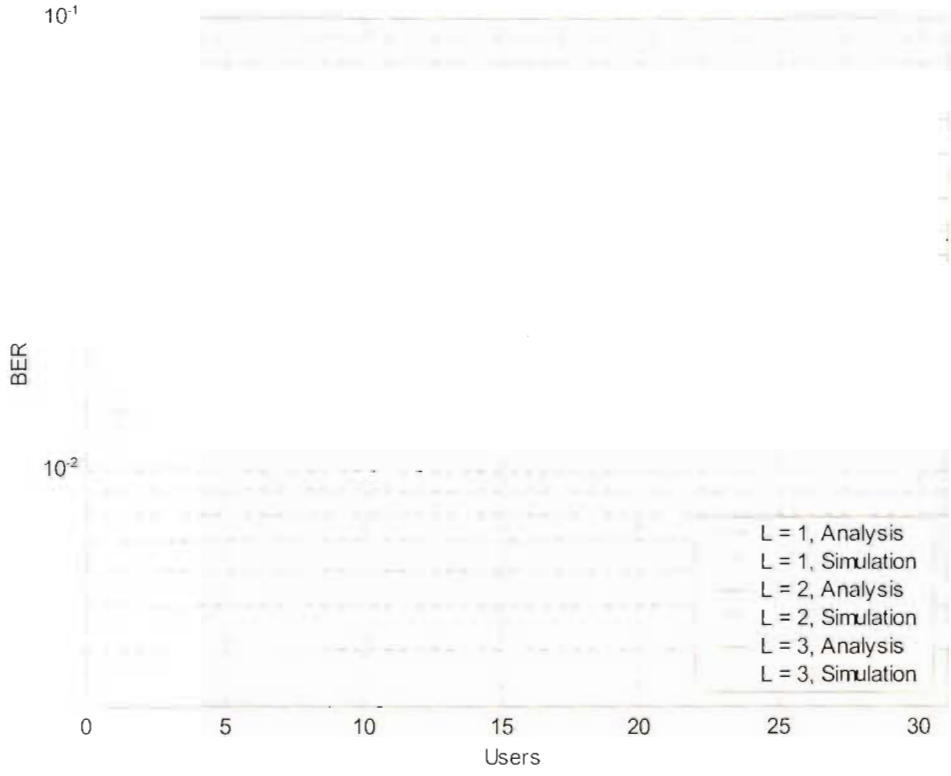

Figure 5-12 Diversity reduction with fewer multipath receivers. P = M = L_{tot} = 3. Mean SNR 5dB.

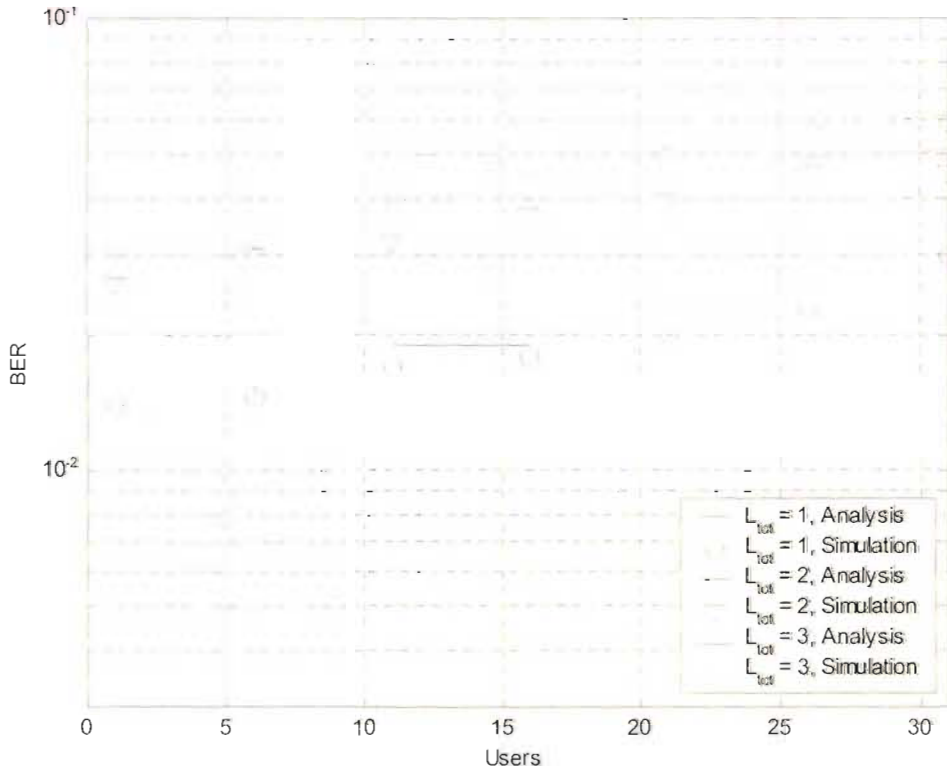

Figure 5-13 Performance reduction with increased frequency selective fading and 1 multipath receiver. P = M = 3, L = 1. Mean SNR 5dB.

5.7 Summary

This chapter presented a new ST-MUD architecture, which used the joint space-frequency-multipath MMSE solution, to enhance the reception of MC-DS-CDMA in a frequency selective, Rayleigh fading channel. The MC-DS-CDMA transmitter model and frequency selective fading channel was given. A space-frequency-correlated vector channel model was used to show the form of the received vector of samples. Using this received vector of samples, the MMSE solution was derived. The decision statistic of the ST-MUD was used as the starting point to compute the SINR at the output of the ST-MUD. This could then be directly related to the BER of the receiver, and thus constituted the core of the analysis technique that was used to predict the performance of the receiver. The SINR of the receiver, under various configurations and conditions, was computed using a custom software environment. From these results, bit error rates were computed and performance curves plotted. The communications channel was simulated with a custom software environment to validate the analysis results.

The MAI suppression capability of the ST-MUD was illustrated in figures 5-4, 5-5, and diversity enhancement in 5-6. Fading correlation effects were analysed in 5-7, and the reduction in diversity with correlation was demonstrated. Figures 5-8 and 5-9 showed performance gain of the ST-MUD architecture over the conventional matched filter receiver. This could be attributed to the ST-MUD's better combination strategy for the subcarrier components, diversity gain from multiple antennas and multipath receivers, and its ability to suppresses MAI and ISI. The amount of performance degradation due to reducing the number of antenna elements, subcarriers and multipath receivers was investigated in figures 5-10, 5-11, and 5-12, respectively. The frequency selectivity of the fading was shown to degrade performance when only one multipath receiver was employed, figure 5-13, otherwise the resolvable multipaths proved to be a valuable source of diversity.

Chapter 6 Subspace Techniques

6.1 Introduction

The ST-MUD problem has been well formulated [65], but unfortunately optimal array processing and optimal MUD are not feasible to implement as algorithms, because they are analytically intractable to solve. In other words, they require too much computing hardware that is either currently available or economically viable. Sub-optimal techniques, including linear techniques, have been developed which can be implemented adaptively [44], [73], (ie. with training sequences) or blindly [50]. Adaptive techniques are generally the most feasible form of implementation, and make use of well-understood digital signal processing techniques [62]. The MMSE solution, discussed in the preceding chapter, is an example of a linear technique that can be implemented adaptively.

The convergence and tracking performance of adaptive algorithms suffers a performance penalty as the number of filter coefficients to adapt increases. Subspace techniques arise out of the need to reduce the number of coefficients, for improved performance [9]. The length of the received vector of samples, $\left(PML\bar{N}\times 1\right)$, that the ST-MUD filters, is equal to the number of filter coefficients to adapt. This value grows rapidly as the number of antenna elements, subcarriers and multipath receivers increases, thus necessitating the need for subspace techniques.

In this ST-MUD context, the received vector of samples lies in the $\mathbb{R}_{PML\bar{N}\times 1}$ space, that is, the subspace spanned by all real vectors of dimension $\left[PML\bar{N}\times 1\right]$. This space is often overdetermined (excessively large) for finding the MMSE solution, which is especially true in the case when there are only a few active users in a cell. The real space $\mathbb{R}_{PML\bar{N}\times 1}$ can therefore be decomposed into a subspace spanning all the interferers' waveforms, and an orthogonal subspace spanning the noise space. Nothing can be done to suppress random noise, but the MMSE solution on the lower dimension interference subspace can be computed. The method

for computing the two subspaces usually involves computing an eigen- (or singular value) decomposition of the received vector covariance matrix.

Subspace based high-resolution methods play an important role in spectrum analysis, sensor array processing and general parameter estimation. To date the focus of research in subspace techniques for CDMA systems, has been in adaptive MUD [50], [74], [11] and STAP [78], [53], [79], and not ST-MUD. Subspace MUD of MC-CDMA has been analysed in [51], [52] and [80]. These papers do not include the effect of fading correlation between the subcarriers.

Better convergence and tracking is usually achieved by choosing a linear subspace with the smallest dimension that contains all the desired signature waveforms and all the interfering waveforms, which reach the receiver with sufficient energy. This chapter looks at three subspaces, namely: a Reduced Rank (Principle Components) Subspace [9], Cross Spectral Subspace [75] and a Partially Despread Subspace [55]. The MMSE solution is then found on these subspaces to perform ST-MUD. Insights into the performance of the subspace techniques are gained through simulation, where there is correlation between the fading terms of the subcarriers and antenna elements, and frequency selective fading per subcarrier.

6.2 Subspace Projection

Fundamental to the subspace techniques under discussion is the subspace projection. The subspace projection operation projects the received vector of samples on to a particular subspace. It is on this subspace that the MMSE solution is subsequently computed. The projected received vector is given by

$$\tilde{\mathbf{r}} = \mathbf{M}_d^T \mathbf{r} \tag{6.1}$$

where $\mathbf{M}_d$ is the subspace projection matrix of dimension d. The dimension d can range in value from 1 up to the length of $\mathbf{r}$, where $\mathbf{r}$ is $\left(PML\bar{N} \times 1\right)$ vector. When $d < PML\bar{N}$ (less than the length of $\mathbf{r}$) then the subspace technique is often referred to as a reduced rank approach. The reduced rank nomenclature is because the dimensionality (or rank) of the problem has been reduced and the receiver algorithm effectively has fewer degrees of freedom to find an optimal solution.

Reducing the rank can often yield benefits in terms of the convergence rates of adaptive algorithms. When d approaches 1, the performance of the receiver will approach that of the matched filter, since it now has no degrees of freedom to cancel out any MAI. When filter coef-

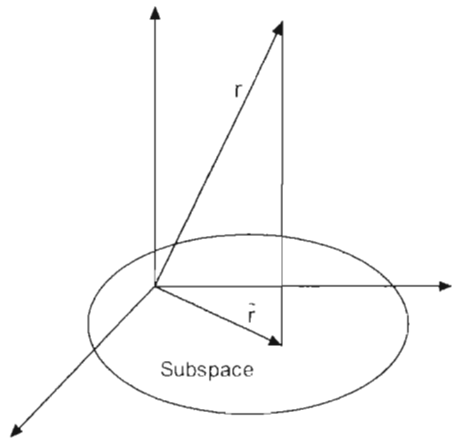

Figure 6-1 Interpretation of a projection on to a 2-dimensional subspace.

ficients used by the subspace algorithm are $\tilde{\mathbf{w}}$, then the MSE on this subspace is given by used by the subspace algorithm are $\tilde{\mathbf{w}}$, then the MSE on this subspace is given by

$$MSE_d = E\left\{\left|b_1 - \tilde{\mathbf{w}}^H \tilde{\mathbf{r}}\right|^2\right\} \tag{6.2}$$

The MMSE solution on this subspace has the same structure as the conventional MMSE solution (5.13), and is given by [9]

$$\tilde{\mathbf{w}} = \tilde{\mathbf{R}}^{-1}\tilde{\boldsymbol{\alpha}}_k \tag{6.3}$$

where

$$\tilde{\mathbf{R}} = \mathbf{M}_d^T \mathbf{R} \mathbf{M}_d \tag{6.4}$$

$$\tilde{\boldsymbol{\alpha}}_k = \mathbf{M}_d^T \boldsymbol{\alpha}_k \tag{6.5}$$

6.3 Principle Components

The principle components method, also known as reduced-rank filtering [75], finds the subspace of $\mathbf{R}$ that contains the most energy. The matrix $\mathbf{M}_d$ is a $\left(PML\bar{N} \times d\right)$ matrix composed of d linearly independent vectors, of length $\left(PML\bar{N} \times 1\right)$. These vectors span the subspace of $\mathbf{R}$ that contains the most energy, out of all subspaces of that same dimension. To find this particular subspace $\mathbf{M}_d$, an eigen-decomposition of the covariance matrix $\mathbf{R}$ is performed,

$$\mathbf{R} = \mathbf{Q}\boldsymbol{\Lambda}\mathbf{Q}^T \tag{6.6}$$

where $\mathbf{Q}$ is an orthonormal matrix of eigenvectors of $\mathbf{R}$, and $\mathbf{\Lambda}$ is a diagonal matrix of the corresponding eigenvalues. A projection matrix $\mathbf{M}_d$ is then made up of d eigenvectors corresponding to the d largest eigenvalues.

6.4 Cross-Spectral Filtering

The cross-spectral technique is similar to the principle components method; the difference is the criterion with which the eigenvectors are chosen. The projection matrix $\mathbf{M}_d$ is made up of the d eigenvectors that maximise the cost function

$$cs(\lambda_n) = \left| \mathbf{q}_n^T \mathbf{c}_k / \lambda_n \right|^2 \tag{6.7}$$

where $\mathbf{q}_n$ is the nth eigenvector of $\mathbf{Q}$ with associated eigen value λ_n, and $\mathbf{c}_k$ is the desired user's spreading code. Equation (6.7) inversely weights the eigenvalues, which is contrary to the principle components technique.

The difference between the principle components technique and the cross-spectral technique can be accounted for if one considers the near-far problem. When other interfering users are either closer to the base station, or are transmitting at a higher power level, their signal can completely swamp the desired user's signal. The subspace of the covariance matrix with the most power would probably correspond to the interfering user and not the desired user under these conditions. The cross-spectral technique introduces information known about the desired user, the spreading code $\mathbf{c}_k$, to form a subspace that can potentially produce better results.

6.5 Partial Despreading

The partial despreading technique provides a mechanism to scale the performance of the receiver from that of the full rank MMSE solution to that of the conventional matched filter. The trade off of performance corresponds to a reduction in the hardware complexity that comes with the reduction of rank.

The partial despreading technique takes m consecutive bits at a time, of the received vector $\mathbf{r}$, and multiplies them by the corresponding m bits of the desired user's spreading code $\mathbf{c}_k$ to form a partially despread representation of the received vector. This operation can be represented as a projection on to a subspace of dimension

$$d = \lceil N/m \rceil \cdot PML \tag{6.8}$$

When $P = M = L = 1$ the subspace projection matrix takes the form

$$\mathbf{M}_d = \begin{bmatrix} \begin{bmatrix} c_k(1) \\ \vdots \\ c_k(m) \end{bmatrix} & 0 & 0 & 0 \\ 0 & \begin{bmatrix} c_k(m+1) \\ \vdots \\ c_k(2m+1) \end{bmatrix} & 0 & 0 \\ 0 & 0 & \ddots & 0 \\ 0 & 0 & 0 & \begin{bmatrix} c_k((d-1)m+1) \\ \vdots \\ c_k(dm+1) \end{bmatrix} \end{bmatrix} \tag{6.9}$$

For the higher dimension cases, where there are multiple receiver antennas, subcarriers and multipaths, $\mathbf{M}_d$ takes on a block diagonal form. This block matrix $\boxed{\mathbf{M}}_d$, has dimension $(PML \times PML)$ where each element along its main diagonal is the matrix in (6.9).

$$\boxed{\mathbf{M}}_d = \begin{bmatrix} \mathbf{M}_{d,1} & & 0 \\ & \ddots & \\ 0 & & \mathbf{M}_{d,PML} \end{bmatrix} \tag{6.10}$$

The appropriate shifts are made in the $\mathbf{c}_i$'s, that construct the $\mathbf{M}_d$'s, that correspond to the time offset of the multipaths. The value of m is known as the despread factor, and when $m = 1$, the partial despreading technique corresponds to the full MMSE solution.

6.6 Results

A receiver architecture comprising 1 antenna element, 1 subcarrier and 1 multipath receiver was used in figure 6-2 to illustrate the importance the choice of rank has on the performance of the receiver. The system was configured with 10 users transmitting asynchronously using length 31 Gold codes. A Rayleigh fading channel was modelled where the mean SNR was set to 5dB and there is only one resolvable multipath per user. The conventional matched filter and MMSE receiver performance is shown as upper and lower limits to the performance of the receivers. The cross-spectral technique converges faster than the principle components technique, and as the rank of the receiver approaches the number of users, the cross-spectral technique converges towards the performance of the MMSE solution. The partial despreading technique's performance falls between that of the matched filter and the MMSE solution, depending on the despread factor. To compare the performance of the subspace techniques and the partial

despreading method, the despread factor went from 31 to 1, as the rank went from 1 to 31. It is immediately evident that the subspace techniques allow a reduction in the number of filter coefficients, while still achieving performance comparable to that of the full MMSE receiver.

The performance curves in figures (6-3), (6-4), (6-5), and (6-6), of the subspace and MMSE techniques, are computed using a receiver architecture comprising 2 antenna elements, 2 subcarriers and 2 multipath receivers. A Space-frequency correlated Rayleigh fading channel is modelled where the standard deviation of the AOA's, Δ, is set to 40°, and $\sigma_\tau = 1.0\mu s$ for the frequency correlation function. The conventional matched filter receiver, which is used for comparative purposes, receives only the strongest out of the 2 resolvable multipaths. It makes use of only one antenna element and uses equal gain combining on the subcarriers.

The performance gap between the matched filter receiver and MMSE receiver is more pronounced in figure 6-3 because of the antenna and multipath diversity the MMSE receiver exploits. Figure 6-3 most importantly illustrates the large reduction in rank (filter coefficients)

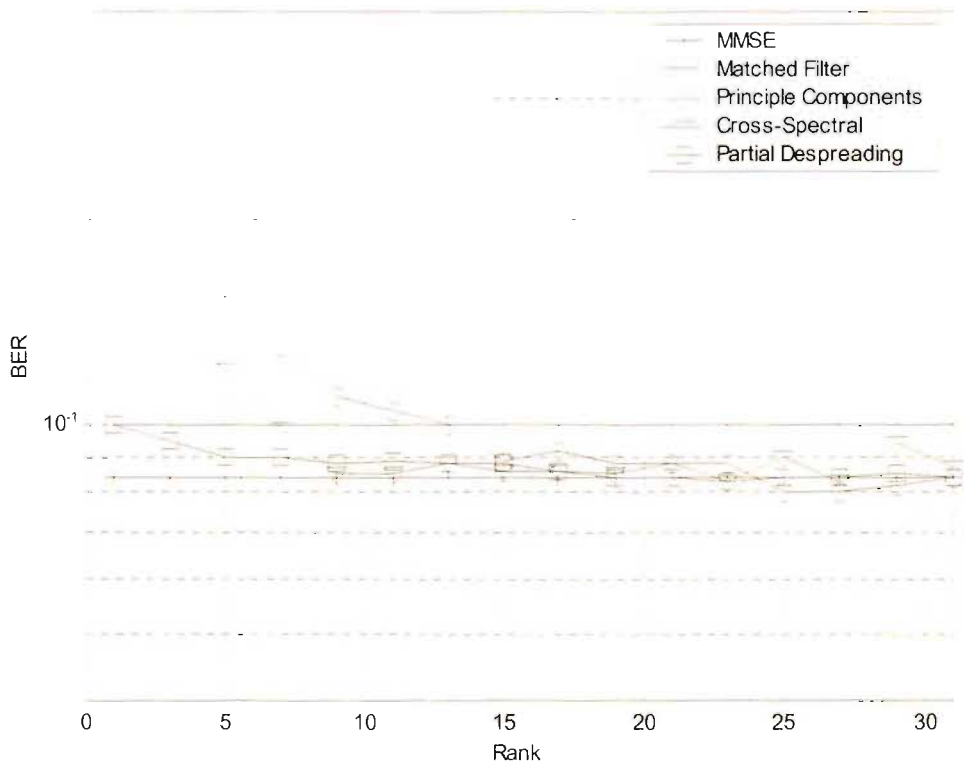

Figure 6-2 P = M = L = L_{tot} = 1. 10 user (asynchronous) system. Rayleigh fading with a mean SNR of 5 dB.

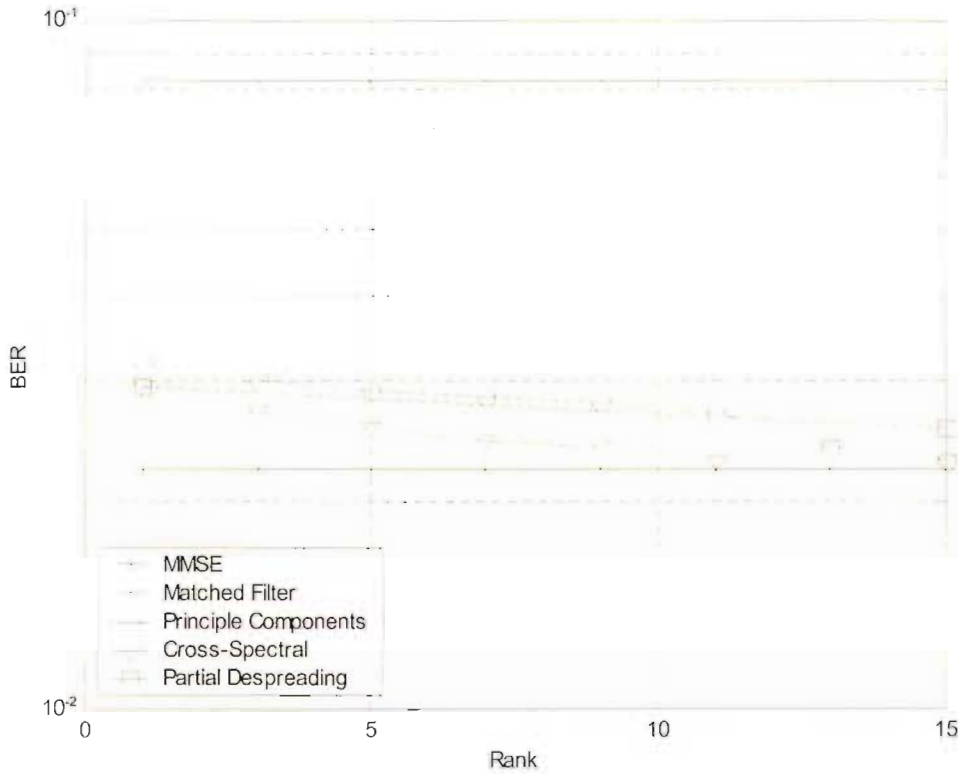

Figure 6-3 Effect of rank on the receiver's performance. P = M = L = L_{tot} = 2. 10 user (asynchronous) system. Rayleigh fading with mean SNR of 5 dB.

that is possible with the subspace techniques, when multiple antenna elements, subcarriers and multipath receivers are involved. An adaptive MMSE receiver, based on this configuration, would have 256 filter coefficients to adapt,

$$P \times M \times L \times \bar{N} = 2 \times 2 \times 2 \times 32 = 256 \tag{6.11}$$

The subspace techniques achieve performance levels comparable to the MMSE solution with just a fraction of this number of filter coefficients. The dimension of the partial despreading technique is a multiple of *PML*, as shown in (6.8). This limits the minimum filter length to 8, for the specific configuration. Rank values of 1 and 15 correspond to partial despread values of 1 and 2, which enables the comparison of the eigen-based methods to the partial despreading method on the same set of axes, as partial despread values of 1 and 2 correspond to filter lengths of 8 and 16. The partial despreading methods greatly outperforms the matched filter receiver in figure 6-3, even with a partial despread factor of 1, because of the diversity gained from the extra antenna element and multipath receiver. The MMSE solution on the partially despread subspace effectively combines the antenna elements, subcarriers, and multipath receivers in the maximal ratio sense. The receiver gains the ability to suppress part of the MAI when the partial despread factor is increased from 1 to 2, and the resulting lower BER is evident in figure 6-3.

Figure 6-4 reiterates the importance of the choice of rank on the receiver, and the relationship between the rank and the number of users, for the eigen-space techniques. The cross-spectral and principle components techniques both converge (with increasing rank) more slowly towards the MMSE performance mark, when there are more users in the system. The optimal choice of rank, for this particular system, can be deduced as being close to the number of users. This result is sensible as there is an exponential MIP, which reduces the amount of MAI that the second multipath introduces. The number of users is then equivalent to the number of degrees of freedom the receiver requires to suppress the bulk of the MAI. Rank values of 1, 15 and 23 correspond to partial despread values of 1, 2 and 3, which in turn correspond to length 8, 16, 24 implementations of the partial despreading method.

The relative performance of the subspace techniques, when they all have the same rank, is further illustrated in figures 6-5 and 6-6. In figure 6-5, the SNR is fixed at 5 dB, rank is set to 8, and the partial despread factor is 1; in figure 6-6, the number of users is set to 10. Figure 6-5 shows a widening of the performance gap between the subspace techniques and the MMSE solution as the number of users increases, thus illustrating the performance penalty incurred as the number of users exceeds the rank of the receiver. It is evident from this figure that if there is

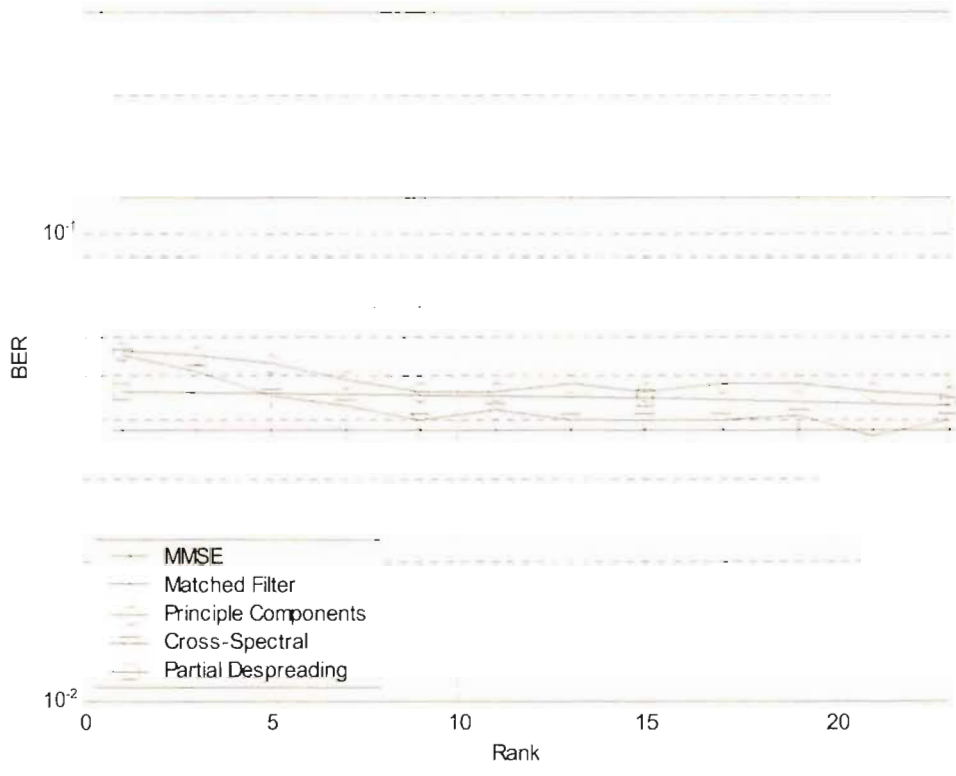

Figure 6-4 Effect of rank on the receiver's performance. P = M = L = L_{tot} = 2. 20 user asyn. system. Mean SNR 5 dB.

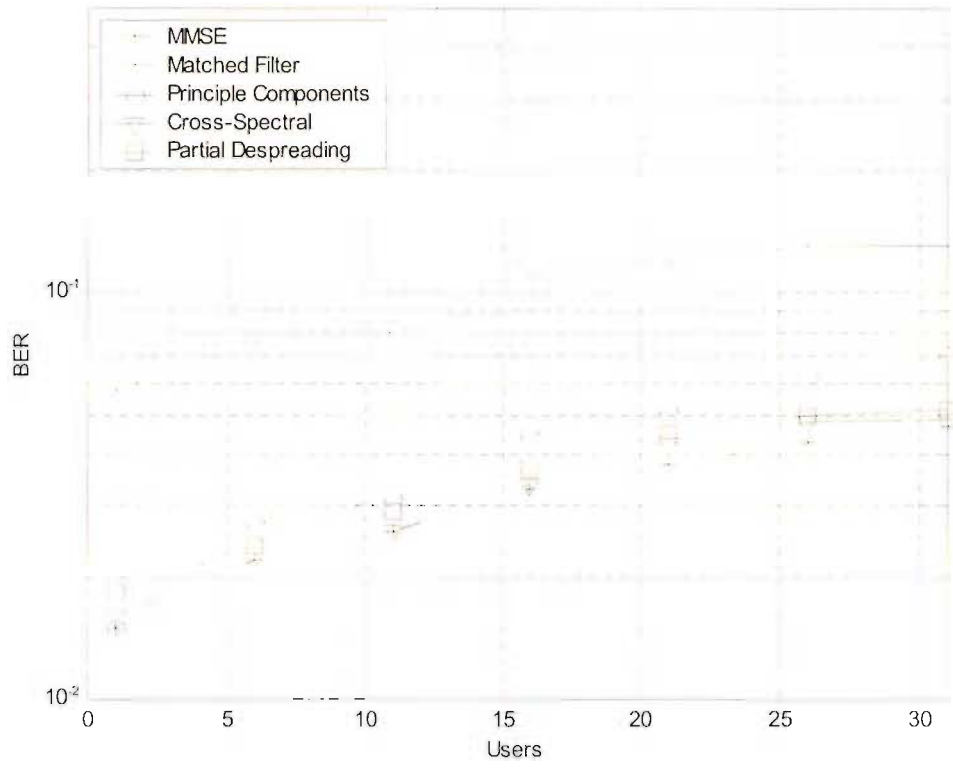

Figure 6-5 Relative performance of subspace techniques, compared to MMSE and matched filter performance. P = M = L =

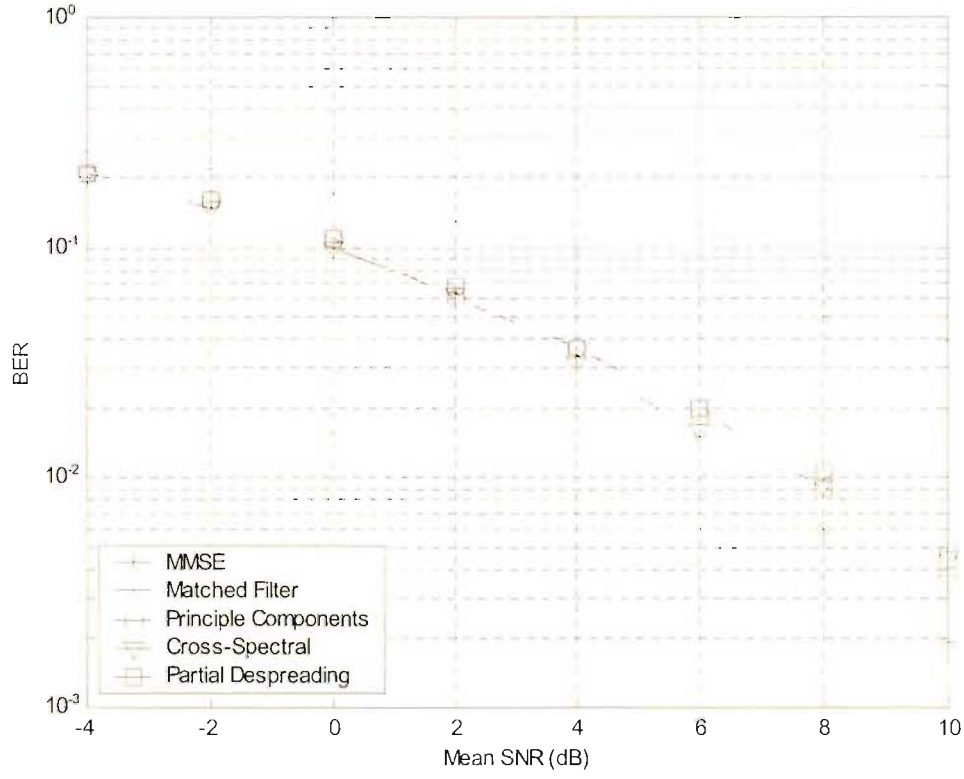

Figure 6-6 Relative performance of subspace techniques, compared to MMSE and matched filter performance, with a varying mean SNR. 2 antenna elements, 2 subcarriers, 2 multipath receivers and two resolvable multipaths in the channel. Rayleigh fading with 10 asynchronous users. Rank is set to 8 for all subspace techniques.

a constraint length on the adaptive FIR filter of the receiver, then the cross-spectral technique offers the best performance. When the SNR increases, the dominant error-causing phenomenon is the MAI, and no longer the AWGN. Figure 6-6 illustrates this point, as well as the various subspace techniques' MAI suppression capability. In the low SNR region, all the receivers have a comparable performance as they are all affected by AWGN in the same manner. In the higher SNR region, the performance of the subspace techniques deviates from the MMSE performance, because of their reduced MAI suppression capability.

6.7 Summary

The most viable implementation of the MMSE ST-MUD is with an adaptive scheme, but the number of filter coefficients to adapt is prohibitively large, thus necessitating the need for subspace techniques. The projection of the concatenated received vector of samples on to a subspace was presented and the generalised MMSE solution on that subspace was illustrated. The use of subspace techniques was motivated through their ability to improve the tracking and convergence properties of adaptive algorithms [9], [11]. The simulation results provide the best performance the ST-MUD architecture can achieve on a given subspace, and were compared to the conventional matched filter receiver and the MMSE solution.

The relative performance of three different subspace techniques was investigated in a frequency selective fading vector channel, where there was fading correlation between the subcarriers and antenna elements. The performance of the subspace techniques was shown to be heavily dependent on the choice of dimension (or rank). The eigen-space techniques can offer improvements over partial despreading, but at the cost of a higher computational complexity. The cross-spectral filtering technique performed, on average, marginally better than the principle components technique. The partial despreading technique provided a mechanism to scale the performance and complexity of the receiver, between the matched filter receiver and that of the full MMSE receiver. Both performance and complexity increases with a lower despread factor.

The disadvantage of subspace techniques in general is the inherent complexity of estimating the correct subspace. Subspace tracking techniques have been proposed to reduce this complexity [81].

Chapter 7 Conclusion

3G universal mobile communications will need to make use of advanced signal processing techniques to enable the provision of spectrally efficient broadband multimedia services, and simultaneously be economically and technically viable. These techniques can include the use of MUD and smart antennas. This dissertation has covered the use of ST-MUD, which encompasses both MUD and smart antennas, and can potentially provide the kinds of improvement necessary to make 3G PCN's possible. The ST-MUD system presented in this dissertation can exploit the characteristics of MC-DS-CDMA, by making use of space, frequency and multipath diversity whilst also suppressing MAI.

7.1 Dissertation Summary

A broad overview of the 3G research interest groups and motivation for ST-MUD was provided in the introductory chapter.

In chapter 2 an overview of radio communications channel models was presented with emphasis on fading and vector channel models. A frequency selective Rayleigh fading model along with the array response vector was used to devise the vector impulse response of the channel. A model that computes the fading correlation coefficient in the frequency domain was given. An outline of vector channel models was presented with their respective applications. The vector channel concept was extended to the frequency domain to define a space-frequency correlation matrix. This space-frequency correlation matrix had a block matrix form and allowed the modelling of the fading correlation between the subcarriers and antenna elements of the ST-MUD receiver.

Chapter 3 showed how smart antennas can be used for optimising and enhancing the performance of CDMA based cellular networks. Diversity techniques were discussed and their ability to combat multipath fading was illustrated. Four applications of smart antennas were discussed, namely: diversity, sectorisation, switched beam and optimal array processing. The concept of the radiation pattern of an antenna array was illustrated, and it was shown how this

pattern could be manipulated electronically using a digital processor. The concept of space-time processing for CDMA systems was presented.

MUD terminology and performance criteria were discussed in chapter 4. A synchronous and an asynchronous DS-CDMA model were also presented in this chapter. MAI suppression, near-far resistance, and the general receiver structure of the MMSE MUD scheme for DS-CDMA communication systems were illustrated. The improvement possible over a conventional receiver was therefore evident, and the use of MUD for advanced 3G receiver structures further emphasised. The asymptotic multiuser efficiency was shown to be a valuable analytical tool for quantifying the MAI suppression capability of different MUD schemes, and was computed for a selection of common MUD techniques. The structures of different MUD schemes were also illustrated in chapter 4. Focus was given to the MMSE and decorrelating MUD schemes. The decorrelating detector was covered as some of the performance metrics of the MMSE scheme are derived from it. The MMSE scheme was important as it provided the framework to derive the MMSE ST-MUD detector of the following chapter. The implementation of the decentralised MMSE MUD using a digital FIR filter along with an adaptive algorithm was shown, which provided a mechanism for the realisation of the MMSE ST-MUD.

In chapter 5, the DS-CDMA model of chapter 4 was extended to model a MC-DS-CDMA system. A MMSE ST-MUD receiver model was designed for a MC-DS-CDMA system with the capability of receiving up to L resolvable multipaths. Using the structure of the receiver and the vector impulse response of the channel, the received vector of samples was derived. This was a concatenated vector containing the signals arriving on different multipaths, antenna elements and subcarriers. The joint space-frequency-multipath MMSE solution was derived, which permitted the performance analysis of the MMSE ST-MUD. It used the decision statistic of the ST-MUD to compute the SINR at the output of the ST-MUD, which could be directly related to the BER of the receiver. The analysis of the ST-MUD, using the realistic vector channel model with space-frequency fading correlation, was plotted and compared to simulation results. A custom software environment, created by the author, generated the simulations results.

The simulation and analysis results concurred, and they illustrated the MAI suppression capability of the receiver. The performance enhancement through diversity was shown, as well as the reduction in diversity through fading correlation. The ST-MUD architecture greatly outperformed the conventional matched filter receiver because it better combined the subcarrier components, had diversity gain from multiple antennas and multipath receivers, and suppressed MAI and ISI. The amount of performance degradation due to reducing the number of antenna elements, subcarriers and multipath receivers was also investigated. The frequency selectivity of the fading was shown to degrade performance if only one multipath receiver was employed,

because of the increased amounts of MAI and ISI in the channel. ISI distorts and interferes with the desired user's waveform thereby reducing performance. MAI increases with more resolvable multipaths because each multipath, of other the users, appears like another user in the system to the receiver.

Chapter 6 extended the joint MMSE space-frequency-multipath solution to three different subspaces. The concept of a projection matrix and subspace was illustrated. A novel block matrix form was used for the partial despreading projection matrix. The use of the subspace techniques was motivated and their respective disadvantages and trade offs were covered. The relative performance of three different subspace techniques was investigated in a frequency selective fading vector channel, where there was fading correlation between the subcarriers and antenna elements. The effect of the choice of rank, and the number of users and SNR was investigated. The eigen-space techniques can offer improvements over partial despreading, but at the cost of a higher computational complexity. The partial despreading technique provided a mechanism to scale the performance, and complexity, of the receiver between the matched filter receiver and that of the full MMSE receiver. The simulation results provide the best performance the ST-MUD architecture can achieve on a given subspace. Their performance was compared to the conventional matched filter receiver and the MMSE solution.

7.2 Future Directions

There are some future research possibilities to build on the work presented in this dissertation:

- The effects of inter-carrier interference (ICI) could be studied in the ST-MUD context. ICI arises when there is a slight frequency shift between adjacent subcarriers and they interfere with each other. It would be an interesting MUD problem to try and suppress ICI.
- The performance of the MMSE ST-MUD could also be analysed in the presence of loose power control, or in bad near-far scenarios. A log-normally distributed variable could be used to adjust the mean transmit power of all the users in a cell, which would model these effects.
- Subspace techniques have been presented in this dissertation, but the performance analysis of blind subspace techniques as well as blind adaptive subspace techniques for ST-MUD, could prove to be a valuable avenue of research.

Appendix A Received Vector of Samples

The received vector of samples can be decomposed into

$$\mathbf{r}(i) = \dot{\mathbf{r}}(i) + \ddot{\mathbf{r}}(i) \tag{A.1}$$

where $\dot{\mathbf{r}}(i)$ is the desired signal component and $\ddot{\mathbf{r}}(i)$ is the inter-symbol interference (ISI) plus multiaccess interference (MAI) plus noise term. The desired signal component (user k) is given by

$$\dot{\mathbf{r}}_{k,p,m,l}(i) = A_k b_k(i) a_{k,p,m,l} g_{k,p,m,l} \mathbf{s}_{k,l} \tag{A.2}$$

and the ISI plus MAI plus noise term is given by

$$\ddot{\mathbf{r}}_{k,p,m,l}(i) = A_k b_k(i) \sum_{\substack{l'=1 \\ l' \neq l}}^{L} \xi_{k,p,m,l'} \mathbf{s}_{k,l'} + \sum_{\substack{k'=1 \\ k' \neq k}}^{K} A_{k'} b_{k'}(i) \sum_{l'=1}^{L} \xi_{k',p,m,l'} \mathbf{s}_{k',l'} + \mathbf{n}_{pm} \tag{A.3}$$

where

$$\xi_{k',p,m,l'} = a_{k',p,m,l'} g_{k',p,m,l'} \cos\left(\theta_{k,p,m,l} - \theta_{k',p,m,l'}\right) \tag{A.4}$$

and $\xi_{k,p,m,l'}$ is similarly defined. $\mathbf{s}_{k,l}$ is the discretised version of the kth users spreading waveform delayed by l-chips. To simplify the performance analysis, the ISI term in (A.3) is ignored, as in [51], [83], [84], to give a new expression

$$\ddot{\mathbf{r}}_{k,p,m,l}(i) = \sum_{\substack{k'=1 \\ k' \neq k}}^{K} A_{k'} b_{k'}(i) \sum_{l'=1}^{L} \xi_{k',p,m,l'} \mathbf{s}_{k',l'} + \mathbf{n}_{pm} \tag{A.5}$$

Appendix B Structure of Sample Covariance Matrix

The sample covariance matrix can be decomposed into the desired signal component and the MAI component

$$\mathbf{R} = \dot{\mathbf{R}} + \ddot{\mathbf{R}} \tag{B.1}$$

where the desired signal covariance matrix is given by

$$\begin{aligned} \dot{\mathbf{R}} &= E\left\{\dot{\mathbf{r}}\dot{\mathbf{r}}^{H} \mid \mathbf{p}\right\} \\ &= \boldsymbol{\alpha}\boldsymbol{\alpha}^{H} \end{aligned} \tag{B.2}$$

The concatenation of the received vector of samples imparts a strong block matrix form to the sample covariance matrix. This is illustrated using the desired signal covariance matrix,

$$\dot{\mathbf{R}} = \begin{bmatrix} \begin{bmatrix} \dot{R}_{111111} & \cdots & \dot{R}_{11111L} \\ \vdots & \ddots & \vdots \\ \dot{R}_{11112} & \cdots & \dot{R}_{11112L} \end{bmatrix} & \cdots & \dot{R}_{111M} & & \\ \vdots & \ddots & \vdots & \cdots & \dot{R}_{1P} \\ \dot{R}_{11M1} & \cdots & \dot{R}_{11MM} & & \\ \begin{bmatrix} \vdots \\ \dot{R}_{P1} \end{bmatrix} & & & \ddots & \vdots \\ & & & \cdots & \dot{R}_{PP'} \end{bmatrix} \tag{B.3}$$

Using the notation where $[\mathbf{A}]_{i,j}$ is the ith row and jth column element of matrix $\mathbf{A}$. The elements of the desired signal covariance matrix are given by

$$\begin{aligned} \left[\dot{R}_{pp'mm'll'}\right]_{i,j} &= \sqrt{\text{power}(l)}\sqrt{\text{power}(l')}\,c_{1,l}(i)\cdot c_{1,l'}(j)\zeta(i,j,l,l') && \text{if } i \neq j \text{ or } p \neq p' \text{ or } m \neq m' \text{ or } l \neq l' \\ &= \sqrt{\text{power}(l)}\sqrt{\text{power}(l')}\,c_{1,l}(i)\cdot c_{1,l'}(j)\zeta(i,j,l,l') + \sigma^2 && \text{if } i = j \text{ and } p \neq p' \text{ and } m \neq m' \text{ and } l \neq l' \end{aligned} \tag{B.4}$$

and the MAI covariance matrix is given by

$$\ddot{\mathbf{R}} = E\left\{\ddot{\mathbf{r}}\ddot{\mathbf{r}}^{H} \mid \mathbf{p}\right\} \tag{B.5}$$

The MAI covariance matrix also has a block diagonal form where the elements of the block matrix are given by

$$\begin{aligned}\left[\ddot{R}_{ppmmll'}\right]_{i,j} &= \sum_{k=2}^{K}\sum_{l=1}^{L_{kp}} \tfrac{1}{2}\text{power}(l)c_{k,l}(i)\cdot c_{k,l}(j)\zeta(i,j,\tau_{k,l}) \qquad \text{if } i \neq j \\ &= \sum_{k=2}^{K}\sum_{l=1}^{L_{kp}} \tfrac{1}{2}\text{power}(l)c_{k,l}(i)\cdot c_{k,l}(j)\zeta(i,j,\tau_{k,l}) + \sigma^2 \quad \text{if } i = j\end{aligned} \tag{B.6}$$

where *power(l)* is the fraction of power on multipath *l*. For simplicity all users have the same number of multipaths and the multipath intensity profile (MIP) is the same for all users. It is possible for the received vector of samples to span up to three different of data bits, since the length of $\mathbf{r}$ is $\bar{N}$, (5.7). The $\zeta(.)$ function checks if the *i*th and *j*th elements of the code vector, $\mathbf{c}_{k,l}$, correspond to the same bit epoch of the received vector.

$$\mathbf{r}_{p,m,l} = [\text{last bit current bit next bit}] \tag{B.7}$$

$$\begin{aligned}\zeta(i,j,\tau_{k,l}) = 1 \quad &\text{if} \quad i \text{ and } j \leq \tau_{k,l} \text{ or} \\ &\tau_{k,l} < i \text{ and } j < \tau_{k,l} + N \text{ or} \\ &i \text{ and } j \geq \tau_{k,l} + N \\ = 0 \quad &\text{else}\end{aligned} \tag{B.8}$$

The $\zeta(.)$ function performs the same operation in (B.4), except $\tau_{k,l}$ is replaced with $|l - l'|$. There is no correlation between the current and successive values of the data bits, and so the $\zeta(.)$ function causes some rectangular zero blocks to appear in the corners of $\dot{\mathbf{R}}_{pp'mm'll'}$ and $\ddot{\mathbf{R}}_{ppmmll'}$.

The off block diagonal elements (where $p \neq p'$, $m \neq m'$, $l \neq l'$) of $\ddot{\mathbf{R}}$ are zero,

$$\left[\ddot{R}_{pp'mm'll'}\right]_{i,j} = 0 \tag{B.9}$$

Appendix C Custom Software Environment Configuration

The custom software environment was created using *Borland C++*, to run as a 32 bit *Microsoft Windows* application. *IMSL C* math libraries were used for random number generation, eigen-analysis and matrix inversion. The code was structured in an object-oriented fashion with one parent class controlling the flow of the simulation and storing all simulation, receiver and channel parameters. This parent class would instantiate the *transmit* and the *receiver* class to perform the operations of computing the received vector of samples and decoding the desired user's transmitted bit respectively. These two classes in turn instantiated their own hierarchy of subclasses to perform functions pertaining to that class. For example, the transmit class would use a correlated Rayleigh random number generator class and the receiver class would instantiate a subspace projection class, if the receiver was configured as such.

C.1 Simulation Parameters

The custom simulation environment made use of length 31 Gold Codes [19]. The calculation of the MIP assumed a chip duration of $0.5\mu s$, which corresponded to a data rate of $1/(0.5\mu s \times 31) \cong 64$ kbits.s^{-1}. The relative fraction of power contained in each multipath, where there is either 1, 2 or 3 total number of resolvable multipaths per user, is given in table 3. The multipath powers are calculated using (2.10). The time separating the resolvable multipaths is equal to 1 chip period.

Fraction power in multipath	$L_{tot} = 1$	$L_{tot} = 2$	$L_{tot} = 3$
1	1.0000	0.6225	0.5064
2	0.0000	0.3775	0.3072
3	0.0000	0.0000	0.1863

Table 3 Multipath Intensity Profile.

All angles of arrival (AOA) for all users and their multipaths were randomised and kept constant during all simulations and analyses. The AOA's were uniformly distributed between $[-\pi, \pi]$. The start times of all interfering users were also randomised (uniformly on $[0,30]$) and kept constant for the duration of the simulations and analyses.

The Rayleigh fade variates, g, were generated with normal random variables having a standard deviation, σ, of $\frac{1}{\sqrt{2}}$, thus keeping the total received power unchanged,

$$E\{g^2\} = 2\sigma^2 = 2\times\left(\frac{1}{\sqrt{2}}\right)^2 = 1 \tag{C.1}$$

For a single simulation run (one data point) there were two criteria that had to be met before the calculated BER was deemed statistically valid. The first criterion was a minimum number of iterations (or transmitted bits) to be processed, and the second criterion was the minimum number of error events to occur.

For figures: 5-4, 5-5, 5-6, 5-7, and 6-2, the minimum number of iterations per data point was set to 50000 and minimum number error events to occur were 1000.

For figures: 5-8, 5-9, 5-10, 5-11, 5-12, 5-13, 6-3, 6-4, 6-5, and 6-6, the minimum number of iterations per data point was set to 5000 and minimum number error events to occur was 100. These numbers were reduced, as the processing time became prohibitive using 50000 and 1000 with these higher dimensional cases.

The standard ST-MUD model consisted of 3 antenna elements, 3 subcarriers, 3 multipath receivers and 3 resolvable multipaths in the channel. The space-frequency correlation matrix (as defined in (2.27), (2.28)), used by this standard system is

$$\mathbf{R}_{sf,\Delta=40,\sigma_d=1} = \begin{bmatrix} 1.0000 & 0.3705 & 0.2715 & 0.4311 & 0.1597 & 0.1170 & 0.2350 & 0.0871 & 0.0638 \\ 0.3705 & 1.0000 & 0.3705 & 0.1597 & 0.4311 & 0.1597 & 0.0871 & 0.2350 & 0.0871 \\ 0.2715 & 0.3705 & 1.0000 & 0.1170 & 0.1597 & 0.4311 & 0.0638 & 0.0871 & 0.2350 \\ 0.4311 & 0.1597 & 0.1170 & 1.0000 & 0.3705 & 0.2715 & 0.4311 & 0.1597 & 0.1170 \\ 0.1597 & 0.4311 & 0.1597 & 0.3705 & 1.0000 & 0.3705 & 0.1597 & 0.4311 & 0.1597 \\ 0.1170 & 0.1597 & 0.4311 & 0.2715 & 0.3705 & 1.0000 & 0.1170 & 0.1597 & 0.4311 \\ 0.2350 & 0.0871 & 0.0638 & 0.4311 & 0.1597 & 0.1170 & 1.0000 & 0.3705 & 0.2715 \\ 0.0871 & 0.2350 & 0.0871 & 0.1597 & 0.4311 & 0.1597 & 0.3705 & 1.0000 & 0.3705 \\ 0.0638 & 0.0871 & 0.2350 & 0.1170 & 0.1597 & 0.4311 & 0.2715 & 0.3705 & 1.0000 \end{bmatrix}$$

C.2 Correlation Control of the Fading coefficients

The fading coefficients of the received signal at the different antenna elements and on different subcarriers may be correlated. In order to simulate the channel, a vector of fade values $\mathbf{g}$, needs to be generated for every user, and for all the users' multipaths. The elements of the vector correspond to the fading coefficients on the different antenna elements and subcarriers, of a particular user's multipath(s). The vector of fade values must have a correlation matrix that corresponds to the values predicted by the space-frequency correlation function (2.26).

$$\mathbf{C} = E\{\mathbf{g}\mathbf{g}^H\} \tag{C.2}$$

where

$$[\mathbf{C}]_{pp'mm'} = \mathbf{R}_{sf}(m-m', p-p') \tag{C.3}$$

The vector $\tilde{\mathbf{g}}$, of uncorrelated Rayleigh random variables, can be made correlated by taking linear combinations of the elements of $\tilde{\mathbf{g}}$.

$$\mathbf{g} = \mathbf{M}\tilde{\mathbf{g}} \tag{C.4}$$

where $\mathbf{M}$ is given by

$$\mathbf{M} = \mathbf{U}\boldsymbol{\Lambda}^{1/2} \tag{C.5}$$

and $\mathbf{U}$ is the matrix of eigenvectors of $\mathbf{C}$ and $\boldsymbol{\Lambda}$ is the associated diagonal matrix of eigenvalues of $\mathbf{C}$. This technique is based on the work done in [82], and can be used to generate correlated Rayleigh random variables with any non-negative definite correlation matrix $\mathbf{C}$.

References

[1] T. Ojanperä, R. Prasad, "An Overview of Air Interface Multiple Access for IMT-2000/UMTS," *IEEE Comms. Mag.*, pp. 82-95, Sept. 1998.

[2] L. B. Milstein, "A Conceptual Overview of Wideband Code Division Multiple Access," *Proc. Of ISSSTA*, pp. 226-229, 2000.

[3] S. Hara, R. Prasad, "Overview of Multicarrier CDMA," *IEEE Comms.* Mag, pp. 126-133, Dec. 1997.

[4] R. Prasad, T. Ojanperä, "An Overview of CDMA Evolution Toward Wideband CDMA," *IEEE Communications Surveys*, pp. 2-29, Fourth Quarter, 1998.

[5] E. Dahlman, *et al*, "UMTS/IMT-2000 Based on Wideband CDMA," *IEEE Comms. Mag.*, pp. 70-80, Sept. 1998.

[6] S. Ponnekanti, "An Overview of Smart Antenna Technology for Heterogeneous Networks," *IEEE Communications Surveys*, pp. 14-23, Vol. 2, No. 4, Fourth Quarter 1999.

[7] H. Lehne, M. Pettersen, "An Overview of Smart Antenna Technology for Mobile Communications Systems," *IEEE Communications Surveys*, pp. 2-13, Vol. 2, No. 4, Fourth Quarter 1999.

[8] A. J. Paulraj, C. B. Papadias, "Space-Time Processing for Wireless Communications," *IEEE Signal Proc. Mag.*, pp. 49-83, Nov. 1997.

[9] M. Honig, M. K. Tsatsanis, "Adaptive Techniques for Multiuser CDMA Receivers," *IEEE Signal Processing Magazine*, pp. 49-61, May 2000.

[10] S. Verdú, *Multiuser Detection*, Cambridge University Press, 1998.

[11] M. Honig, "A Comparison of Subspace Adaptive Filtering Techniques for DS-CDMA Interference Suppression," *Proc. of Milcom*, Monterey, CA, pp. 836-840, Nov 1997.

[12] M. P. Lötter, P. van Rooyen, "Cellular Channel Modeling and the Performance of DS-CDMA Systems with Antenna Arrays," *IEEE JSAC*, pp. 2181-2196, Vol. 17, No. 12, Dec 1999.

[13] R. B. Ertel, T. S. Rappaport, J. H. Reed, *et al*, "Overview of Spatial Channel Models for Antenna Array Communication Systems," *IEEE Personal Comms. Mag*, pp. 10-21, Feb. 1998.

[14] A. Neskovic, N. Neskovic, G. Paunovic, "Modern Approaches in Modelling of Mobile Radio Systems Propogation Environment," *IEEE Communication Surveys*, Third Quarter, 2000.

[15] A. Shah, A. M. Haimovich, "Performance Analysis of Optimum Combining in Wireless Communications with Rayleigh Fading and Cochannel Interference," *IEEE Trans. Comm.*, Vol. 46, pp. 473-479, April 1998.

[16] M. Zeng, A. Annamalai, V. Bhargava, "Recent Advances in Cellular Wireless Communications," *IEEE Comm. Mag.*, pp. 128-138, Sept. 1999.

[17] D. Parsons, *The Mobile Radio Propagation Channel*, Pentech Press, 1992.

[18] Editor R. C. V. Macario, *Modern Personal Radio Systems*. IEE Press, 1996.

[19] J. G. Proakis. *Digital Communications*, 4th Ed., McGraw-Hill, 2001.

[20] COST 207 Document 207 TD (86)51 rev 3.

[21] V. Tarokh, N. Seshadri, A. R. Calderbank, "Space-Time Codes for High data Wireless Communication: Performance Criterion and Code Construction," *IEEE Trans. Info. Theor.*, Vol. 44, No. 2, pp. 744-765, March 1998.

[22] S. Choi, D. Shim, T. Sarkar, "A Comparison of Tracking-Beam Arrays and Switching-Beam Arrays Operating in a CDMA Mobile Communication Channel," *IEEE Antennas and Propagation Mag.*, Vol. 41, No. 6, pp. 10-21, Dec. 1999.

[23] W. C. Y. Lee, *Mobile Communications Engineering*, McGraw-Hill, 1982.

[24] P. van Rooyen, M. Lötter, D. van Wyk, *Space-Time Processing For CDMA Mobile Communications*, Kluwer Academic Publishers, 2000.

[25] D. Aszetly, *On Antenna Arrays in Mobile Communications Systems: Fast Fading and GSM Base Station Receiver Algorithms*, Ph.D. Dissertation, Royal Institute of Technology, March 1996.

[26] R. B. Ertel, "Vector Channel Model Evaluation," Tech. Report, SW Bell Tech. Resources, August 1997.

[27] J. S. Salz, J. H. Winters, "Effect of fading correlation on adaptive arrays in digital wireless communications," *IEEE Trans. Veh. Technol.*, Vol. 43, pp. 1049-1057, Nov. 1994.

[28] A. F. Naguib, PhD Dissertation "Adaptive Antennas for CDMA Wireless Networks," Stanford University, 1996.

[29] M. Dell' Anna, A. H. Aghvami, "Performance of Optimum and Suboptimum Combining at the Antenna Array of a W-CDMA System," *IEEE JSAC*, pp. 2123-2137, Vol. 17, No. 12, Dec. 1999.

[30] A. Özyildirim, Y. Tanik, "Outage Probability Analysis of a CDMA System with Antenna Arrays in a Correlated Rayleigh Environment," *Proc. Of IEEE VTC Spring*, pp. , 1999.

[31] A. Özyildirim, Y. Tanik, "SIR Statistics in Antenna Arrays in the Presence of Correlated Rayleigh Fading," *Proc. Of IEEE VTC Fall*, pp. 67-71, 1999.

[32] L. C. Van Atta, "Electromagnetic Reflections," U.S. Patent 2908002, October 6, 1959.

[33] B. Widrow, P. E. Mantey, L. J. Griffiths, "Adaptive Antenna Systems" *Proc. Of IEEE*, Vol. 55, No. 12, pp. 2143-2159, Dec. 1967.

[34] H. Krim, M. Viberg, "Two Decades of Array Signal Processing Research," *IEEE Sign. Proc. Mag.*, pp. 33-59, July 1996.

[35] X. Wang, H. V. Poor, "Space-Time Processing in Multiple-Access Systems," *Proc of WCNC*, pp.129-133, 1999.

[36] L. E. Brennan, I. S. Reed, "Theory of Adaptive Radar," IEEE Trans. On Aerospace and Electronics, AES-9, Vol. 2, pp. 237-252, March 1973.

[37] Y. T. Lo, "A Mathematical Theory of Antenna Arrays with Randomly Spaced Elements," *IEEE Trans. Antennas Propag.*, Vol. AP-12, pp. 257-268, May 1964.

[38] T. K. Moon, W. C. Stirling, *Mathematical Methods and Algorithms for Signal Processing*, Prentice Hall, 2000.

[39] R. A. Monzingo, T. W. Miller, *Introduction to Adaptive Arrays*, Wiley, 1980.

[40] W. L. Melvin, "Space-Time Adaptive Processing and Adaptive Arrays: Special Collection of Papers," *IEEE Trans. On Aeropsace and Electronic Systems*, Vol. 36, No. 2, pp. 508-509, April 2000.

[41] W. F. Gabriel, "Adaptive Processing Array Systems," *Proc Of IEEE*, Vol. 80, No. 1, pp. 152-162, Jan. 1992.

[42] R. Wang, S. D. Blostein, "Spatial-Temporal CDMA Receiver Structures for a Rayleigh fading Channels," *Proc. Of ICC*, pp. 549-554, 1999.

[43] S. Verdú, "Minimum Probability of Error for Asynchronous Gaussian Multiple Access," *IEEE Trans. IT.*, Vol. IT-32, No. 1, pp. 85–96, Jan. 1986.

[44] M. Honig, U. Madhow, S. Verdú, "Blind Adaptive Multiuser Detection," *IEEE Trans. On Information Theory*, Vol. 41, No. 4, pp. 944-960, July 1995.

[45] Xiaohua Li, H. Howard Fan, "Direct Blind Multiuser Detection for CDMA in Multipath without Channel Estimation," *IEEE Trans. Sign. Proc.*, Vol. 49, No. 1, pp. 63-73, Jan. 2001.

[46] G. Cherubini, *et al*, *IEEE Journal on Selected Areas of Communications – Multiuser Detection Techniques with Application to Wired and Wireless Communications Systems I*, Vol. 19, N0. 8, Aug. 2001.

[47] H. Vincent Poor, S. Verdú, "Probability of Error in MMSE Multiuser Detection," *IEEE Trans. On Information Theory*, Vol. 43, No. 3, pp. 858-871, May 1997.

[48] U. Madhow, M. L. Honig, "MMSE interference suppression for direct-sequence spread spectrum CDMA," *IEEE Trans. Comm.*, Vol. 42, pp. 3178-3188, Dec. 1994.

[49] S. L. Miller, M. L. Honig, L. B. Milstein, "Performance Analysis of MMSE Receivers for DS-CDMA in Frequency Selective Channels," *IEEE Trans. Comms*, Vol. 48, pp. 1919-1929, Nov. 2000.

[50] X. Wang, H. Vincent Poor, "Blind Multiuser Detection: A Subspace Approach," *IEEE Trans. On Inform. Theory*, Vol. 44, No. 2, pp. 677-690, March 1998.

[51] W. Xu, L. B. Milstein, "MMSE Interference Suppression for Multicarrier DS-CDMA in Frequency Selective Channels," *Proc. of Globecom*, pp. 259-264, 1998.

[52] S. L. Miller, B. J. Rainbolt, "MMSE Detection of Multi-Carrier CDMA," *IEEE JSAC*, Vol. 18, No. 11, pp. 2356-2362, Nov. 2000.

[53] J. R. Guerci, J. S. Goldstein, I. S. Reed, "Optimal and Adaptive Reduced-Rank STAP," *IEEE Trans. On Aeropsace and Electronic Systems*, Vol. 36, No. 2, pp. 508-509, April 2000.

[54] B. Ninness, S. R. Weller, "Performance aspects of linear multiuser receivers," *Proc. Of Globecom*, pp. 31-35, 2000.

[55] R. Singh, L. B. Milstein, "Interference Suppression for DS/CDMA," *IEEE Trans. Comms*, Vol. 47, pp. 446-453, March 1999.

[56] X. Wang, H. Vincent Poor, "Blind Equalization and Multiuser Detection in Dispersive CDMA Channels," *IEEE Trans. Comms*, Vol. 46, pp. 91-103, Jan. 1997.

[57] M. L. Honig, S. L. Miller, M. J. Shensa, "Performance of Adaptive Linear Interference Suppression in the Presence of Dynamic Fading," *IEEE Trans. Comm.*, Vol. 49, pp. 635-645, April 2001.

[58] H. Howard Fan, X. Li, "Linear Prediction Approach for Joint Blind Equalization and Blind Multiuser Detecttion in CDMA Systems," *IEEE Trans. Sign. Proc.*, Vol. 48, pp. 3134-3145, Nov. 2000.

[59] M. Honig, M. K. Tsatsanis, "Adaptive Techniques for Multiuser CDMA Receivers," *IEEE Signal Proc. Mag.*, pp 49-61, May 2000.

[60] S. L. Miller, M. L. Honig, L. B. Milstein, "Performance Analysis of MMSE Receivers for DS-CDMA in Frequency Selective Channels", *IEEE Trans. Comms.*, Vol. 48, No. 11, pp. 1919-1929, Nov. 2000.

[61] H. Gao, P. J. Smith, M. V. Clark, "Theoretical Reliability of MMSE Linear Diversity Combining in Raleigh-Fading Additive Interference Channels," *IEEE Trans. Comms*, Vol. 46, pp. 666-672, May 1998.

[62] E. C. Ifeachor, B. W. Jervis, *Digital Signal Processing*, Addison-Wesley, 1993.

[63] H. C. Huang, S. Schwartz, S. Verdú, "Combined multipath and spatial resolution for multiuser detection: Potentials and problems," in *Proc. Of IEEE Int. Symp. Inform. Theory*, Whistler, B.C., Canada, 1995, pp. 205.

[64] C. Vaidyanathan, K. Buckely, "An Adaptive Decision Feedback Equaliser antenna array for Multiuser CDMA Wireless Communications," in *Proc. Of 30th Asilomar Conf. Circuits, Syst., Comput.*, Pacific Grove, CA, Nov. 1995.

[65] X. Wang, H. V. Poor, "Space-Time Multiuser Detection in Multipath CDMA Channels," *IEEE Trans. On Signal Processing*, Vol. 47, No. 9, pp. 2356-2374, September 1999.

[66] M. Honig, "A Comparison of Subspace Adaptive Filtering Techniques for DS-CDMA Interference Suppression," *Proc. of MILCOM*, Monterey, CA, pp. 836-840, November 1997.

[67] U. Madhow, E. Visotsky, D. Warrier, "Multiuser Space-Time Communication," *IEEE ITW*, Kruger National Park, South Africa, June 1999.

[68] X. Wang, H. V. Poor, "Blind Adaptive Space-Time Multiuser Detection in Multipath CDMA Channels," in *Proc. Of WCNC'99*, pp. 1033-1037.

[69] H. Dai, H. Vincent Poor, "Iterative Space-Time Processing for Multiuser Detection in CDMA Systems," in *Proc of ISSSTA*, pp. 343-347, 2000.

[70] S. Moshavi, J. C. Liberti, P. G. Zablocky, "Combined Space Time Adaptive Processing in Multi-User Detection for Enhanced Reverse Link IS-95 CDMA Reception with Experimental Results," in *Proc of ISSSTA*, pp. 449-454, 2000.

[71] W. A. Hamouda, P. J. McLane, "Performance Analysis of Space-Time MMSE Detection in Synchronous Multiuser DS-CDMA," in *Proc of ISSSTA*, pp. 6-10, 2000.

[72] S. Kondo, L. B. Milstein, "On the Performance of Multicarrier DS CDMA Systems," *IEEE Trans. Comms*, pp. 238-246, Vol. 44, Feb. 1996.

[73] U. Madhow, L. J. Zhu, L. Galup, "Differential MMSE: new adaptive algorithms for equalization, interference suppression, and beamforming," *Proc. 32nd Asilomar Conf. Signals, Systems and Computers (Asilomar'98)*, Pacific Grove, CA, October 1998.

[74] S. Kraut, L. Scharf, L. Todd McWorter, "Adaptive Subspace Detectors," *IEEE Trans. Sign. Proc.*, Vol. 49, No. 1, pp. 1-16, Jan. 2001.

[75] J. S. Goldstein, I. S. Reed, "Reduced Rank Adaptive Filtering," *IEEE Trans. Sign. Proc.*, Vol. 45, No. 2, pp. 492-496, Feb. 1997.

[76] A. Özyildirim, Y. Tanik, "SIR Statistics in Antenna Arrays in the Presence of Correlated Rayleigh Fading," *Proc. Of VTC*, pp. 67-71, Fall 1999.

[77] J. Salz, J. Winters, "Effect of fading correlation on adaptive arrays in digital wireless communications," *IEEE Trans. Veh. Technol.*, Vol. 43, pp. 1049-1057, Nov. 1994.

[78] C. D. Peckham, *et al*, "Reduced-Rank STAP Performance Analysis," *IEEE Trans. On Aeropsace and Electronic Systems*, Vol. 36, No. 2, pp. 508-509, April 2000.

[79] Alle-Jan van der Veen, S. Talwar, A. J. Paulraj, "A Subspace Approach to Blind Space-Time Signal Processing for Wireless Communication Systems," *IEEE Trans. On Signal Processing*, Vol. 45, No. 1, pp. 173-190, Jan. 1997.

[80] J. Namgoong, T. F. Wong, J. S. Lehnert, "Subspace Multiuser Detection for Multicarrier DS-CDMA," *IEEE Trans. Comms*, Vol. 48, No. 11, pp. 1897-1908, Nov. 2000.

[81] C.E. Davila, "Efficient, High Performance, Subspace Tracking for Time Domain Data," *IEEE Trans. on Sign. Pro.*, pp. 3307-3315, Vol. 48, No. 12, Dec. 2000.

[82] T. Poutanen, J. Kolu, "Correlation Control in the Multichannel Fading Simulators," *Proc. Of Spring VTC*, Greece, 2001.

[83] W. Xu, L. B. Milstein, "On The Performance of Multicarrier RAKE Systems," *Proc. Of Globecom*, pp. 295-299, 1997.

[84] T. Eng, L. B. Milstein, "Coherent DS-CDMA Performance in Nakagami Multipath Fading," *IEEE Trans. Comms*, 1134-1143, Vol. 43, No. 3, March 1995.